Industrial Chemistry & Materials

ROYAL SOCIETY OF CHEMISTRY

REVIEW

View Article Online
View Journal

Check for updates

Cite this: DOI: 10.1039/d6im00033a

Hydrogen barrier coatings for pure hydrogen/hydrogen-blended natural gas pipelines: a focused review

Yuxi Chen, [ab] Cailin Wang,*[ab] Cuiwei Liu,[ab] Xiusai Xu,[ab] Lianfeng Wu,[cd] Junjie Huang [ab] and Yuxing Li *[ab]

Constructing new hydrogen pipelines or utilizing existing natural gas networks represents an effective pathway for large-scale hydrogen energy transport. However, the permeation of hydrogen atoms into metallic materials during transport can induce hydrogen embrittlement (HE), posing a severe threat to pipeline safety. Developing hydrogen barrier coatings (HBCs) with superior pipeline adaptability is a critical strategy to mitigate this issue. This paper systematically reviews four HBC material systems: metal-based, ceramic-based, 2D materials, and polymer-based composites. Beyond a comparative analysis of their barrier performance, we deeply elucidate the hydrogen barrier mechanisms, including the physical/chemical barriers and hydrogen trapping effects in inorganic materials, as well as the synergistic mechanisms between organic polymer matrices and functional fillers. A key contribution of this review, which distinguishes it from existing literature, is the construction of a comprehensive full-chain evaluation framework. This framework integrates "Preparation Quality (density, adhesion, thickness) – Hydrogen Barrier Efficiency (permeation rate, permeation reduction factor) – Protection Performance (HE resistance, fatigue resistance) – Pipeline Applicability (environmental coupling, coating–substrate interactions)", thereby providing a standardized basis for assessment. Finally, considering the specific requirements of hydrogen transport scenarios, the paper outlines current pipeline coating application requirements and proposes future research directions to support the development of safe and efficient hydrogen transport infrastructure.

Keywords: Hydrogen pipeline transportation; Hydrogen barrier coatings; Hydrogen barrier mechanism; Coating evaluation; Hydrogen permeation.

Received 22nd January 2026,
Accepted 13th May 2026

DOI: 10.1039/d6im00033a

rsc.li/icm

Open Access Article. Published on 14 May 2026. Downloaded on 6/5/2026 2:11:30 AM.
This article is licensed under a Creative Commons Attribution-NonCommercial 3.0 Unported Licence.

1 Introduction

Amid the global urgency to combat climate change and accelerate the energy transition, hydrogen has emerged as a cornerstone of future sustainable energy systems, distinguished by its zero-carbon footprint and high energy density.[1,2] Retrofitting existing natural gas infrastructure for hydrogen blending, or constructing dedicated pure hydrogen pipelines, is widely regarded as the most viable pathway for achieving large-scale, cost-effective hydrogen transport. Consequently, the deployment of hydrogen transport infrastructure has accelerated worldwide. Notable initiatives include the United States' HyBlend program, the European Union's ambitious "European Hydrogen Backbone" and "SoutH2 Corridor"—projecting over 40 000 km of pipelines—

[a] College of Pipeline and Civil Engineering, China University of Petroleum (East China), Qingdao, 266580, China
[b] Shandong Provincial Key Laboratory of Oil, Gas and New Energy Storage and Transportation Safety, China University of Petroleum (East China), Qingdao, 266580, China
[c] Marine Chemical Research Institute Co., Ltd., Qingdao 266071, China
[d] State Key Laboratory of Coatings for Advanced Equipment, Qingdao 266071, China

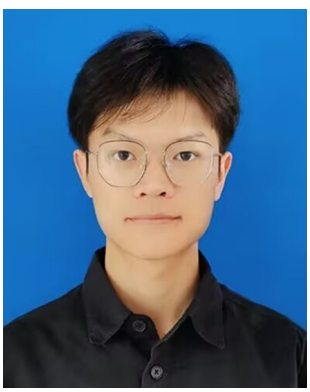

Yuxi Chen

Yuxi Chen is currently a postgraduate student at China University of Petroleum (East China). His research focuses on the control of hydrogen embrittlement in hydrogen transport pipelines.

© 2026 The Author(s). Co-published by the Institute of Process Engineering, Chinese Academy of Sciences and Royal Society of Chemistry

Open Access Article. Published on 14 May 2026. Downloaded on 6/5/2026 2:11:30 AM. This article is licensed under a Creative Commons Attribution-NonCommercial 3.0 Unported Licence.

and China's active planning of extensive long-distance hydrogen networks.[3–5]

However, implementing this strategy confronts critical material safety challenges. During transport, hydrogen atoms readily permeate into metallic materials, inducing degradation modes such as HE, hydrogen-induced cracking (HIC), and blistering. Decarburization and hydrogen attack may be triggered by high-temperature and high-pressure environments, thereby compromising pipeline integrity.[6] HE, in particular, has been identified as a fundamental bottleneck that hinders the advancement of hydrogen transport infrastructure. Experimental evidence demonstrates that typical pipeline steels suffer a 30–50% reduction in fracture toughness and significantly accelerated fatigue crack growth rates upon hydrogen exposure.[7,8] While various theoretical models—including Hydrogen Enhanced Decohesion (HEDE), Adsorption Induced Dislocation Emission (AIDE), and Hydrogen Enhanced Localized Plasticity (HELP)—have been proposed to elucidate these mechanisms,[9] there is a consensus that the fundamental mitigation strategy lies in effectively blocking hydrogen entry into the metal matrix.

The concept of Hydrogen Barrier Coatings (HBCs), introduced by Fowler *et al.* in the late 1970s,[10] offers a potent solution. By establishing physical or chemical barriers, HBCs can reduce hydrogen permeation flux by over 99%. Existing reviews have established a solid foundation for the material design, performance regulation, and permeation evaluation of HBCs. Based on hydrogen permeation mechanisms, Rönnebro *et al.*[11] reviewed gaseous and electrochemical permeation testing methods. However, this work primarily focused on the hydrogen isotope barrier performance and radiation tolerance of inorganic materials in nuclear irradiation environments. Conversely, Yuan *et al.*[3] emphasized the microstructural design of polymer-based composite barrier materials, analyzing the effects of structural parameters—such as free volume and crystallinity—on hydrogen barrier performance. Centering on permeation evaluation methodologies, Liu *et al.*[12] systematically discussed the influence of coating materials and fabrication methods on the permeation reduction factor (PRF). Furthermore, Akbari-Kharaji *et al.*[13] established an intrinsic correlation between deposition-induced coating defects and hydrogen permeation behaviors. Despite these significant advancements in material design and barrier performance evaluation, prior studies have predominantly been confined to singular permeation characterizations under ideal laboratory conditions. Such limited scopes are inadequate for evaluating the multidimensional service performance of coatings in practical engineering scenarios. Pipeline environments impose unique service constraints distinguishable from other fields: (1) extensive networks demand coatings with exceptional economic viability and the potential for wide-scale use; (2) the difficulty of maintaining hundreds of kilometers of buried pipelines necessitates extreme coating longevity; and (3) complex operating conditions—including pressure fluctuations, temperature gradients, and coupled mechanical stresses—challenge the overall structural integrity of the coating. While the report *Coatings and Liners for Hydrogen Service Pipelines* published by the CSA Group highlights the importance of pipeline coatings, existing standards like CSA Z662 and ASME B31.12 fail to address critical requirements. These include standardized test methods and acceptance criteria for HBCs about hydrogen barrier efficiency, embrittlement protection, and long-term durability.[14,15]

In light of these challenges, this review aims to establish a comprehensive, full-chain evaluation framework tailored for the industrial application of hydrogen transport pipelines. Beyond covering coating quality and hydrogen barrier efficiency, this framework innovatively incorporates the protective effect and adaptability to complex pipeline conditions into a unified evaluation system. By unifying

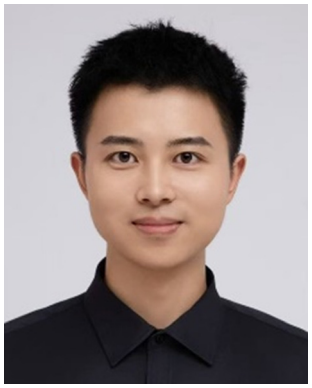

Cailin Wang

Cailin Wang is an Associate Professor and Master Supervisor at China University of Petroleum (East China). He received his B.S. and PhD in Oil and Gas Storage and Transportation from China University of Petroleum (East China). From 2019 to 2021, he conducted joint PhD research at the University of Leeds, UK. His research focuses on the storage and transportation of new energy, including hydrogen, CO_2, methanol, ammonia, etc. He is a Taishan Scholar Young Expert and was selected for the Young Talent Lifting Project by the China Association for Science and Technology (CAST).

Yuxing Li

Yuxing Li is a Professor and PhD supervisor at China University of Petroleum (East China). He received his PhD from China University of Petroleum (Beijing) and was a visiting scholar at the University of Tulsa, USA. As Chief Scientist of the National Key Research and Development Program, he focuses on transportation theory and safety for new energy (hydrogen, ammonia, methanol, CO_2) and oil/gas pipelines. He directs the National Virtual Simulation Experimental Teaching Center and the Shandong Provincial Key Laboratory for Oil, Gas and New Energy Storage and Transportation Safety.

© 2026 The Author(s). Co-published by the Institute of Process Engineering, Chinese Academy of Sciences and Royal Society of Chemistry

Open Access Article. Published on 14 May 2026. Downloaded on 6/5/2026 2:11:30 AM.
This article is licensed under a Creative Commons Attribution-NonCommercial 3.0 Unported Licence.

disparate performance indexes, this full-chain framework addresses the lack of evaluation methodological consistency in existing literature. The proposed framework provides theoretical guidance for the development of industrial standards and the large-scale deployment of HBCs. The logical structure and the weighted decision-making components of this full-chain evaluation framework are illustrated in Fig. 1.

The paper is organized as follows: section 2 systematically examines four dominant material systems (metal-based, ceramic-based, 2D materials, and polymer-based composites) with a focus on their intrinsic hydrogen resistance. Building upon a profound analysis of hydrogen permeation phenomena and embrittlement mechanisms, section 3 elucidates the fundamental hydrogen barrier mechanisms governing various coating systems. These include the physical/chemical barrier and trapping effects inherent in inorganic coatings, as well as the synergetic mechanisms identified within polymer-based composites. Section 4 summarizes current preparation methods, laying the groundwork for section 5, which proposes the novel full-chain evaluation framework. This framework encompasses preparation quality (density, adhesion, thickness), hydrogen barrier efficiency (hydrogen permeation rate, PRF), protective effect (HE resistance, fatigue resistance), and pipeline applicability (environmental coupling, coating–substrate interactions). Finally, section 6 evaluates the technological maturity and economic viability of current coating solutions within the hydrogen energy sector, while section 7 suggests targeted research directions for the future development and deployment of HBCs in service pipeline scenarios.

2 Classification system for HBCs

HBCs, serving as highly effective hydrogen permeation barriers, are widely applied in fields such as nuclear energy and hydrogen storage systems. Based on coating material types, they can be categorized into metal-based coatings, ceramic-based coatings, 2D material coatings, and polymer-based composite coatings, as shown in Fig. 2. To evaluate the hydrogen permeation barrier efficiency, researchers introduced the PRF (defined as the ratio of hydrogen permeation rates between the substrate material without coating and with coating). This metric quantitatively describes the coating's hydrogen barrier capability. Compared to other coatings, polymer-based composite coating systems offer promising technology for protecting hydrogen transportation infrastructure due to their excellent hydrogen barrier properties and comprehensive adaptability.

2.1 Metal-based coatings

Metal-based coatings are defined as functional layers predominantly consisting of metallic elements, which are fabricated on substrate surfaces *via* surface engineering methods such as deposition or diffusion coating. These coatings are characterized by a metallic bond-dominated continuous phase and a densely packed atomic arrangement. Their compositions include pure metals, alloys, intermetallic compounds, and metal-matrix composites. Based on primary constituent elements and structural features, metal-based HBCs can be classified into the following categories for detailed discussion: noble metal coatings, transition metal coatings, intermetallic compound coatings, and high-entropy alloy coatings.

2.1.1 Noble metal coatings. Noble metal coatings are fabricated from materials such as Au, Pt, Ag, and their alloys. These coatings exhibit extremely low hydrogen permeability, excellent chemical stability, and high resistance to elevated temperatures, making them essential for applications that require high barrier performance or extreme environmental tolerance. In a study by Noga,[16] a gold coating was applied

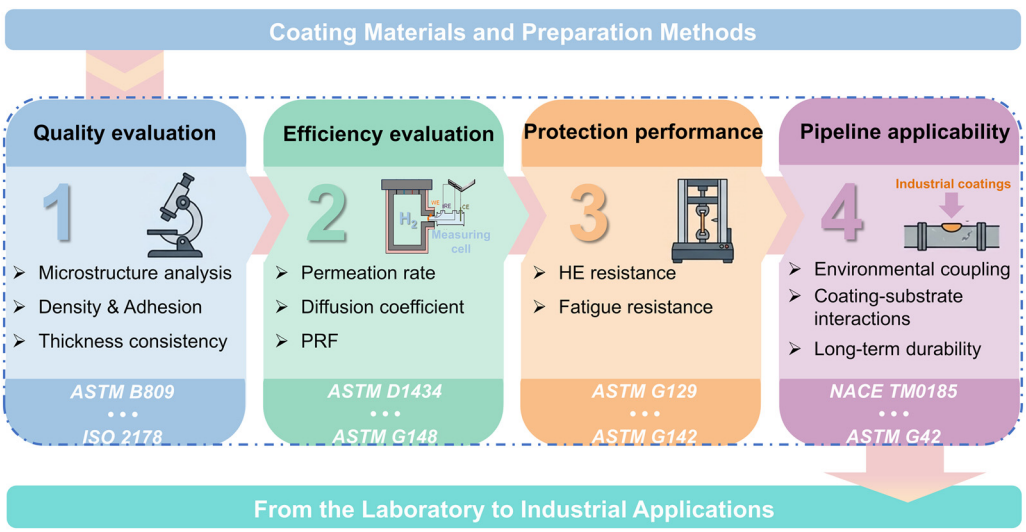

Fig. 1 Logic structure of the full-chain evaluation framework for HBCs in industrial pipelines.

© 2026 The Author(s). Co-published by the Institute of Process Engineering, Chinese Academy of Sciences and Royal Society of Chemistry

Open Access Article. Published on 14 May 2026. Downloaded on 6/5/2026 2:11:30 AM.
This article is licensed under a Creative Commons Attribution-NonCommercial 3.0 Unported Licence.

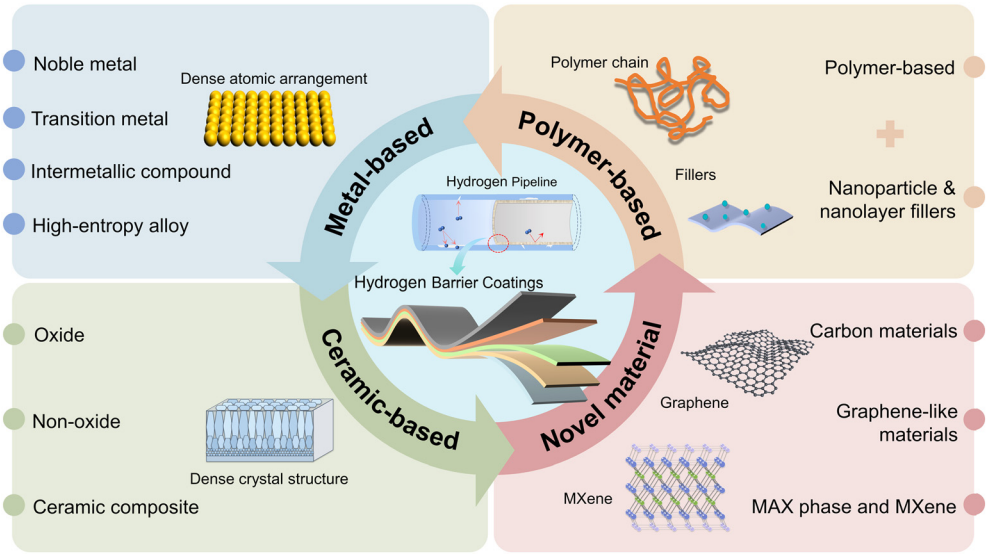

Fig. 2 Classification systems for HBCs.

via electrodeposition onto the pressure tube material of a CANDU-PHW nuclear reactor, which resulted in up to a 45-fold reduction in hydrogen absorption. The gold coating acts as a barrier by reducing hydrogen solubility, thereby lowering permeability. However, such coatings are associated with high cost, typically accounting for approximately 80% of material expenditures. Moreover, noble metal coatings such as Pt or Au often exhibit poor adhesion to steel substrates, necessitating the use of intermediate layers for improved bonding. These limitations increase the process complexity for large-scale applications and have restricted investigations into their use in long-distance hydrogen pipeline systems.

2.1.2 Transition metal coatings. The primary advantage of transition metal coatings as hydrogen barriers stems from the intrinsic properties of the constituent materials, such as nickel, chromium, and their alloys, which are characterized by low hydrogen solubility and low diffusion coefficients. However, in early studies, such coatings prepared by electroplating introduced a critical drawback: hydrogen was incorporated into the substrate during deposition, thereby counteracting the intended barrier function. As a result, electroplating is now seldom used for this purpose. Current research focuses on non-electroplating deposition technologies to avoid hydrogen incorporation. Further enhancement of hydrogen barrier performance is achieved through compositional modification (*e.g.*, alloying) and microstructural design, such as the formation of diffusion barriers or amorphous structures.

Early studies utilizing single-element transition metal layers indicated theoretical potential for hydrogen barrier applications. However, their practical effectiveness was significantly compromised by the presence of microdefects. In the work by Chalfoun,[17] high-purity tungsten layers were deposited onto F82H steel using magnetron sputtering. The resulting PRF values were found to vary widely, ranging from 3 to 4006. This study explicitly attributed the large dispersion in PRF values primarily to submicron-scale pinhole defects, rather than to coating thickness or substrate treatment processes. In contrast to single-element coatings, improved overall hydrogen barrier performance has been achieved in alloyed coatings, owing to synergistic effects between constituent elements. The limitations of single-element coatings were overcome by Samanta[18] through the deposition of an amorphous NiP (11.3 wt% P) alloy coating onto API X70 steel *via* electroless plating. Experimental results demonstrated that, compared with conventional electroplated nickel coatings, the nickel–phosphorus alloy significantly reduced the hydrogen permeation flux and exhibited superior corrosion resistance to chloride ions. These findings confirmed the advantages of alloying combined with an amorphous structural design. Furthermore, enhanced interdiffusion at the coating/substrate interface was promoted to form a gradient transition layer, which effectively alleviated thermal expansion mismatch and improved hydrogen barrier performance. In a related study, Meng *et al.*[19] deposited a Ni–Cr alloy onto X70 steel by magnetron sputtering, followed by an annealing process. This treatment resulted in a dual-layer mosaic structure consisting of an inner Fe–Ni solid solution layer and an outer Fe–Ni–Cr diffusion layer, with a maximum diffusion thickness of 2.6 μm. The structure enhanced the bonding strength with the substrate. Simultaneously, the Cr/Fe_xNi_y interfaces within this mosaic architecture served as physical hydrogen trapping sites, facilitated by stable bonding among Cr, Ni, and H atoms. Consequently, a substantial reduction in hydrogen permeability was achieved, yielding a PRF of 204.

2.1.3 Intermetallic compound coatings. Intermetallic compound coatings are primarily composed of iron–aluminum and other metallic compound systems. These coatings exhibit characteristics of both intermetallic compounds and certain properties of solid solutions. The

© 2026 The Author(s). Co-published by the Institute of Process Engineering, Chinese Academy of Sciences and Royal Society of Chemistry

Open Access Article. Published on 14 May 2026. Downloaded on 6/5/2026 2:11:30 AM. This article is licensed under a Creative Commons Attribution-NonCommercial 3.0 Unported Licence.

primary distinction from conventional alloy coatings lies in their hybrid bonding nature—comprising both metallic and partial covalent bonds—as well as their long-range ordered crystal structure. The formation of such coatings is based on the diffusion of introduced metallic elements into the substrate, followed by *in situ* reactions. Therefore, common preparation technologies are typically employed to enhance interdiffusion and reaction, such as hot-dip aluminizing, physical or chemical vapor deposition (PVD/CVD), and pack aluminizing.

Iron aluminides are the most widely used intermetallic compounds in hydrogen barrier applications and have been extensively studied since the 1930s.[11] These coatings are typically formed by controlling the diffusion of aluminum into the substrate metal, followed by *in situ* reactions, resulting in a gradient distribution of aluminum content across the thickness and providing excellent hydrogen barrier properties. However, inherent limitations such as insufficient thermal stability have severely restricted the practical application of iron–aluminum intermetallic coatings in high-temperature engineering environments compared to other metallic coatings. To address this challenge, research has mainly focused on two strategies: performance evaluation and material modification. In a study by Kalin *et al.*,[20] coatings containing $FeAl_3$, FeAl, and Fe_3Al phases were deposited onto austenitic stainless steel through a hot-dip aluminizing process. It was found that the hydrogen barrier performance of the coating was highly sensitive to the preparation temperature and time. For instance, a 10-micron coating prepared at 700 °C for 5 hours exhibited a PRF value of 2700, while the PRF decreased to 2000 when the temperature was reduced to 600 °C. An $FeAl/FeAl_3$ layer was achieved on 316 L stainless steel by Hollenberg[21] through aluminum diffusion, which exhibited a high PRF of 10 000. However, the hydrogen barrier performance was significantly degraded under irradiation conditions, further underscoring concerns regarding environmental stability. In light of these performance limitations, research efforts have been directed toward improving the comprehensive properties of iron–aluminum intermetallic coatings through elemental modification, particularly their resistance to high-temperature oxidation and hot corrosion.[22–25] A systematic investigation revealed that among single-element modifiers (such as Si, Cr, Co, Pt, Pd, and rare earth elements), Pt effectively promotes the selective oxidation of aluminum, leading to the formation of a dense and well-adhered Al_2O_3 protective layer, thereby markedly enhancing the high-temperature stability of the coating. Building on achievements in single-element modification, subsequent studies have extended to multi-element co-modification strategies, including binary, ternary, and higher-order systems incorporating elements such as Pt and rare earths. These approaches have been demonstrated to synergistically enhance the high-temperature oxidation and corrosion resistance of ferroaluminide coatings more effectively, offering a critical pathway for their application in severe engineering environments.

2.1.4 High-entropy alloy coatings. High-entropy alloy coatings effectively obstruct hydrogen permeation due to the high-entropy effect, wherein the interaction of multiple principal elements causes severe lattice distortion and sluggish diffusion. However, the multi-component nature of these coatings results in hydrogen barrier performance that is highly dependent on environmental conditions, requiring targeted optimization of elemental composition to achieve synergistic properties. This environmental dependency was demonstrated in a study by Hong *et al.*[26] AlCrFeMoTi coatings deposited *via* magnetron sputtering exhibited optimal hydrogen barrier performance (PRF = 63) in high-temperature gaseous hydrogen permeation tests. In contrast, AlCrFeTiNb coatings showed degraded performance due to excessive Fe content, which led to the formation of porous oxides. Conversely, in electrochemical hydrogen permeation tests simulating corrosive environments, the corrosion-resistant AlCrMoNbZr coating outperformed others, while AlCrFeMoTi coatings failed as a result of spallation. Based on a similar high-entropy concept, high-entropy oxides (HEOs) composed of optimized elemental combinations have been developed for extremely high-temperature applications. For instance, Hu *et al.*[27] fabricated a (TiVAlCrZr)O coating using five elements characterized by low thermal neutron cross-sections and high melting points. This coating achieved a PRF of 1608 at 500 °C, demonstrating exceptional hydrogen barrier performance and high-temperature stability. Therefore, through strategic selection and optimization of principal elements according to specific operational requirements, synergistic enhancement of hydrogen barrier performance alongside other functional properties can be realized.

2.2 Ceramic-based coatings

Ceramic-based coatings are functional layers fabricated on metal substrates using technologies such as plasma spraying or sol–gel processing. These coatings consist of inorganic non-metallic compounds as the matrix phase, bonded through ionic or covalent interactions. The hydrogen barrier property is primarily attributed to the inherently dense physical barrier provided by the ceramic phase, complemented by its chemical inertness and hydrogen trapping capability, which collectively hinder the permeation of hydrogen atoms. However, the high intrinsic brittleness of ceramics and the significant mismatch in thermal expansion coefficients between the coating and the metal substrate can readily lead to delamination, cracking, and spallation.[4] More critically, once cracks develop, corrosive media can penetrate rapidly, accelerating coating degradation. Therefore, refining the microstructure of ceramic-based coatings—for instance, by increasing density and optimizing grain boundary structure and properties—has become a major research direction for enhancing their hydrogen barrier performance

© 2026 The Author(s). Co-published by the Institute of Process Engineering, Chinese Academy of Sciences and Royal Society of Chemistry

Open Access Article. Published on 14 May 2026. Downloaded on 6/5/2026 2:11:30 AM.
This article is licensed under a Creative Commons Attribution-NonCommercial 3.0 Unported Licence.

and environmental durability. This approach also provides a foundation for further investigation into optimization strategies for various types of ceramic coatings.

2.2.1 Oxide coatings. Oxide coatings, as the earliest hydrogen barrier system to be systematically studied, are typically formed either by direct oxidation of the substrate or through *in situ* oxidation of the deposited layer. Their structure consists of a continuous matrix composed of metallic or non-metallic oxides. In comparison with intermetallic compound coatings, oxide coatings generally exhibit higher melting points and superior chemical stability. Under high-temperature conditions or in oxygen-containing atmospheres, a dense and adherent protective oxide layer is spontaneously formed on most reactive metals. Hydrogen permeation is effectively obstructed by this layer, owing to its inherently dense crystalline structure. Among various oxides, aluminum oxide (Al_2O_3), chromium oxide (Cr_2O_3), and zirconium oxide (ZrO_2) are considered the most widely applied and representative HBCs, due to their well-balanced comprehensive properties and substantial research background. Additionally, rare-earth oxides such as erbium oxide (Er_2O_3) and yttrium oxide (Y_2O_3) have also been investigated. However, the high cost of rare-earth elements like erbium and yttrium restricts their economic viability for large-scale applications.

Alumina (Al_2O_3) coatings are regarded as a central material in oxide coating research owing to their exceptional hydrogen barrier performance. The technologies for their preparation and application are well-established, including physical vapor deposition (PVD), chemical vapor deposition (CVD), sol–gel processes, plasma spraying (PS), hot-dip aluminizing (HDA), and pack cementation (PC).[28] Although alumina can exist in multiple crystalline phases, only the thermodynamically stable α phase exhibits outstanding hydrogen barrier properties, whereas other phases show significantly inferior performance. The α-Al_2O_3 phase is widely recognized for its exceptional resistance to hydrogen permeation, typically achieving PRF exceeding 1000. This high performance is attributed to the fact that hydrogen atoms encounter the greatest diffusion energy barrier at the first oxygen atomic layer on the α-Al_2O_3 surface.[29,30] The hydrogen barrier performance of alumina coatings is highly dependent on the preparation technology and temperature. Studies by Serra *et al.*[31,32] have shown that Al_2O_3 coatings fabricated on martensitic stainless steel through hot-dip aluminizing exhibit considerable variation in the PRF with temperature, decreasing to 260 at 743 K but reaching 1000 at 573 K. In contrast, coatings produced by magnetron sputtering demonstrate superior performance, with PRF up to four orders of magnitude higher. Feng *et al.*[33,34] reported a PRF of 1000 for Al_2O_3 coatings deposited on SS316 L stainless steel *via* plasma electrolytic oxidation. Despite their excellent hydrogen barrier properties, Al_2O_3 coatings face significant challenges. The large difference in thermal expansion coefficients between the coating and the metallic substrate renders the coating highly prone to cracking and delamination, both during fabrication and under service conditions involving severe thermal fluctuations. To mitigate thermal mismatch issues, Li *et al.*[35] successfully deposited a surface-dense, uniform, crack-free amorphous Al_2O_3 coating on SS316L using metal organic chemical vapor deposition (MOCVD). Although the hydrogen barrier performance of this amorphous coating was inferior to that of α-Al_2O_3—reducing hydrogen permeability by only 51–60 times at 860–960 K—this study illustrates that amorphization can effectively improve interfacial compatibility between the coating and substrate. This approach offers a promising strategy for mitigating thermally induced stress. In summary, α-Al_2O_3 coatings are recognized as one of the most effective hydrogen barrier oxide systems, exhibiting ultra-high resistance to hydrogen permeation (PRF $>$ 1000). Nevertheless, their practical application is still constrained by inherent brittleness and interfacial failure resulting from thermal mismatch. Therefore, investigating amorphous or other microstructural designs that alleviate thermal stress remains a crucial research direction for improving engineering applicability.

In comparison with alumina coatings, chromium oxide (Cr_2O_3) and zirconia (ZrO_2) coatings exhibit relatively inferior hydrogen barrier performance, which has led to a smaller number of related studies. Research on chromium oxide coatings has primarily focused on mitigating microdefects, such as micropores, introduced by conventional fabrication processes. These defects act as diffusion channels for hydrogen, substantially compromising the coating's barrier effectiveness. Terai *et al.*[36] utilized chemical densification technology (CDC) to fabricate Cr_2O_3 coatings on austenitic stainless steel, achieving a PRF greater than 100. However, this method inherently tends to generate surface pores, which restrict further improvement in performance. To overcome the porosity associated with CDC, Kulsartov *et al.*[37] introduced $CrPO_4$ as a pore-filling agent into the process, resulting in enhanced coating density and improved hydrogen barrier properties. In another study, Li *et al.*[38] deposited Cr_2O_3 coatings on 316L stainless steel using RF magnetron sputtering. This finding indicated that the hydrogen barrier performance is highly temperature-dependent: a PRF of 152 was achieved at 400 °C, but it decreased markedly to 48 at 700 °C. This degradation is attributed to the penetration of hydrogen atoms at elevated temperatures, which disrupts intergranular bonding within the Cr_2O_3 structure and promotes the formation of cracks and defects.

A common method for preparing zirconia coatings is through thermally induced oxidation, which generates an *in situ* ZrO_2 layer on zirconium or zirconium alloy surfaces to serve as a hydrogen barrier. Using micro-arc oxidation technology, Wang *et al.*[39] successfully fabricated a thick, multiphase ZrO_2 film on a zirconium hydride alloy substrate. The coating consisted of monoclinic (m-ZrO_2), tetragonal (t-ZrO_2), and minor cubic (c-ZrO_2) phases. This multi-phase zirconia coating demonstrated significantly

© 2026 The Author(s). Co-published by the Institute of Process Engineering, Chinese Academy of Sciences and Royal Society of Chemistry

Open Access Article. Published on 14 May 2026. Downloaded on 6/5/2026 2:11:30 AM. This article is licensed under a Creative Commons Attribution-NonCommercial 3.0 Unported Licence.

improved hydrogen barrier performance, achieving a PRF of 13.3, which indicates its potential for hydrogen inhibition applications. Nevertheless, the overall hydrogen barrier performance still requires further enhancement.

2.2.2 Non-oxide coatings. Non-oxide ceramic-based coatings mainly include silicides, nitrides, and carbides.

Silicide coatings are composed of covalent compounds formed between silicon and elements such as C and N, primarily SiC, Si_3N_4, and SiN. These coatings generally exhibit high wear resistance, exceptional hardness, strong corrosion resistance, and excellent high-temperature oxidation resistance, making them highly promising hydrogen barrier materials among non-oxide ceramic systems. During hydrogen diffusion within such coatings, hydrogen atoms readily form stable chemical bonds—such as C–H, N–H, and Si–H—with carbon, nitrogen, and silicon atoms. This results in the trapping of hydrogen atoms, which effectively block diffusion pathways. Amorphous SiN coatings with high hydrogen content have been shown to exhibit particularly high hydrogen barrier properties. Using radio-frequency magnetron sputtering, Nemanič *et al.*[40] prepared SiN coatings and demonstrated that films containing 6–7 at% trapped hydrogen achieved a PRF exceeding 2000 at a thickness of only 500 nm. This performance is significantly superior to that of hydrogen-free amorphous SiN structures, which exhibited a PRF of only 25. Wu *et al.*[41] evaluated the influence of SiC films deposited *via* magnetron sputtering at 473 K and 673 K on deuterium permeation behavior. The results demonstrated that the PRF was approximately 200 and 3, respectively. They attributed the significantly lower barrier performance at higher deposition temperatures to degraded film adhesion, which led to the formation of cracks and delamination. Additionally, the adhesion between the silicide coating and the steel substrate is generally weak. With increasing coating thickness, the risk of cracking and delamination due to accumulated internal stresses rises significantly.[41–45] Therefore, optimizing the coating microstructure at the atomic scale to enhance interfacial adhesion—thereby suppressing cracking and delamination—and developing more adaptable deposition processes constitute critical challenges that must be addressed to advance practical engineering applications.

Nitride and carbide coatings have been extensively investigated in the field of hydrogen barrier technologies. Among these, TiN and TiC have shown considerable promise as hydrogen permeation barriers.[46] Using magnetron sputtering, Liu *et al.*[47] deposited a dense CrN coating on X70 pipeline steel, which reduced the apparent hydrogen diffusion coefficient by a factor of 52.6 and the hydrogen permeation coefficient by 24.1. Studies by Matějíček *et al.*[48] suggest that nitrides such as CrN, WN, and ZrN are suitable for hydrogen barrier applications, with ZrN exhibiting particularly superior performance. Ohtsu[49] demonstrated that increasing the NbN concentration in NbN/Nb gradient layers—fabricated on niobium substrates *via* plasma nitrocarburizing—effectively suppresses hydrogen permeation, even for hydrogen-absorbing substrates. However, among the aforementioned non-oxide ceramic coatings, titanium-containing ceramic coatings, which are commonly employed, encounter significant challenges under high-temperature service conditions. TiC coatings are prone to defects such as pores and microcracks during deposition, which can act as rapid diffusion pathways for hydrogen and potentially increase permeation risks.[50] Furthermore, titanium-containing coatings undergo rapid and detrimental oxidation when exposed to temperatures above 450 °C, leading to marked degradation of hydrogen barrier performance and loss of structural integrity.[51]

2.2.3 Ceramic composite coatings. Single-layer ceramic coatings are limited in practical applications due to their inherent brittleness and inadequate adhesion to metallic substrates. As a result, ceramic composite coating systems have attracted extensive research attention. Through multilayer structural design and elemental doping, ceramic composite coatings can overcome the performance limitations of single-layer coatings, achieving enhanced adhesion and hydrogen barrier properties.[52,53] In multilayer structural design, Cr_2O_3 is widely adopted as the hydrogen barrier layer in composite coatings due to its favorable thermal expansion coefficient matching with the steel substrate.[54] Using MOCVD, He *et al.*[55] fabricated a Cr_2O_3/Al_2O_3 composite coating on 316L stainless steel comprising a 156 nm Cr_2O_3 inner layer and a 174 nm Al_2O_3 outer layer. Wu *et al.*[56] prepared a Cr_2O_3/Y_2O_3 composite coating with a 50 nm Cr_2O_3 inner layer and a 420 nm Y_2O_3 outer layer. At temperatures ranging from 823 to 973 K, the PRF of the Cr_2O_3/Al_2O_3 composite structure was 230–544, significantly outperforming single-layer Al_2O_3 and Cr_2O_3 coatings of equivalent thickness. Within the same temperature range, the PRF of the Cr_2O_3/Y_2O_3 composite structure was 167–477, while the PRF of the single-layer Y_2O_3 coating was only 96–292. These results indicate that multilayer ceramic coatings exhibit superior hydrogen barrier properties. Regarding elemental doping, Chen *et al.*[57] prepared La_2O_3/Y_2O_3-doped Cr_2O_3-based composite coatings *via* plasma spraying. They revealed that La_2O_3/Y_2O_3 synergistically modulates grain boundaries, oxygen vacancy defects, and lattice strain to optimize hydrogen capture and diffusion behavior in the Cr_2O_3-based coating.

2.3 2D nanomaterials and MAX/MXene phases

2.3.1 Carbon materials. Graphene (Gr), an allotrope of carbon, consists of a single layer of carbon atoms arranged in a hexagonal honeycomb lattice through sp^2 hybridization. As shown in Fig. 3a, as a typical two-dimensional material and the thinnest known substance, graphene exhibits outstanding impermeability despite its atomic-scale thickness. The dense lattice-structured electron cloud distribution provides strong barrier properties against various molecules, atoms, and ions, rendering it an exceptional impermeable material.[58] Graphene flakes with well-defined thin-film structures can be

© 2026 The Author(s). Co-published by the Institute of Process Engineering, Chinese Academy of Sciences and Royal Society of Chemistry

Open Access Article. Published on 14 May 2026. Downloaded on 6/5/2026 2:11:30 AM.
This article is licensed under a Creative Commons Attribution-NonCommercial 3.0 Unported Licence.

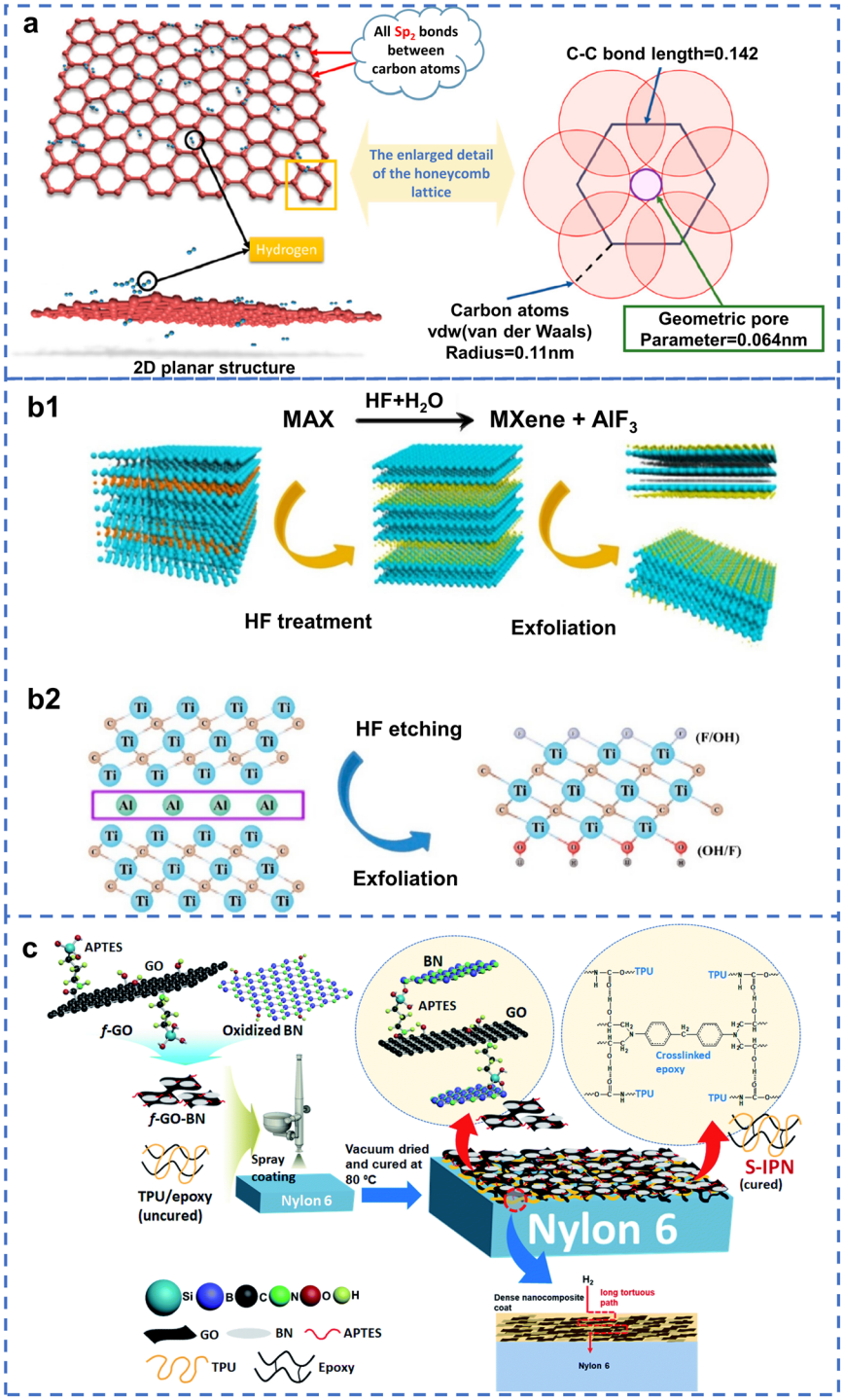

Fig. 3 (a) Hydrogen permeation through the hexagonal honeycomb lattice of graphene, highlighting a geometric pore size of 0.064 nm that renders it virtually impermeable to gas molecules. Reproduced with permission.[58] Copyright 2023, American Chemical Society; typical method for synthesizing MXene from MAX phases: (b1) selective etching of the A-layer (*e.g.*, Al) from the bulk MAX phase using hydrofluoric acid, followed by mechanical exfoliation to yield few- or single-layer MXene nanosheets, (b2) atomic-scale schematic of the structural transformation. Reproduced with permission.[71] Copyright 2025, Elsevier; (c) fabrication of the f-GO-BN reinforced TPU/EP semi-interpenetrating network (S-IPN) nanocomposite coating for hydrogen barrier applications. Reproduced with permission.[64] Copyright 2022, Royal Society of Chemistry.

directly formed on substrate surfaces using chemical vapor deposition.[59] Additionally, graphene—a representative two-dimensional nanomaterial characterized by a high aspect ratio and specific surface area—can significantly extend the permeation pathway of hydrogen when incorporated as a filler within other coating materials. As a result, it is widely utilized in composite systems combined with other matrices.[12] The most common application involves using

© 2026 The Author(s). Co-published by the Institute of Process Engineering, Chinese Academy of Sciences and Royal Society of Chemistry

Open Access Article. Published on 14 May 2026. Downloaded on 6/5/2026 2:11:30 AM.
This article is licensed under a Creative Commons Attribution-NonCommercial 3.0 Unported Licence.

graphene sheets as a hydrogen-barrier reinforcing phase in polymer matrices. However, due to the lack of functional groups, direct incorporation often leads to agglomeration, which impairs dispersion and limits the utilization of its inherent barrier properties as a two-dimensional sheet material. Therefore, graphene is usually modified prior to compositing with polymers to improve its dispersibility, as further discussed in section 2.4 on polymer-based composite coatings.

Graphene oxide (GO), similar to graphene, is a two-dimensional material characterized by a high aspect ratio and large specific surface area, and is frequently utilized in composite forms with other materials. A GO-Al_2O_3 composite coating was prepared by Yang *et al.*[60] *via* a sol–gel method. The introduction of GO was shown to increase the PRF by nine-fold compared to Al_2O_3 coatings. However, excessive addition of GO may reduce coating density, thereby compromising hydrogen barrier performance. Furthermore, GO contains abundant oxygen-containing functional groups, which provide improved compatibility with polymer matrices. Simple modification can effectively mitigate agglomeration and enhance dispersion within polymers, making GO more suitable than graphene as a functional filler for enhancing hydrogen barrier properties in polymer-based composite coatings. Wan *et al.*[61] chemically modified graphene oxide with polyethylene glycol diglycidyl ether (EGDE) to produce modified GO (mGO). A multilayer coating with an EP/mGO/EP sandwich structure was designed, in which the tightly stacked mGO interlayer extended the diffusion path for hydrogen permeation. Compared to a single-layer epoxy (EP) coating, this multilayer architecture achieved an 80% improvement in hydrogen barrier efficiency.

Diamond-like carbon (DLC) is primarily composed of amorphous carbon incorporating small amounts of diamond (sp^3 bonds) and graphite (sp^2 bonds) microcrystals. DLC coatings are characterized by high hardness, excellent wear resistance, and high electrical insulation, which make them suitable for a wide range of applications. However, the unique physicochemical properties of DLC lead to significant incompatibilities with most substrate materials. A typical challenge is the thermal expansion mismatch with metallic substrates, combined with weak interfacial chemical bonding. Direct deposition of DLC onto metals often generates high residual stresses, resulting in internal stress accumulation that can cause cracking or spallation. To address the poor adhesion at the DLC–metal interface, the introduction of a transition layer is commonly employed.

Tamura *et al.*[62] employed a 0.6 μm Cr–CrN buffer layer between a DLC coating and a 316L stainless steel substrate to improve adhesion. The results indicated that, compared to coatings without a buffer layer, the hydrogen permeability of the DLC coating with 20 at% hydrogen content was reduced by an order of magnitude. Specifically, hydrogen permeability decreased by more than 1000 times relative to the uncoated substrate. In a separate study, Garitano[63] used Cr as a continuous matrix phase on AISI 4130 low-carbon steel substrates, taking advantage of its high compatibility and ductility to alleviate thermal stresses. Tungsten carbide was introduced as a bridging layer to interface with DLC. The resulting DLC coating, with a thickness of 2500 nm and a hydrogen content of 20 at%, reduced the hydrogen diffusion rate by a factor of 22 and the permeability by a factor of 179. Both studies further indicated that the hydrogen barrier performance of DLC coatings is highly dependent on hydrogen content. Hydrogen atoms incorporated during deposition act as static obstacles, forcing subsequent hydrogen atoms to traverse longer paths or overcome higher energy barriers, thereby significantly extending the diffusion time and enhancing barrier properties. However, when the hydrogen content becomes excessive, the trapping sites approach saturation, which reduces trapping efficiency and degrades barrier performance. Although research on diamond-like carbon as a hydrogen permeation barrier remains limited, current findings underscore its significant potential for high-performance hydrogen barrier applications.

2.3.2 Graphene-like materials. Graphene-like two-dimensional materials, such as hexagonal boron nitride (h-BN), cubic boron nitride (c-BN), molybdenum disulfide (MoS_2), silicene, and germanene, exhibit physical properties reminiscent of those of graphene. These materials have been demonstrated to effectively suppress hydrogen permeability and enhance barrier performance against hydrogen diffusion to varying degrees, making them promising candidates for hydrogen barrier coating applications.

Currently, boron nitride is the most widely used material in hydrogen barrier applications, encompassing both cubic boron nitride (c-BN) and hexagonal boron nitride (h-BN), which are also two-dimensional layered nanomaterials. Owing to its exceptional thermal stability and electrical insulation properties, boron nitride has been widely investigated as a functional filler for enhancing hydrogen barrier performance.[64] Cubic boron nitride consists of atoms interconnected by sp^3 covalent bonds in a three-dimensional network, which contains no weakly bonded planes. This structure contributes to its outstanding hydrogen barrier characteristics. For instance, a 1 μm-thick c-BN coating deposited on a 0.5 μm SiC interlayer has been shown to reduce hydrogen permeability by two orders of magnitude.[65] However, the substantial difference in thermal expansion coefficient between c-BN and common substrates often leads to high interfacial stress. This stress can readily cause coating cracking, thereby necessitating the design of appropriate buffer layers. In hexagonal boron nitride (h-BN), interlayer bonding is governed by van der Waals forces. This structure permits hydrogen to diffuse readily through interlayer gaps or along weakly bonded grain boundaries. As a result, the hydrogen barrier performance of h-BN is highly influenced by the preparation process and crystal orientation. Checchetto *et al.*[66] utilized ion beam assisted deposition to synthesize h-BN coatings with (002) planes oriented perpendicular to the substrate. However, these coatings were

© 2026 The Author(s). Co-published by the Institute of Process Engineering, Chinese Academy of Sciences and Royal Society of Chemistry

Open Access Article. Published on 14 May 2026. Downloaded on 6/5/2026 2:11:30 AM. This article is licensed under a Creative Commons Attribution-NonCommercial 3.0 Unported Licence.

found to exhibit relatively high hydrogen permeability and unsatisfactory barrier performance. In contrast, h-BN coatings fabricated by magnetron sputtering demonstrated significantly improved hydrogen barrier properties. This difference arises because when the (002) plane of h-BN is aligned vertically, hydrogen diffusion is facilitated along the interlayer pathways within the (002) plane. In this configuration, hydrogen bypasses the high-energy barrier presented by the covalent boron–nitrogen planes, leading to reduced barrier effectiveness. Therefore, achieving low-stress interface design for c-BN and oriented crystal plane growth technologies for h-BN will be crucial for optimizing their hydrogen barrier properties.

2.3.3 MAX phase and MXene. MAX phases are a group of ternary ceramic compounds that combine the outstanding properties of ceramics and metals. They are composed of the following elements: M—transition metals (Sc, Ti, V, Cr, Zr, Cr, Nb, Mo); A—group A elements (primarily Al, Si, P, S, Ga, Ge, Pb); X—carbon or nitrogen. MAX phase ceramic materials, such as Cr_2AlC, Ti_2AlC, and TiAlN, have been investigated for applications such as hydrogen isotope barrier layers or nuclear cladding materials. Tang *et al.*[67] quantitatively evaluated the hydrogen barrier performance of Cr_2AlC and Ti_2AlC coatings deposited on Zr-4 alloy. It was confirmed that a MAX-phase coating with a thickness of only 5 μm provides hydrogen resistance equivalent to that of a 30 μm-thick ZrO_2 pre-oxidized layer, thereby significantly reducing the required coating thickness. Ling *et al.*[68] confirmed this finding through first-principles calculations. Theoretical calculations indicate that the Al atomic layer in Cr_2AlC forms a high diffusion energy barrier, forcing hydrogen to diffuse parallel to the atomic layer surface rather than penetrate vertically. Building upon the excellent hydrogen barrier properties of single-layer MAX phase coatings, attention has also been directed toward the development of multilayer or composite MAX phase coatings, which are expected to exhibit theoretically superior performance. A TiAlN/TiMoN multilayer coating was fabricated on AISI 316L stainless steel using arc ion plating by Tamura *et al.*[69] This structure reduced hydrogen permeability to one-thousandth of that of the uncoated substrate. Kim *et al.*[70] introduced a TiZrN-C composite coating prepared *via* laser carburization, through which a grain size reduction of 11% was achieved. The composite coating showed an 80% decrease in hydrogen permeability and maintained stable barrier performance at elevated temperatures (573–773 K). These results indicate that multilayer architecture and grain boundary engineering are effective strategies for enhancing the efficiency of HBCs.

MXene is a novel class of two-dimensional layered materials obtained by selectively etching the A-atom layer from MAX phases, resulting in transition metal carbides/nitrides.[71] It is generally represented by the chemical formula Mn + $1X_nTx$ (n = 1, 2, 3), where M stands for a transition metal (such as Ti, Cr, or Nb), X denotes carbon or nitrogen, and T represents functional groups. A typical synthesis route for MXene derived from MAX phases is illustrated in Fig. 3b. Similar to MAX phases, MXene exhibits a combination of metallic and ceramic properties. Owing to its layered structure and distinctive characteristics, MXene demonstrates broad potential for applications across multiple fields. A Ti_3C_2Tx coating was deposited on X70 pipeline steel *via* spin coating by Shi *et al.*,[72] which achieved a hydrogen permeability only one-third of that of the bare steel substrate. Further exploring the potential of MXene for hydrogen barriers, Auh *et al.*[73] developed a composite system incorporating two-dimensional MXene nanosheets with polymers. Through layer-by-layer (LBL) self-assembly driven by hydrogen bonding under acidic conditions, negatively charged MXene was combined with polyacrylic acid (PAA), forming a dense, pinhole-free multilayer barrier membrane. This membrane reduced hydrogen permeability by up to 9000 times compared to an uncoated niobium substrate.

2.4 Polymer-based composite coatings

Compared with the aforementioned metal- and ceramic-based coatings, polymer-based coatings generally exhibit higher hydrogen permeability coefficients due to the intrinsic free volume within their amorphous polymer chains. Nevertheless, for large-scale infrastructure such as long-distance pipelines, polymer-based coatings remain the most practically viable engineering solution owing to their superior flexibility, cost-effectiveness, and feasibility for *in situ* low-temperature application.

Industrially, polymer coatings such as polyethylene (PE), polyamide (PA), and epoxy resins (EP) are widely employed to protect against corrosion from moisture, CO_2, and H_2S.[74–76] While effective against the ingress of these larger gaseous molecules, pure polymer matrices theoretically struggle to completely impede hydrogen—which possesses the smallest molecular diameter—from diffusing through the free volume to reach the steel substrate.[77,78] Nevertheless, recent industrial-scale validation from the EUROPIPE project has demonstrated that specifically formulated epoxy-based coatings can provide sufficient hydrogen barrier protection even under 10 MPa pure hydrogen environments.[79] This finding substantiates the significant potential of epoxy resins as internal barrier coatings for hydrogen transport pipelines.

To overcome the intrinsic porosity caused by free volume and significantly enhance hydrogen resistance, current research focuses on composite modification strategies. A primary approach involves incorporating barrier fillers and constructing multi-level structures. These fillers mainly consist of 2D laminar materials (*e.g.*, graphene, MXene) or hydrogen-trapping nanoparticles (*e.g.*, Al_2O_3, SiC).[80–82] Mechanistically, these fillers densify the matrix by occupying free volume and retard hydrogen permeation by extending diffusion pathways or trapping hydrogen atoms. Cai *et al.*[81] incorporated graphene and silicon carbide (SiC) into an epoxy matrix, fabricating a "Gr-EP/SiC-EP/Gr-EP" sandwich

© 2026 The Author(s). Co-published by the Institute of Process Engineering, Chinese Academy of Sciences and Royal Society of Chemistry

Open Access Article. Published on 14 May 2026. Downloaded on 6/5/2026 2:11:30 AM. This article is licensed under a Creative Commons Attribution-NonCommercial 3.0 Unported Licence.

structure *via* spin coating. This design effectively combined barrier and trapping mechanisms, demonstrating superior hydrogen resistance. Similarly, Yuan *et al.*[83] designed a bilayer structure comprising a thermoplastic polyurethane (TPU) primer to block electrochemical corrosion pathways and a modified epoxy topcoat to enhance hydrogen barrier properties. Furthermore, Lei *et al.*[82] co-modified epoxy with montmorillonite (MMT) as a gas barrier agent and polyethylene glycol (PEG) as a toughening agent. This strategy simultaneously optimized gas impermeability and low-temperature mechanical properties, resolving the performance trade-offs typically associated with single-filler modifications.

However, the direct incorporation of 2D laminar fillers, such as graphene, into polymer matrices often leads to agglomeration. This results in the formation of micro-voids that serve as rapid hydrogen diffusion channels, thereby compromising the barrier performance of the composite coating.[84] Consequently, prior surface modification of fillers *via* covalent or non-covalent methods is a critical strategy to enhance their dispersion and compatibility within the polymer matrix. Common covalent modifiers include silane coupling agents, small amine molecules, and isocyanates. In contrast, non-covalent approaches—relying on electrostatic interactions, hydrogen bonding, or π–π stacking—offer high efficiency and operational simplicity while preserving the intrinsic chemical structure of the fillers.[83] Huang *et al.*[85] demonstrated that covalent modification of graphene oxide (GO) with 3-aminopropyltriethoxysilane (APTES) significantly improved its dispersion in zinc-rich epoxy resins. This modification increased the coating's PRF from 21.4 (unmodified) to 43.9. Given the advantages of modified fillers, Guo *et al.*[86] utilized silane-modified boron nitride (BN) as a barrier filler in epoxy resin. Their results indicated a 66.9% reduction in the hydrogen permeation coefficient and a two-order-of-magnitude increase in corrosion impedance compared to the neat epoxy coating. Building on these studies, Saha *et al.*[64] proposed an innovative strategy by dispersing APTES-crosslinked f-GO-BN hybrid nanosheets into a TPU/EP copolymer system (Fig. 3c). This design not only leveraged the synergistic barrier effect of the hybrid fillers but also utilized the semi-interpenetrating network formed by the flexible TPU segments and rigid epoxy chains to effectively prevent crack initiation and propagation within the coating.

In summary, although the aforementioned strategies of filler modification and structural design have significantly reduced hydrogen permeability and improved mechanical properties, the long-term barrier stability under complex coupled environments in long-distance pipelines (*e.g.*, high-pressure hydrogen, stress, and temperature fluctuations) remains to be fully explored. This gap represents a primary focus of the current review. Therefore, future research must prioritize the optimization of functional fillers and precise structural designs to achieve multi-functional integration and synergistic enhancement. Such advancements are essential to overcome the intrinsic limitations of polymers and meet the practical demands of hydrogen transport infrastructure.

2.5 Performance comparison of representative HBCs

The selection of fabrication and evaluation for HBCs depends on both coating and substrate materials, which determines the PRF of the coatings. Table 1 summarizes representative research findings across four material systems, explicitly demonstrating this material–process–performance correlation.

2.6 Controversies and challenges

While laboratory-scale evaluations have yielded promising results for diverse HBCs, their integration into large-scale industrial frameworks faces significant bottlenecks. These critical impediments are categorized into three primary areas:

(1) There is a core imbalance between achieving high barrier efficiency and meeting the economic demands of industrial scalability. The prevalent focus on maximizing PRF values in laboratory settings creates a 'performance-centric' bias, neglecting the practicalities of large-scale manufacturing. Taking ceramic-based coatings as an example, although they exhibit extremely high PRF under controlled laboratory conditions, their mainstream preparation methods suffer from disadvantages such as high equipment costs, complex processes, and low energy efficiency. For long-distance hydrogen transport pipelines, their industrial competitiveness in terms of life-cycle costs and construction feasibility is relatively weak. Consequently, future research must shift from the singular pursuit of extreme laboratory performance to a comprehensive, optimized design that balances operational stability, pipeline compatibility, and total life-cycle costs.

(2) A severe discrepancy exists between the ideal performance data obtained in the laboratory and the practical requirements of pipeline service scenarios. Laboratory evaluations typically rely on smooth, planar specimens under conditions devoid of external mechanical damage or environmental fluctuations. Under these idealized conditions, 2D nanomaterials can construct near-perfect lamellar barrier networks, thereby exhibiting exceptional hydrogen barrier properties. Nevertheless, in the actual service environments of long-distance hydrogen transport pipelines, complex factors—including cyclic loading, impurity gases, and cathodic protection—severely degrade the coatings' hydrogen barrier performance. Moreover, irregular pipeline geometries, such as complex curved surfaces and discontinuous weld zones, invariably subject the coatings to residual stresses. Consequently, it is imperative that coatings possess extraordinary toughness to withstand stress concentrations in these critical regions. This reality fundamentally explains why the industrial sector overwhelmingly prioritizes polymer-based coatings as the mainstream strategy in ongoing pilot projects for hydrogen-blended natural gas and pure hydrogen pipelines

© 2026 The Author(s). Co-published by the Institute of Process Engineering, Chinese Academy of Sciences and Royal Society of Chemistry

Open Access Article. Published on 14 May 2026. Downloaded on 6/5/2026 2:11:30 AM.
This article is licensed under a Creative Commons Attribution-NonCommercial 3.0 Unported Licence.

Table 1 Comparison of hydrogen barrier properties for typical coatings

	Materials	Substrates	Techniques	PRF	Test methods	Test temperature (°C)	Test pressure (kPa)	Thickness	Advantages	Disadvantages	Ref.
Metal-based	W	F82 H steel	Magnetron sputtering	3–4006	Gaseous hydrogen permeation tests	30/50/70	100	100/300 nm	With low hydrogen permeability, a high melting point, and excellent radiation resistance	Susceptible to defects, submicron-level pores cause PRF fluctuations	17
	Fe–Al	Austenitic stainless steel	Hot-dip aluminum	400–2700	Vacuum gaseous hydrogen permeation tests	High temperature	100	5/7/10/13 μm	Excellent hydrogen barrier properties and mature preparation process	Hydrogen barrier performance is significantly influenced by preparation temperature	20
	AlCrFeMoTi	CLF-1 steel	Magnetron sputtering	63	Vacuum gaseous hydrogen permeation tests	600	30	—	Excellent hydrogen barrier properties in high-temperature environments	Significantly affected by environmental conditions and not resistant to corrosion	26
Ceramic-based	Cr_2O_3	316L stainless steel	Radio frequency magnetron sputtering	48–152	Vacuum gaseous hydrogen permeation test	400–700	120	0.5 μm	High adhesion to the substrate, it can serve as a transition layer for composite coatings	Prone to forming microcracks, leading to severe degradation of hydrogen barrier performance	38
	ZrO_2	Zirconium hydride alloy	Micro-arc oxidation	13	Thermal desorption spectrometry test	600	Vacuum	110 μm	High adhesion to the substrate	Failure at 900 °C	39
	Al_2O_3	MANET steel	Hot-dip aluminum	260–1000	Vacuum gaseous hydrogen permeation test	300–500	100	About 200 μm	Mature preparation process and good hydrogen barrier properties	Significant difference in coefficient of thermal expansion from the substrate and prone to delamination	31
		MANET steel	Magnetron sputtering	~10 000		260–500	100	1.5 μm			32
		316L stainless steel	Plasma electrolytic oxidation	>1000		500/600/700	—	6 μm			33, 34
		316L stainless steel	MOCVD	51–60		587–687	100	1 μm			35
	Al_2O_3/Cr_2O_3	316L stainless steel	MOCVD	230–544	Vacuum gaseous hydrogen permeation test	550–700	100	330 nm	The chromium oxide layer enhances the adhesion between the aluminum oxide coating and the substrate	The preparation process readily generates high-valent chromium, which impairs the hydrogen barrier coating's properties	55

© 2026 The Author(s). Co-published by the Institute of Process Engineering, Chinese Academy of Sciences and Royal Society of Chemistry

Open Access Article. Published on 14 May 2026. Downloaded on 6/5/2026 2:11:30 AM.
This article is licensed under a Creative Commons Attribution-NonCommercial 3.0 Unported Licence.

Table 1 *(continued)*

	Materials	Substrates	Techniques	PRF	Test methods	Test temperature (°C)	Test pressure (kPa)	Thickness	Advantages	Disadvantages	Ref.
	SiN	Eurofer steel	Radio frequency magnetron sputtering	>2000	Vacuum gaseous hydrogen permeation test	400	100	712 nm	Excellent hydrogen barrier properties	Highly brittle, prone to cracking and flaking, demanding high surface quality of the substrate	40
	SiC	F82 H steel	Radio frequency magnetron sputtering	~1000	Vacuum gaseous hydrogen permeation test	450–550	80	1.5 μm	Well hydrogen barrier properties	Significant difference in coefficient of thermal expansion compared to steel substrates and prone to cracking	44
2D materials	TiAlN/TiMoN	316L stainless steel	Arc ion plating	~1000	Vacuum gaseous hydrogen permeation test	300	400	2.0–2.6 μm	Surface-dense and excellent hydrogen barrier properties	Hydrogen barrier performance degradation in high-temperature environments	69
Polymer-based	PEI/GO	PET	Layer-by-layer self-assembly	~17	Vacuum gaseous hydrogen permeation test	23	100	4.24 nm	Able to form an ordered, dense structure with excellent hydrogen barrier properties	Complex preparation process	87
	BN-AH/PTFE/EP	PET	Low-temperature curing film formation method	1.4	Vacuum gaseous hydrogen permeation test	25	100	141 μm	Easy to prepare	High-temperature hydrogen-blocking adaptability is unclear	86
	(Gr-EP)/(SiC-EP)/(Gr-EP)	316L stainless steel	Low-temperature curing film formation method	59	Electrochemical hydrogen permeation test	Room temperature	Atmospheric pressure	250 μm	No high-temperature preparation required, with good hydrogen barrier properties	Requires multiple coats and curing	81
	(APTES-GO)-Zn-EP	X80 steel	Low-temperature curing film formation method	33.5–43.9	Electrochemical hydrogen permeation test	Room temperature	Atmospheric pressure	72 μm	Enhanced hydrogen barrier properties without high-temperature preparation	High-temperature hydrogen-blocking adaptability is unclear	85

Note: since PRF values are based on different test methods and vary depending on test conditions, they cannot be directly compared across different tests.

© 2026 The Author(s). Co-published by the Institute of Process Engineering, Chinese Academy of Sciences and Royal Society of Chemistry

Open Access Article. Published on 14 May 2026. Downloaded on 6/5/2026 2:11:30 AM.
This article is licensed under a Creative Commons Attribution-NonCommercial 3.0 Unported Licence.

globally (*e.g.*, the EUROPIPE project), despite their inferior hydrogen barrier performance in laboratory tests. The core advantage lies in the capacity of polymer matrices to effectively tolerate pipeline deformations induced by geological settlement and mechanical impacts during construction. Ultimately, this robust adaptability to complex engineering environments offers substantially greater practical value than idealized barrier performance.

(3) Significant controversy persists regarding the evaluation frameworks for the long-term service stability of coatings. At present, the academic community predominantly relies on short-term dynamic hydrogen permeation tests—ranging from several hours to a few hundred hours—to predict coating performance. However, such methodologies are fundamentally inadequate for accurately reflecting the degradation behavior of coatings over a typical 30-year pipeline service lifespan. Under the coupled effects of hydrogen pressure fluctuations and corrosive environments, the physical aging and internal microstructural evolution of the coatings can lead to the deterioration of their hydrogen barrier performance. Consequently, future research should perhaps not be confined to developing static barriers that strictly pursue "high-efficiency hydrogen barrier", but rather transition towards dynamic defense strategies for long-term service, emphasizing "monitoring and healing". From this perspective, polymer-based composite coatings modified with functional fillers exhibit substantial advantages. The development of self-healing polymer composite coatings, integrated with intelligent in-pipe monitoring technologies, facilitates the establishment of an engineering protection system that permits trace hydrogen permeation while remaining controllable, monitorable, and repairable. Compared to the pursuit of prohibitively expensive and fragile "perfect" hydrogen barriers, this methodology aligns more comprehensively with the pragmatic demands of future energy infrastructure development.

3 Theoretical analysis of hydrogen barrier mechanisms

3.1 Hydrogen permeation and embrittlement mechanisms

The transport of high-pressure gaseous hydrogen is a core component of large-scale hydrogen storage and transportation systems, yet the hydrogen embrittlement (HE) of pipeline steels remains a primary obstacle to long-term operational safety. As the prerequisite for HE, hydrogen permeation initiates a deleterious interaction between hydrogen and the metallic matrix that macroscopically degrades mechanical performance. The transition from hydrogen permeation to material failure involves several critical stages: dissociative adsorption, atomic hydrogen ingress, lattice diffusion, localized accumulation at hydrogen traps, and ultimately, hydrogen-induced crack initiation and propagation.[88] These mechanisms establish the theoretical framework for the material selection, structural design, and performance optimization of HBCs.

3.1.1 Gaseous hydrogen permeation. Depending on the governing regime mechanisms, hydrogen permeation is primarily categorized into three distinct stages: solution, diffusion, and accumulation.

During the dissolution stage, hydrogen molecules dissociate into hydrogen atoms at the gas–solid interface *via* physisorption and chemisorption. These active hydrogen atoms gradually enter the steel and occupy interstitial sites within the surface lattice. This equilibrium process is governed by Sieverts' law, which states that the equilibrium solubility (C_H) is proportional to the square root of the hydrogen partial pressure (P_{H_2}):[89]

$$C_H = S\cdot\sqrt{P_{H_2}} \quad (1)$$

where C_H is the concentration of hydrogen atoms dissolved in the steel, S is the solubility coefficient, and P_{H_2} represents the hydrogen partial pressure. A higher hydrogen partial pressure increases the concentration of dissolved hydrogen, establishing a concentration gradient that drives hydrogen permeation into the material. Furthermore, factors such as temperature and interface conditions indirectly modulate solubility by affecting the efficiency of hydrogen adsorption and dissociation.

During the diffusion stage, hydrogen atoms that have entered the lattice migrate *via* interstitial jumping.[90] Influenced by concentration gradients, the diffusion of hydrogen atoms follows Fick's law:

$$\begin{cases} J = -D\nabla C_H \\ \dfrac{\partial C}{\partial t} = -D\nabla^2 C_H \end{cases} \quad (2)$$

where J is the hydrogen diffusion flux and D is the diffusion coefficient, which quantifies the effects of temperature and medium properties on diffusion. An increase in temperature significantly enhances the diffusion coefficient, thereby accelerating the hydrogen diffusion process.[89] In an ideal crystal, the resistance to diffusion primarily originates from the lattice potential barrier, and hydrogen atoms are expected to distribute uniformly throughout the crystal structure. However, in the presence of defects or stress fields, the concentration gradient no longer accurately describes the diffusion direction. In such cases, the diffusion behavior is dominated by the chemical potential gradient.

During the accumulation stage, diffusing hydrogen atoms are often captured by numerous hydrogen traps.[91] Pipeline steel is not an ideal material. It contains various microscopic defects, such as grain boundaries, dislocations, precipitates, and non-metallic inclusions.[92] These defects act as hydrogen traps, exerting a binding effect on diffusing hydrogen atoms through their binding energy (E_b). Based on the strength of this energy, hydrogen traps are classified into reversible traps ($E_b < 60$ kJ mol^{-1}) and irreversible traps ($E_b > 60$ kJ mol^{-1}).[88] Reversible traps have lower binding energies, allowing hydrogen atoms to escape easily and continue diffusing. In contrast, irreversible traps possess high binding energies that effectively capture hydrogen atoms, preventing their

© 2026 The Author(s). Co-published by the Institute of Process Engineering, Chinese Academy of Sciences and Royal Society of Chemistry

Open Access Article. Published on 14 May 2026. Downloaded on 6/5/2026 2:11:30 AM. This article is licensed under a Creative Commons Attribution-NonCommercial 3.0 Unported Licence.

accumulation in critical regions such as crack tips. The presence of these traps significantly alters hydrogen diffusion behaviour, leading to localized non-uniform accumulation.

3.1.2 HE mechanisms. When the local hydrogen concentration exceeds the critical hydrogen concentration of the material, the mechanical properties of pipeline steel deteriorate significantly, ultimately triggering HE failure. At present, the academic consensus recognizes four classic HE mechanisms: hydrogen pressure theory (HP), HEDE, HELP, and AIDE. However, under the complex service conditions of high-pressure pure hydrogen or hydrogen-blended natural gas pipelines, a single mechanism is often insufficient to fully elucidate the nature of macro-scale failure.

The HP is the only mechanism focused on the physical effects of molecular hydrogen. This theory posits that hydrogen atoms accumulated at material defects tend to recombine into hydrogen molecules. Large quantities of gathered hydrogen molecules cannot diffuse through the metal lattice, thereby generating extremely high internal pressure within closed cavities. When the stress exerted by this hydrogen pressure on microvoids exceeds the local tensile strength of the material, cracks initiate and propagate. Although the HP effectively explains the hydrogen blistering phenomenon under supersaturated hydrogen permeation during cathodic protection, it fails to account for the sudden brittle fracture of high-strength steel systems under low hydrogen partial pressure. Consequently, researchers have shifted their focus toward the interactions between atomic hydrogen and the material's microstructure. The HEDE focuses on the influence of interstitial hydrogen on the atomic lattice and microstructural interfaces. According to this theory, hydrogen atoms segregated at the crack tip reduce lattice cohesion strength by interfering with the d-orbital overlap between metal atoms, causing the material to undergo brittle fracture along grain boundaries or cleavage planes even under low stress.[93] This is the primary explanation for sudden brittle fracture in high-strength steel. The HELP focuses on the impact of hydrogen on dislocation mobility.[12,94] It posits that the segregation of interstitial hydrogen atoms within the dislocation stress field creates an elastic shielding effect, which reduces the local resistance to dislocation slip. This effect significantly promotes dislocation emission and multiplication, inducing the premature nucleation and coalescence of microvoids at grain or phase boundaries. Consequently, the characteristic phenomenon of "microscopic enhanced plasticity and macroscopic brittle fracture" is observed. Regarding the AIDE, hydrogen atoms at free surfaces or crack tips are focused upon. This theory incorporates both the decohesion concept from HEDE and the dislocation promotion from HELP. According to the AIDE, atomic bonding at the crack tip is weakened by adsorbed hydrogen, which significantly reduces the critical stress required for dislocation nucleation and emission. A large number of directionally emitted dislocations are then induced to form slip steps, directly driving the crack growth at extremely low plastic strains.

In fact, extensive research has been conducted to clarify whether hydrogen-enhanced decohesion or enhanced localized plasticity dominates.[9,95] However, it is increasingly evident that the validity of each mechanism, or their synergetic effects, depends on the specific hydrogen concentration and microstructural conditions. For coating–substrate systems, the complexity of the overall embrittlement mechanism is further intensified by potential film-induced brittleness.[96,97] Therefore, when HBCs are introduced to pipeline steel, the evolution of HE must be analyzed by considering the coating and the substrate as an integrated system.

3.2 Hydrogen barrier mechanisms

The hydrogen permeability is determined by both the diffusion coefficient and the hydrogen solubility. Although the diffusion coefficient is the dominant factor governing hydrogen permeability, solubility also influences the achievement of low permeation rates.[98] In inorganic materials, hydrogen dissolves and diffuses in atomic form. The hydrogen barrier effect of coatings is manifested through three primary mechanisms: first, the barrier against external hydrogen involves the dissociation and adsorption of hydrogen molecules on the coating surface, a process that determines the concentration of hydrogen atoms entering the coating. Second, the microstructure of the coating imposes diffusion resistance on hydrogen atoms within the material, governing their mobility. Finally, the physical and chemical trapping capabilities of the coating reduce the concentration of freely diffusing hydrogen atoms. In contrast, hydrogen diffusion in organic polymers occurs mainly in molecular form. The hydrogen barrier mechanism in polymers relies on the synergistic effect between the polymer matrix and incorporated fillers.

3.2.1 Physical barrier mechanism. The physical barrier mechanism is considered the most fundamental and prevalent approach for HBCs. As show in Fig. 4a, this mechanism primarily relies on the construction of a dense barrier that reduces hydrogen solubility, thereby isolating the substrate from high hydrogen concentrations in the service environment and providing a physical blocking function. On a macroscopic level, nearly all coatings exhibit a certain degree of physical barrier effect, which is highly influenced by coating thickness. Generally, the barrier performance improves with increasing thickness until a critical threshold is reached. Beyond this point, excessively thick coatings are prone to cracking and microcrack formation or even delamination under practical service conditions, compromising both structural integrity and hydrogen resistance. From a microscopic perspective, a dense crystalline structure and low porosity are crucial for an effective physical barrier. These characteristics minimize pathways for hydrogen dissolution and diffusion, ultimately becoming the dominant factors in hydrogen resistance, overshadowing the effect of thickness. For instance, Gilbert

© 2026 The Author(s). Co-published by the Institute of Process Engineering, Chinese Academy of Sciences and Royal Society of Chemistry

Open Access Article. Published on 14 May 2026. Downloaded on 6/5/2026 2:11:30 AM.
This article is licensed under a Creative Commons Attribution-NonCommercial 3.0 Unported Licence.

et al.[99] demonstrated that a relatively thin iron aluminide layer on 316L stainless steel provided superior hydrogen barrier performance. This was attributed to the facilitated oxidation of aluminum within the thin layer, resulting in the formation of a dense Al_2O_3 layer with a compact microstructure. Among various coating systems, metal-based coatings, ceramic-based coatings, and novel two-dimensional materials have been shown to exhibit prominent physical barrier effects.

Metal-based coatings function as hydrogen permeation barriers primarily due to the lower hydrogen solubility of their constituent phases compared to iron-based substrates. The dense atomic arrangement and strong metallic bonding within the coating significantly hinder hydrogen dissolution and penetration at the atomic scale. This effectively prevents the ingress of hydrogen atoms from the service environment, maintaining minimal hydrogen concentration at the coating/substrate interface. As a result, even if limited hydrogen diffusion occurs at this interface, the low hydrogen concentration generates insufficient thermodynamic driving force to support further penetration into the substrate.

Ceramic coatings primarily function as hydrogen barriers through their dense crystalline structures acting as physical barriers.[47,97] However, the effectiveness of this barrier mechanism is highly dependent on the integrity of the microstructure,[31–34,100] making it challenging to achieve and maintain a fully dense and defect-free morphology. Defects such as microcracks and pores, often introduced during fabrication, can act as preferential diffusion pathways for hydrogen atoms, significantly compromising the barrier performance.

The inherent hydrogen barrier properties of novel 2D layered materials exhibit significant physical barrier effects at the microscopic level. However, defects inevitably introduced during large-scale manufacturing and application compromise the advantages of these intrinsic properties. To effectively harness the physical barrier characteristics of 2D layered materials, layered stacking structures are commonly employed. Such stacking configurations reduce hydrogen permeation sites, lengthen hydrogen permeation pathways, and significantly increase diffusion resistance for hydrogen atoms. Graphene layer stacking has been demonstrated to exhibit a remarkably strong physical barrier effect.[101]

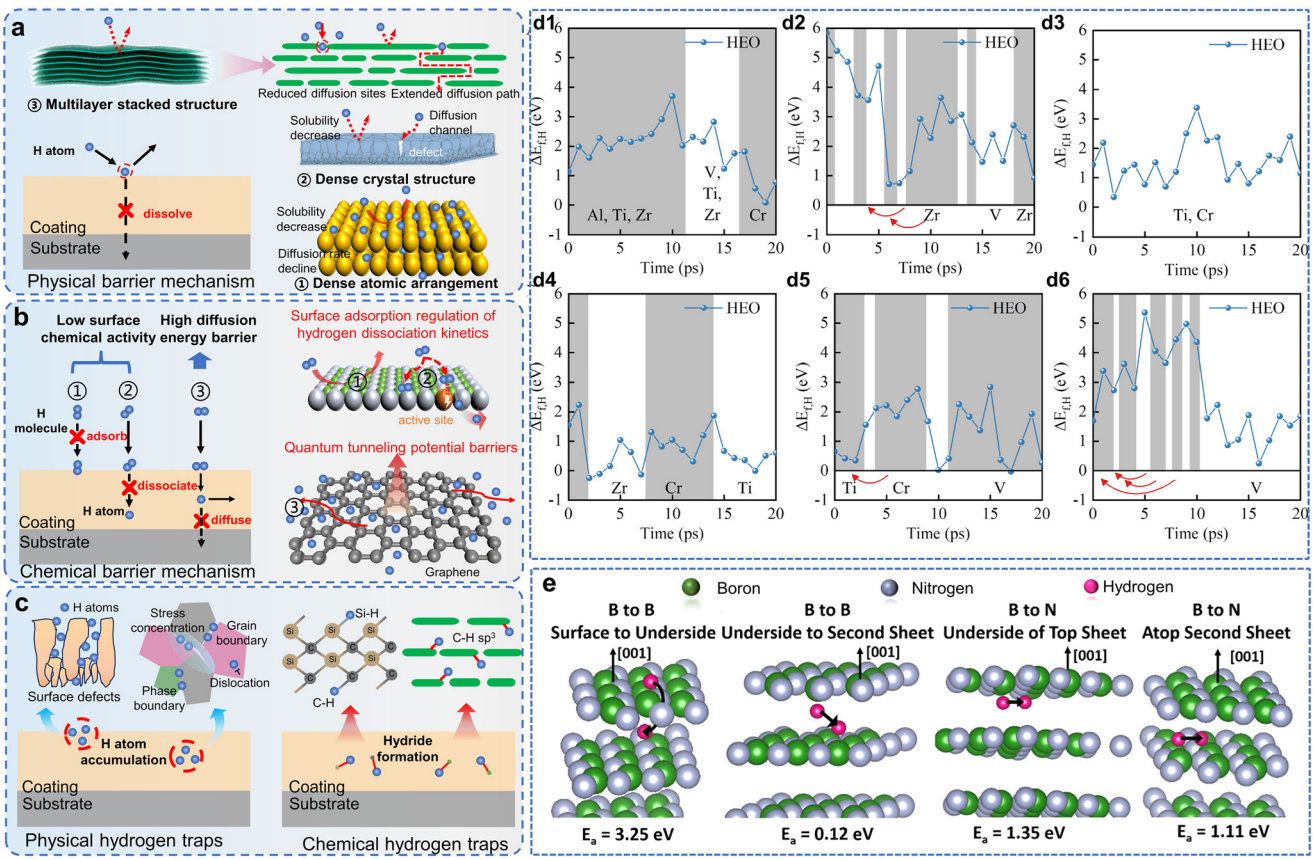

Fig. 4 Schematic diagrams of (a) the physical barrier mechanism, (b) the chemical barrier mechanism, and (c) the trap capture mechanism; (d1–d6) rugged energy barrier diagram for H diffusion in high-entropy metal oxides. Each shaded or white region represents the residence time of H. Return-jump events are marked with red arrows. If hydrogen atoms linger in the vicinity for a longer period, the element name is labelled. Reproduced with permission.[27] Copyright 2022, Elsevier; (e) diffusion pathways of hydrogen atoms between h-BN layers and required activation energy for diffusion. The activation energies required for the four diffusion paths are 3.25, 0.12, 1.35, and 1.11 eV, respectively. Reproduced with permission.[111] Copyright 2021, Elsevier.

© 2026 The Author(s). Co-published by the Institute of Process Engineering, Chinese Academy of Sciences and Royal Society of Chemistry

Open Access Article. Published on 14 May 2026. Downloaded on 6/5/2026 2:11:30 AM. This article is licensed under a Creative Commons Attribution-NonCommercial 3.0 Unported Licence.

Consequently, multilayer stacked structures represent a key design approach for translating the inherent hydrogen barrier properties of two-dimensional layered materials into a feasible and effective macroscopic physical hydrogen barrier.

3.2.2 Chemical barrier mechanism. The chemical barrier mechanism, as shown in Fig. 4b, regulates hydrogen dissociation kinetics through surface chemical adsorption on the one hand, while reducing hydrogen diffusion rates based on the high hydrogen diffusion energy barrier within the hydrogen barrier material on the other. The coating's low surface chemical activity suppresses hydrogen dissociation adsorption, forming the first line of defense in chemical barrier protection. Previous studies have demonstrated that hydrogen atoms entering pipeline steel and causing HIC originate from the dissociative adsorption of hydrogen gas on surfaces.[88,102–107] During dissociative adsorption, hydrogen gas exhibits a high theoretical dissociation energy of 4.48 eV. Physical adsorption primarily involves weak van der Waals interactions, which do not alter the electronic structure of hydrogen gas and thus contribute minimally to the dissociative adsorption process. Chemisorption significantly reduces the dissociation barrier for hydrogen molecules due to strong interactions between hydrogen and the surface, facilitated by active sites.[9] Surfaces like ceramic coatings lack active sites that promote hydrogen dissociation adsorption and exhibit chemical inertness, making it difficult for most hydrogen gas to dissociate into hydrogen atoms. Therefore, reducing active sites on the substrate surface to increase the dissociation adsorption resistance of hydrogen molecules is an effective method for blocking hydrogen permeation. Sun *et al.*[108] demonstrated that hydrogen exhibits higher adsorption energy on Al_2O_3 surfaces than on iron surfaces, inhibiting the dissociative adsorption process. However, this surface chemical hydrogen barrier is also susceptible to defects. They noted that hydrogen exhibits more negative adsorption energies at surface defects, promoting dissociative adsorption and leading to localized hydrogen enrichment. When defects reach critical sizes or densities, they become preferential diffusion pathways for hydrogen atoms.

The high diffusion energy barrier within the coating serves as the second line of defense for chemical barrier protection. For common crystalline materials, the hydrogen diffusion coefficient primarily depends on the energy barrier it must overcome when hopping between interstitial sites within the lattice. Crystalline structures with high density exhibit significantly higher diffusion energy barriers. First-principles calculations by He *et al.*[109] indicate that the diffusion barrier in closely packed face-centered cubic (FCC) or hexagonal close-packed (HCP) structures is approximately eight times that of body-centered cubic (BCC) structures. This elevated barrier effectively reduces the hydrogen diffusion coefficient. Additionally, elements within the material that exhibit higher hydrogen binding energies can significantly increase the hydrogen diffusion barrier. First-principles calculations were conducted by Ling *et al.*[68] to investigate hydrogen diffusion in Cr_2AlC, a typical MAX-phase material. The activation energy for hydrogen diffusion at the Al atomic layer was found to be as low as 0.312 eV. However, a higher diffusion barrier of 1.59 eV was observed at the same layer, indicating strong resistance to hydrogen permeation. High-entropy materials exhibit uniquely rugged energy barriers due to element-specific barrier differences and the broad barrier distribution induced by chemical disorder.[27] As a result, hydrogen diffusion strongly depends on its initial position and surrounding elements. As shown in Fig. 4d1–d6, hydrogen frequently traverses elemental sites with different energy barriers, resulting in irregular diffusion paths. At local energy minima, hydrogen atoms exhibit significantly prolonged residence times (Fig. 4d1 and d2) and demonstrate a "back-jumping" phenomenon (Fig. 4d2, d5 and d6). This rugged energy barrier achieves kinetic suppression of hydrogen diffusion.

For materials such as graphene, scholars have proposed the concept of quantum tunneling potential barriers,[110] attributed to their unique sp^2 hybridized bonds. This represents a quantum-scale repulsive effect exerted by nanoscale tunnels on hydrogen atoms, quantifiable *via* eqn (3).

$$Q = e^{\frac{-2x\sqrt{2m(V-E)}}{h}} \tag{3}$$

where Q is the tunneling potential barrier, dimensionless; x is the barrier width, m; m is the mass of the tunneling hydrogen atom, kg; V is the barrier height, J; E is the kinetic energy of the tunneling hydrogen atom, J; h is the reduced Planck constant, 1.054×10^{-34} J s.

However, for nanoscale two-dimensional layered materials, the differences in energy barriers exhibited by distinct diffusion pathways significantly influence the effectiveness of chemical barriers. Theoretical calculations by Bull *et al.*[111] on the activation energies required for hydrogen atoms along four different diffusion pathways within h-BN layers provide compelling evidence for this. As shown in Fig. 4e, among the four diffusion pathways, the energy barrier for hydrogen atoms traversing the h-BN layer from the adsorption site on surface B atoms is the highest, reaching 3.25 eV. In contrast, the energy barrier for hydrogen atoms diffusing between B atom sites is only 0.12 eV. This disparity indicates that hydrogen atoms preferentially diffuse parallel to the layer surface rather than traversing it vertically. Therefore, the orientation of the layers relative to the hydrogen diffusion direction becomes a critical preparation parameter. To maximize the hydrogen barrier advantage of two-dimensional layered materials, their alignment orientation must be optimized, employing a layer-by-layer stacking approach to extend the hydrogen diffusion path.

3.2.3 Trap capture mechanism. As shown in Fig. 4c, the trap capture mechanism effectively suppresses hydrogen permeation by capturing and storing diffusing hydrogen atoms through various physical or chemical hydrogen traps.

Physical hydrogen traps primarily consist of microstructural defects within materials and the stress fields

© 2026 The Author(s). Co-published by the Institute of Process Engineering, Chinese Academy of Sciences and Royal Society of Chemistry

Open Access Article. Published on 14 May 2026. Downloaded on 6/5/2026 2:11:30 AM.
This article is licensed under a Creative Commons Attribution-NonCommercial 3.0 Unported Licence.

generated around them. Defects such as vacancies (point defects), dislocations (line defects), and grain boundaries (plane defects), along with the stress concentration zones formed around them, serve as preferred sites for hydrogen atom accumulation.[9] Research indicates that lattice distortions in high-entropy alloys can also generate non-uniform stress fields that trap hydrogen atoms.[112,113] Furthermore, while surface microdefects can also function as physical hydrogen traps to capture small amounts of hydrogen atoms, their storage capacity is relatively weak. When defects reach a critical size, hydrogen atoms preferentially diffuse through surface defects instead, reducing the hydrogen barrier performance of the coating. During hydrogen permeation and diffusion, a fraction of hydrogen atoms is initially captured by surface microdefects, while the remaining unbound hydrogen atoms diffuse inward either through surface defects or directly. Subsequently, numerous microstructural defects within the coating—including vacancies, dislocations, and grain boundaries—along with the surrounding stress fields, efficiently capture and store large quantities of hydrogen atoms. This process significantly reduces the concentration of free hydrogen atoms capable of diffusing to the coating/substrate interface, constituting the key mechanism of the physical hydrogen trapping effect. To address the issue that excessive large surface defects may promote hydrogen permeation, surface treatments such as shot peening can be employed to introduce high-density nanoscale microdefects. This enhances surface hydrogen trapping capacity and restricts the initial hydrogen permeation process. Li *et al.*,[114] Huang *et al.*,[115] and Otsuka *et al.*[116] have confirmed the significant role of shot peening in suppressing hydrogen permeation and reducing HE susceptibility. Furthermore, from the perspective of internal hydrogen traps within materials, refining grain size to increase grain boundary density, thereby boosting the number of hydrogen traps and expanding physical hydrogen storage space, may also serve as a key strategy to enhance the physical hydrogen trapping effect.

Chemical hydrogen traps rely on strong chemical bonding interactions between materials and hydrogen atoms to immobilize hydrogen. For example, atoms such as Cr and Ni in metallic materials can form stable bonds with hydrogen atoms, creating hydrogen trap sites.[19] Among non-oxide ceramic materials, substances such as SiC and SiN contain a large number of unsaturated Si-bonds, C-bonds, and N-bonds in their structures. These bonds can form strong chemical bonds with hydrogen atoms, requiring high energy to break, thereby firmly trapping hydrogen atoms.[45] For oxide materials, Li *et al.*[107] demonstrated through density functional theory calculations that hydrogen possesses a more negative adsorption energy on the Fe_2O_3 surface than on the iron surface. While this promotes dissociative adsorption of hydrogen and generates permeating hydrogen atoms, the hydrogen atoms can also be tightly captured by newly formed O–H bonds. Additionally, molecular dynamics studies by Shi *et al.*[101] revealed that unsaturated carbon bonds in graphene can form sp^3-hybridized bonds with hydrogen, creating effective binding interactions. Thus, by forming stable chemical bonds, chemical hydrogen traps provide hydrogen atoms with capture sites that are difficult to escape. Capture efficiency typically depends on the bond energy of the relevant chemical bond; the higher the bond energy, the stronger the capture ability for hydrogen atoms. Bond energy data for selected chemical bonds are presented in the table below (Table 2).

3.2.4 Composite synergistic mechanism. As shown in Fig. 5, the composite synergistic mechanism achieves excellent hydrogen barrier performance through the synergistic interaction between the polymer matrix and inorganic fillers.

The hydrogen barrier mechanism of pure polymers is based on solution-diffusion, differing from that of inorganic material coatings. The core of this mechanism involves gas molecules first dissolving on the organic coating surface, then diffusing through the coating, and finally desorbing on the opposite side.[117] Throughout this process, the chemical properties and microstructure of the polymer itself (such as free volume, crystallinity, *etc.*[3]) jointly determine the solubility and diffusion coefficient of gas molecules within it.

Zheng *et al.*[118] investigated the diffusion behavior of hydrogen molecules in polyethylene (PE) materials. The results revealed that hydrogen diffusion in PE follows a "jumping" mechanism. Initially, hydrogen molecules undergo prolonged, small-amplitude vibrations within voids created by free volume. Subsequently, the molecules rapidly leap to adjacent new voids, exhibiting large-amplitude "jumps". After completing a jump, the molecules resume small-amplitude vibrations while awaiting the next jump. Through repeated cycles of vibration and jumping, hydrogen molecules eventually migrate far from their initial positions and permeate the PE material. Zhao *et al.*[119] employed molecular dynamics simulations to analyze the crystallization process of PE materials with different chain structures. Results indicated that the presence of side chains hindered crystallization behavior, leading to reduced crystallinity and increased hydrogen solubility in the material. Further analysis revealed that the key factor influencing solubility was side chain density, while the effect of side chain length was negligible. Zhao *et al.* proposed that side chains increase the free volume within PE materials, thereby promoting hydrogen diffusion at the glass transition temperature. A higher number of side chains (greater density) result in poorer hydrogen barrier properties of the material.[120] Kanesugi *et al.*[121] investigated the hydrogen permeation characteristics of low-density polyethylene (PE-LD), high-density polyethylene (PE-HD), and polyamide 11 (PA11),

Table 2 Bond energies of different chemical bonds (kJ mol^{-1})

Si–H	C–H	N–H	O–H
318	411	386	459

© 2026 The Author(s). Co-published by the Institute of Process Engineering, Chinese Academy of Sciences and Royal Society of Chemistry

Open Access Article. Published on 14 May 2026. Downloaded on 6/5/2026 2:11:30 AM.
This article is licensed under a Creative Commons Attribution-NonCommercial 3.0 Unported Licence.

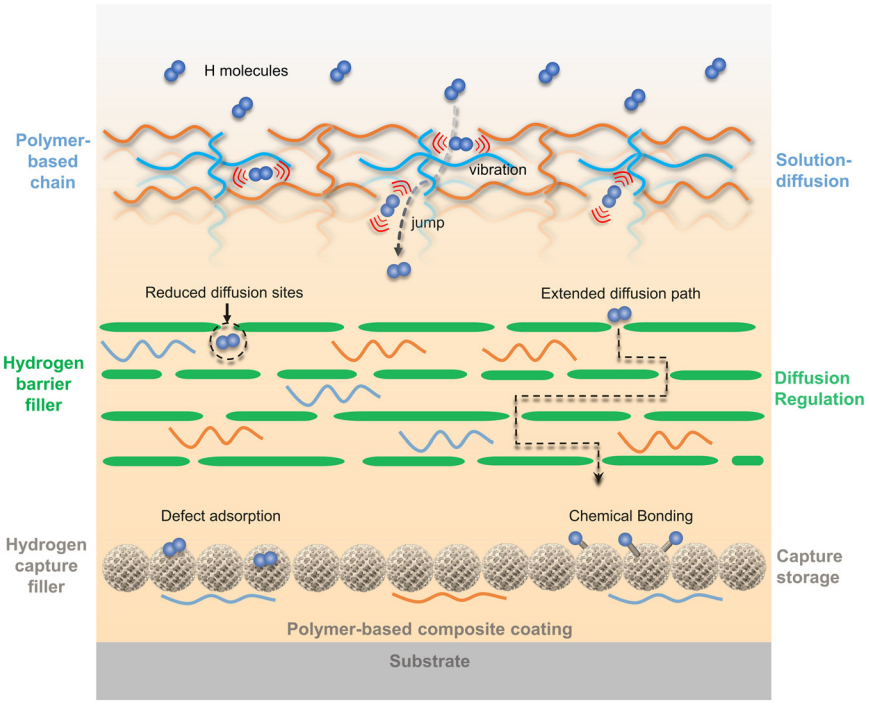

Fig. 5 Schematic diagram of the polymer composite synergistic hydrogen barrier mechanism. Hydrogen molecules vibrate and jump between organic molecular chains and diffuse into the polymer matrix. The green region represents ideally arranged two-dimensional layered fillers, which effectively reduce diffusion sites and extend the diffusion path. The gray balls represent nanoceramic particles, which further capture hydrogen diffusing toward the substrate.

reaching the same conclusion. Jung *et al.*[122,123] measured the permeability parameters of rubber materials with varying densities after exposure to hydrogen-containing environments. They observed that both hydrogen permeability and diffusion rate decreased with increasing density. These findings collectively demonstrate that, under identical conditions, polymer materials with higher density exhibit superior hydrogen barrier properties.

When fillers are incorporated into a polymer matrix, the gas barrier performance of the polymer is markedly improved. Macro-scale effects include the fillers effectively compressing the free volume within the polymer, forming a dense physical structure that increases the tortuosity of gas permeation pathways. This reduces the concentration of hydrogen molecules entering the polymer *via* solution-diffusion mechanisms. At the microscopic level, the targeted orientation of fillers maximizes their hydrogen-blocking effects. This is achieved through two approaches: (1) parallel alignment of two-dimensional layered hydrogen-barrier fillers to regulate hydrogen diffusion pathways; (2) leveraging the porous structure and surface dangling bonds of nano-ceramic particles to physically or chemically adsorb hydrogen, enabling its capture and storage.

In future, exploration of other functional fillers (*e.g.*, self-healing types) holds promise for enhancing the long-term reliability and service life of polymer-based composite coatings under severe pipeline operating conditions. This advancement provides critical technological support for constructing more durable, low-maintenance hydrogen energy infrastructure.

4 Preparation methods of HBCs

In the coating preparation process, even when employing identical processes, different materials and structural designs can lead to significant variations in hydrogen permeability. Fig. 6a shows coating structures in single-layer, multi-layer, gradient, nanolayer, and nanocomposite forms.[124] The rational selection of coating materials and structural design is a prerequisite for preparing HBCs with specific properties.

Currently, the preparation of metal and ceramic HBCs mostly requires high-temperature conditions. Commonly used techniques include Physical Vapor Deposition (PVD), Chemical Vapor Deposition (CVD), sol–gel method, Plasma Spraying (PS), Electrochemical Deposition (ECD), and Plasma Electrolytic Oxidation (PEO). In contrast, polymer-based composite coatings involve the mixed assembly of polymers and fillers, eliminating the need for stringent high-temperature conditions. Primary preparation techniques include Layer-by-Layer Self-Assembly (LBL) and the operationally simple low-temperature curing film formation method.

4.1 Physical vapor deposition

Physical vapor deposition is a method that vaporizes target materials into atomic, molecular, or ionic states through

© 2026 The Author(s). Co-published by the Institute of Process Engineering, Chinese Academy of Sciences and Royal Society of Chemistry

Open Access Article. Published on 14 May 2026. Downloaded on 6/5/2026 2:11:30 AM.
This article is licensed under a Creative Commons Attribution-NonCommercial 3.0 Unported Licence.

evaporation, ionization, or sputtering within a vacuum or low-pressure environment, then condenses and grows them into coatings on substrate surfaces. Primary techniques include vacuum evaporation coating, arc ion plating, sputter coating, and ion beam assisted deposition. Fig. 6b1 illustrates the principle of radiofrequency magnetron sputtering. With PVD, uniform and dense coatings of metals and their alloys, oxides, and non-oxide ceramics can be

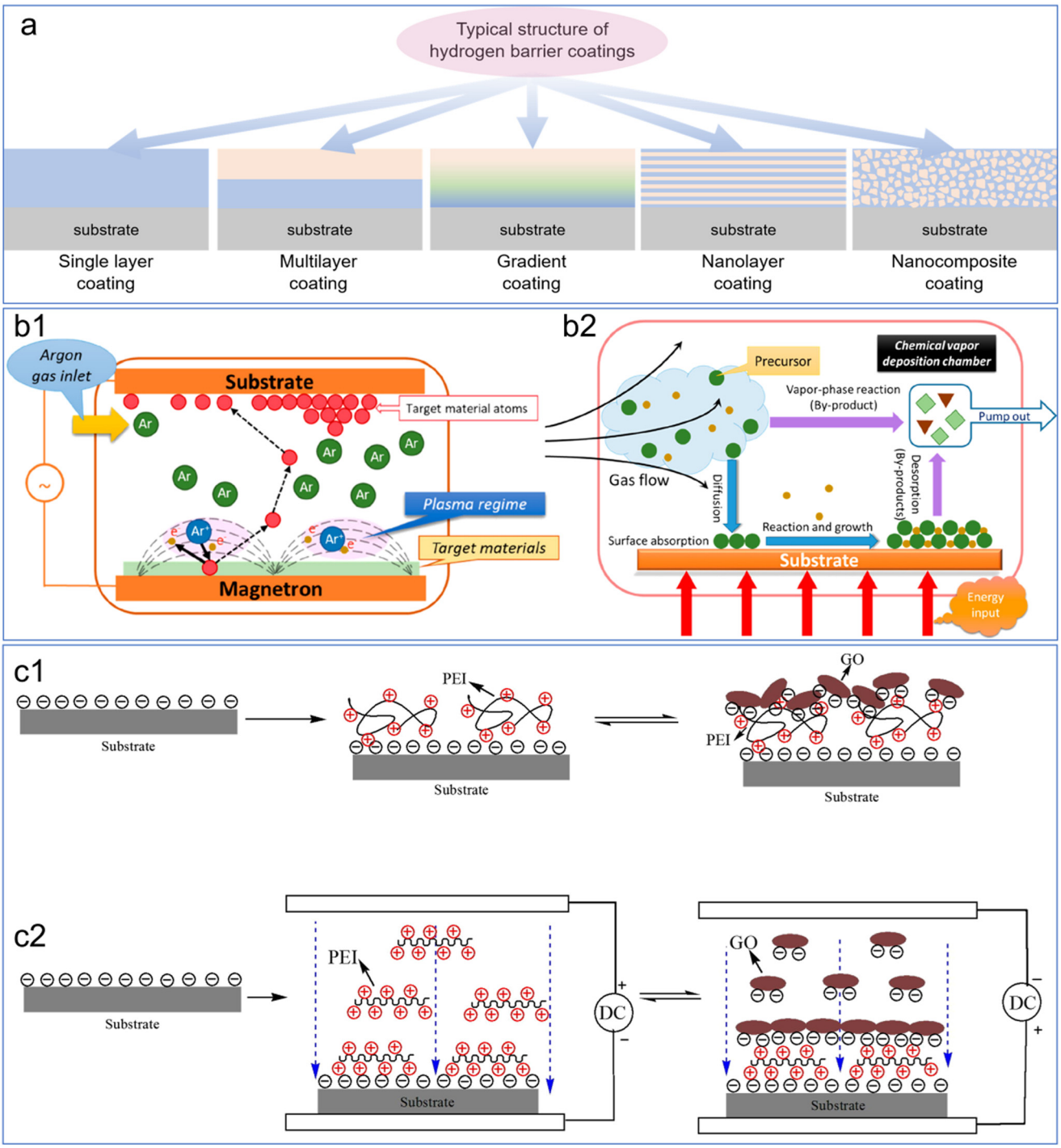

Fig. 6 (a) Structural design types of HBCs; (b1) schematic of radio frequency magnetron sputtering. Argon ions, activated by electron collisions, bombard the target surface with high energy, causing target atoms or molecules to sputter and deposit onto the substrate to form a thin film, (b2) schematic of conventional CVD, showing the core steps of precursor gas-phase diffusion, surface adsorption, surface reaction for film formation, and desorption of byproducts. Reproduced with permission.[58] Copyright 2023, American Chemical Society; (c1) traditional LBL self-assembly. Without an electric field, the PEI chains are randomly coiled, resulting in loose and uneven stacking of GO sheets, (c2) LBL self-assembly regulated by an external electric field. The applied direct current electric field causes the PEI chains to stretch and extend, which increases the deposition rate and promotes a more uniform orientation of the GO sheets. Reproduced with permission.[87] Copyright 2015, Elsevier.

© 2026 The Author(s). Co-published by the Institute of Process Engineering, Chinese Academy of Sciences and Royal Society of Chemistry

Open Access Article. Published on 14 May 2026. Downloaded on 6/5/2026 2:11:30 AM. This article is licensed under a Creative Commons Attribution-NonCommercial 3.0 Unported Licence.

produced. For example, Levchuk *et al.*[125] prepared a dense α-Al_2O_3 coating at 973 K using a negative bias of 200 V, reducing hydrogen permeability by a factor of 1000. Without a bias, the formation of the α-Al_2O_3 phase typically requires temperatures of 1300 K or higher, which adversely affects the microstructure and mechanical properties of the martensitic steel matrix. Subsequently, Al–Cr–O coatings deposited on Eurofer 97 steel surfaces *via* pulsed arc evaporation reduced hydrogen permeability by 2000–3500 times. This method forms a dense corundum-type structure at 823 K. However, the vertical deposition process from the target to the substrate limits PVD deposition on large-area and complex workpieces.[126] Therefore, despite the superior hydrogen barrier performance of PVD coatings, their application in large-scale hydrogen pipelines remains severely challenged. The process is primarily constrained by the inherent vertical deposition mechanism and the reliance on large-scale vacuum chambers, rendering the uniform and continuous coating of long pipeline inner surfaces technically prohibitive. Furthermore, the degradation of mechanical properties induced by excessive deposition temperatures represents an unacceptable risk in engineering practice.

4.2 Chemical vapor deposition

Chemical vapor deposition introduces gaseous precursors into a reaction chamber, where chemical reactions occur on the substrate surface or in the adjacent space. This generates solid deposits that form a coating covering the substrate surface. As shown in Fig. 6b2, conventional chemical vapor deposition primarily involves four processes: (1) diffusion of reactive gas streams onto the substrate surface, (2) adsorption of reactive gas streams onto the substrate surface, (3) chemical reaction on the substrate surface to form a film, and (4) desorption of gaseous byproducts from the substrate surface. HBCs prepared *via* CVD enable *in situ* deposition of ceramic coatings or novel hydrogen barrier layers on container or pipeline inner walls, making it suitable for coating complex or defective surfaces. Young[127] and Fan[128] utilized CVD to fabricate low-defect graphene HBCs on copper substrates and nickel foils.

However, the deposition temperature of conventional CVD typically exceeds 1273 K, thereby limiting the choice of substrate materials. Against this backdrop, metal–organic chemical vapor deposition (MOCVD) has garnered significant attention. In this process, volatile metal organic compounds undergo thermal decomposition at low temperatures, providing favorable conditions for uniform coating deposition and large-scale production. By adjusting conditions in the MOCVD system—such as reactor geometry, flow rate, pressure, and deposition temperature—the composition, microstructure, and crystallinity of the coating can be modified. He *et al.*[129] investigated the effect of MOCVD temperature on the hydrogen permeability of Al_2O_3 coatings. The permeability of crystalline Al_2O_3 coatings annealed at 1173 K was higher than that of amorphous Al_2O_3 coatings annealed at 973 K; however, the former exhibited delamination after hydrogen permeation testing. This was attributed to the formation of the $MnCr_2O_4$ spinel phase on the coating surface after 1173 K annealing, creating rapid hydrogen diffusion pathways that enhanced permeability. Wu *et al.*[130] prepared Y_2O_3 coatings on 316L stainless steel *via* MOCVD, achieving permeability reductions of 240 to 410 times compared to the substrate. Although CVD technology has made significant strides in coating uniformity and adaptability to complex surfaces, its application in large-scale hydrogen pipelines is still constrained by high deposition temperatures and associated energy costs.

4.3 Sol–gel method

The sol–gel process utilizes metal alkoxides or similar compounds as precursor materials, which are typically dissolved in organic solvents such as alcohols or ethers to form a homogeneous solution. Subsequently, through hydrolysis and condensation, the solution transforms into a sol state. As polymerization progresses further and undergoes aging and drying, the sol gradually transitions into a gel state. Finally, thermal processing steps such as sintering remove the solvent and moisture, resulting in the formation of the final ceramic coating. Sol–gel-prepared coatings offer advantages such as high uniformity, single-component composition, controllable processing, simplicity, and adaptability to complex workpiece geometries. Although Al_2O_3 coatings prepared by Wang *et al.*[131] *via* thermal growth and sol–gel methods exhibit surface porosity, they maintain overall density and strong adhesion, theoretically preventing hydrogen permeation. However, the preparation of α-Al_2O_3 crystals requires a calcination temperature of 1373 K, which can damage the substrate. Yao *et al.*[132] prepared Er_2O_3 coatings at 973 K using the sol–gel method with controlled atmosphere and temperature. These coatings exhibited uniform thickness, crack-free structures, and excellent bonding with the substrate. Nevertheless, this method is costly and time-consuming, hindering its large-scale application.

4.4 Plasma spraying

Plasma spraying is a thermal spraying technology that involves propelling powdered materials heated to a molten or semi-molten state within a plasma jet at high velocity onto a substrate to form a coating. It is primarily categorized into atmospheric plasma spraying (APS) and vacuum plasma spraying (VPS). This technology does not require high-temperature preheating of the substrate, enabling coating preparation without altering the substrate's microstructure or strength. It offers large coating areas, ease of repair, and low production costs. However, coatings produced by APS are generally unsuitable for hydrogen barriers, as oxidation during spraying generates numerous defects that increase hydrogen permeation. Residual stresses may also form in

© 2026 The Author(s). Co-published by the Institute of Process Engineering, Chinese Academy of Sciences and Royal Society of Chemistry

Open Access Article. Published on 14 May 2026. Downloaded on 6/5/2026 2:11:30 AM. This article is licensed under a Creative Commons Attribution-NonCommercial 3.0 Unported Licence.

PS-produced coatings due to the rapid cooling of ejected particles, potentially affecting coating adhesion strength.

Fazio *et al.*[133] observed that the permeability of Fe–Cr–Al coatings prepared by VPS decreased by only 2.5-fold. The poor hydrogen resistance may be attributed to oxide layer delamination caused by residual stresses. Perujo *et al.*[153] sprayed aluminum onto martensitic stainless steel, followed by heat treatment to form Al_3Fe and Al_5Fe_2. Hydrogen permeability tests indicated the coating reduced hydrogen permeability by 2–3 orders of magnitude. Liu *et al.*[178] designed a self-healing hydrogen barrier coating and prepared a multi-interface composite coating consisting of TiC + Mixture (TiC/Al_2O_3) + Al_2O_3 *via* APS. After heat treatment, TiC oxidized to TiO_2, and the volume expansion reduced porosity by 90%. Hydrogen permeation decreased, and coating adhesion strength increased. After 40 h of annealing at 923 K, the self-healing coating exhibited reduced cracking and delamination. Hydrogen permeability also decreased by approximately 50% compared to the untreated coating, thereby enhancing its hydrogen resistance. However, while thermal spraying is suitable for industrial-scale production, the pores and cracks formed during thermal spraying remain the primary obstacle to hydrogen barrier applications. Solutions must be found before widespread adoption.

4.5 Electrochemical deposition

Electrochemical deposition utilizes electrolytic principles to cover substrate surfaces with a metallic coating, effectively reducing hydrogen atom permeation. Electroplating represents a typical electrochemical deposition process. Hajjami *et al.*,[134] Boiadjieva *et al.*,[135] and Zhou *et al.*[136] conducted studies on alloy coatings, considering additional factors such as baking and varying electrodeposition parameters, thereby validating the coatings' HE protection capabilities. During the electroplating process, factors including the plating bath system, additives, ultrasonic agitation, and coating structure significantly influence the suppression of HE effects. Nevertheless, the electroplating process involves inherent hydrogen evolution; a portion accumulates as gas diffusing into the environment, while another portion permeates into the coating and substrate. The accumulation of process-induced hydrogen at coating/substrate interface defects can induce delamination and blistering, severely constraining the applicability of this technique. While optimizing operational parameters and incorporating shot peening can alleviate interface lattice mismatch and macroscopic defects, the risk of HE introduced during the plating process remains a critical safety hazard for high-strength pipeline steels.

4.6 Plasma electrolytic oxidation

Plasma electrolytic oxidation, also known as micro-arc oxidation, generates instantaneous high temperatures and pressures on metals such as aluminum, magnesium, titanium, and their alloys through arc discharge, thereby enabling the *in situ* growth of oxide ceramic coatings. This method is simple to operate, and the coatings exhibit high bonding strength due to metallurgical bonding with the substrate, featuring a compact structure that resists peeling. Jun *et al.* employed PEO to deposit Al_2O_3 coatings on SS316L. These coatings demonstrated excellent adhesion to the substrate and superior thermal shock resistance.[33] At 773 K, hydrogen permeability decreased by a factor of 1930. Within the current density range of 30–120 mA cm^{-2}, higher current densities favored the oxidation of Al to Al_2O_3. On the other hand, within the voltage range of 200–500 V, higher voltages promoted the phase transformation from γ-Al_2O_3 to α-Al_2O_3, resulting in enhanced hydrogen barrier properties. Despite these performance advantages, the implementation of PEO on large-scale hydrogen pipelines faces significant material constraints. Since pipeline steels are predominantly iron-based, PEO typically necessitates a pre-deposited aluminum layer on the pipeline's inner wall. This complex "dual-process" requirement substantially escalates both coating production costs and operational complexity.

4.7 Layer-by-layer self-assembly

Layer-by-layer (LBL) self-assembly is a method for constructing functional films layer by layer on a substrate surface by alternately depositing molecules or nanomaterials with opposite charges. Its core principle is electrostatic interaction, though it can also be extended to intermolecular forces such as hydrogen bonding. Since Decher[137] proposed the electrostatic-driven layer-by-layer self-assembly mechanism in 1997, LBL technology has been extensively studied in polymer-based composite coatings. In the field of HBCs, Rajasekar[138] introduced negative charges into polyvinylidene fluoride through sulfonation modification. This material was electrostatically coupled with positively charged poly (diallyldimethylammonium chloride) and alternately deposited. Meanwhile GO served as a nanofiller dispersed within the sulfonated polyvinylidene fluoride. The resulting LBL film, composed of 16 stacked bilayer structures, substantially enhanced the hydrogen barrier properties of the polyethylene terephthalate substrate. However, this method requires a relatively long self-assembly time, and the tendency of GO sheets to wrinkle during filling can compromise the final hydrogen barrier performance. To address this issue, Zhao *et al.*[87] incorporated an externally applied electric field into the LBL technique. This approach not only accelerated the uniform dispersion of GO within polyethyleneimine (PEI) but also suppressed sheet wrinkling, optimized the orientation of GO layers, and enhanced the film's compactness. The hydrogen gas transmission rate (GTR) of the prepared 10-layer self-assembled film reached 81 cm^3 m^{-2} d atm, which is 65% lower than that of the PEI/GO film prepared without an electric field. Fig. 6c1 and c2 illustrate the LBL self-assembly process with and without an electric field. In the absence of an electric field, polymer

© 2026 The Author(s). Co-published by the Institute of Process Engineering, Chinese Academy of Sciences and Royal Society of Chemistry

Open Access Article. Published on 14 May 2026. Downloaded on 6/5/2026 2:11:30 AM.
This article is licensed under a Creative Commons Attribution-NonCommercial 3.0 Unported Licence.

chains in dilute solution adopt a disordered, coiled state that cannot be stretched, hindering polymer deposition and film formation. On the other hand, when GO sheets adsorb onto the substrate, their uniform film formation and spreading are constrained by the morphology and distribution of adsorbed polymer chains. This makes it prone to forming uneven and loosely packed surfaces, resulting in prolonged processing times and poor hydrogen barrier performance. Under an applied electric field, the disordered polymer chains are stretched and extended due to electrostatic repulsion, accelerating deposition rates. Similarly, the adsorption of graphene oxide layers is accelerated by the electric field, resulting in more uniform alignment and orientation. It is evident that the electric field-controlled LBL self-assembly technique achieves higher efficiency and superior hydrogen barrier performance in the resulting coatings.

LBL technology enables molecular-level precision control in preparing hydrogen-barrier coatings, facilitating the fabrication of ultra-thin (nanoscale) layers. However, the primary drawback of LBL technology lies in its low deposition efficiency—a single layer requires 5–20 minutes to deposit. The excessive time cost makes it difficult to meet the demands of industrial-scale coating preparation for long-distance pipeline steel.

4.8 Low-temperature curing film formation method

Low-temperature curing film formation methods are commonly employed in laboratory settings due to their ability to avoid excessively high processing temperatures. Common techniques encompass blade coating, spin coating, and spray coating. In comparison to conventional methods such as CVD and PVD, low-temperature curing film formation offers significant advantages through its ability to operate under mild conditions without requiring complex high-temperature or high-vacuum environments. As a result, it is especially advantageous for the preparation of polymer-based composite coatings and functionalized inorganic–organic hybrid films under laboratory research conditions.

Blade coating is the simplest method, involving the direct application of a liquid polymer precursor onto the substrate surface. After drying and curing at a specific temperature, a protective coating is formed. Spin coating offers a straightforward process with strong film thickness controllability, making it a prominent technique in experimental research on polymer-based HBCs. The core process involves dripping a liquid precursor (such as a sol, polymer solution, or nanocomposite slurry) onto the substrate surface. Centrifugal force generated by high-speed rotation drives the liquid to spread uniformly, accompanied by solvent evaporation or chemical reaction curing, ultimately forming a dense, uniform functional film. However, spin coating imposes stringent requirements on substrate surface flatness, limiting its scalability for large-area or complex geometries. In comparison, spray coating using small spray guns effectively overcomes these limitations, enabling coating preparation on intricate surfaces.

4.9 Comparison of common preparation processes

The hydrogen resistance of coatings depends not only on the properties of the materials but also on the microstructure. By adjusting preparation parameters or combining different processes, the coating structure can be designed and optimized. Table 3 summarizes the research results of various coatings prepared using different techniques.

As indicated in the aforementioned table, it is evident that most preparation processes involve complex procedures and rely on high temperatures, making it difficult to directly apply traditional HBCs to existing industrial pipelines. In contrast, the low-temperature curing film formation method eliminates the need for stringent high-temperature environments, simplifies operational steps, and exhibits excellent adaptability to various surfaces. Consequently, developing and applying an industrially viable low-temperature curing film formation method is key to overcoming the limitations of current engineering applications.

5 Comprehensive evaluation system for HBCs in transport pipelines

Considerable progress has been achieved in laboratory research concerning hydrogen barrier materials, permeation mechanisms, and advanced fabrication processes. However, the translation of these fundamental findings into industry-recognized and standardized engineering specifications and technical guidelines remains a formidable challenge. In practical industrial networks for pure or hydrogen-blended gas, the evaluation of coated pipeline systems extends far beyond the PRF as a singular metric. Within the contexts of industrial certification and practical engineering applications, greater emphasis is placed on the structural integrity and functional durability of coatings under long-term dynamic conditions. The core evaluative dimensions include the bonding stability of the coating–substrate interface, overall hydrogen barrier performance under complex conditions, synergistic HE failure behavior during extended service, and long-term durability within the pipeline environment. Consequently, a multidimensional and comprehensive methodological framework is required to bridge fundamental materials science and engineering requirements. On this basis, a full-chain evaluation framework is established in this section, encompassing four critical dimensions: preparation quality, hydrogen barrier efficiency, protective performance, and pipeline applicability.

5.1 Quality evaluation

The quality of the coating directly affects hydrogen barrier performance. Based on the factors influencing hydrogen barrier performance, coating quality evaluation is primarily

© 2026 The Author(s). Co-published by the Institute of Process Engineering, Chinese Academy of Sciences and Royal Society of Chemistry

Open Access Article. Published on 14 May 2026. Downloaded on 6/5/2026 2:11:30 AM. This article is licensed under a Creative Commons Attribution-NonCommercial 3.0 Unported Licence.

Table 3 Characteristics of the preparation process

Techniques	Materials	Structural design	Features	Ref.
PVD	CrN	Single layer	Ion bombardment during magnetron sputtering reduces the formation of grain boundaries, resulting in a dense coating	139
	α-Al_2O_3	Single layer	At 973 K, applying a 200 V bias voltage enables the preparation of dense α-Al_2O_3 crystals	125
	Ni–Cr	Gradient	By adjusting the sputtering power ratio of Ni/Cr target materials, the coating composition can be controlled. Combined with annealing treatment, this enables elemental interdiffusion to form a gradient structure, thereby enhancing coating adhesion	19
CVD	V-Gr	Nanolayer	Large-area graphene coatings can be synthesized *in situ via* CVD to prevent graphene from tearing during transfer	59
Sol–gel method	Al_2O_3	Single layer	Sol–gel method can be used for coating complex geometric surfaces, such as the inner walls of pipes, but requires high-temperature calcination	131
	Er_2O_3	Single layer	High-temperature calcination with a small amount of oxygen yields excellent coating crystallization	132
PS	Fe–Cr–Al	Single layer	1. APS coatings exhibit more defects than VPS coatings 2. Due to defects caused by residual stresses in the coating, the PRF of the VPS coating is only 2.5, far below the expected 100	133
ECD	ZrO_2	Single layer	ECD can be used to seal pores in coatings	140
LBL	PEI/GO PDDA/SPVDF-GO	Nanolayer	A multilayer hydrogen-barrier composite coating formed by stacking double-layer structures can be prepared without high-temperature conditions. This approach optimizes the two-dimensional packing orientation of the fillers, resulting in a structurally dense coatings, but assembly efficiency remains low	87, 138
Low-temperature curing film formation method	(f-GO-BN)-TPU-EP	Nanocomposite	Combining spraying with *in situ* curing, this method is suitable for coating the inner walls of complex-shaped containers	64
	Gr-PPD-EP/TPU	Multilayer	Spin coating can be repeated multiple times, but it imposes stringent requirements on the substrate surface and exhibits poor surface adaptability	83

divided into three aspects: density evaluation, adhesion evaluation, and thickness evaluation.

5.1.1 Density evaluation. The density of a coating, defined as the uniformity and compactness of its surface structure, serves as a crucial indicator for evaluating its performance. Density is typically characterized using two-dimensional microscopy techniques such as scanning electron microscopy (SEM), transmission electron microscopy (TEM), and electron backscatter diffraction (EBSD). Extensive research indicates that high coating density is a key factor in enhancing hydrogen barrier performance. Yoo *et al.*[141] utilized EBSD to compare three intermetallic compound coatings, finding that coatings with a dense Fe_2Al_5 phase exhibited the best hydrogen barrier properties. Fig. 7 displays the phase map and inverse polar map (IPF) derived from EBSD image analysis, revealing that the Fe_2Al_5 phase possesses the most complete and dense columnar crystal structure. He *et al.*[35,142] confirmed *via* SEM characterization that aluminum oxide coatings with higher surface density exhibit superior hydrogen barrier performance. Liu *et al.*[47] employed field emission scanning electron microscopy to demonstrate that suppressing grain growth *via* energy ion bombardment enhances the density of CrN coatings, thereby improving their hydrogen barrier properties. These studies consistently indicate that optimizing microstructure to increase density is an effective approach for enhancing hydrogen barrier performance. However, the hydrogen barrier efficiency of coatings can be significantly compromised by the presence of defects, particularly pores. Studies by Shi *et al.*[101] and Oliver *et al.*[143] explicitly demonstrate that pores provide direct diffusion pathways for hydrogen atoms, greatly facilitating hydrogen permeation within the coating. Hydrogen atoms permeating into the coating may recombine into hydrogen molecules at microdefects, leading to localized accumulation of hydrogen pressure. The sustained action of this hydrogen pressure induces bubble formation, crack nucleation, and propagation. This damage not only directly compromises the integrity of the metal substrate but also severely impairs the coating's long-term barrier function and durability under demanding service conditions.[98] Therefore, thoroughly investigating the specific influence of coating porosity on hydrogen permeation kinetics and damage mechanisms—particularly determining critical porosity thresholds—is crucial for designing highly reliable HBCs.

Currently, common methods for characterizing porosity include mercury intrusion porosimetry (MIP) and X-ray microcomputed tomography (X-CT) technology. MIP is limited in hydrogen barrier coating evaluation because it cannot image microstructures, locate specific pores, and cause irreversible damage to samples. In contrast, X-CT technology offers non-destructive three-dimensional imaging capabilities, making it a superior choice for coating evaluation. X-CT enables quantitative three-dimensional analysis of film thickness distribution, porosity, and pore

© 2026 The Author(s). Co-published by the Institute of Process Engineering, Chinese Academy of Sciences and Royal Society of Chemistry

Open Access Article. Published on 14 May 2026. Downloaded on 6/5/2026 2:11:30 AM.
This article is licensed under a Creative Commons Attribution-NonCommercial 3.0 Unported Licence.

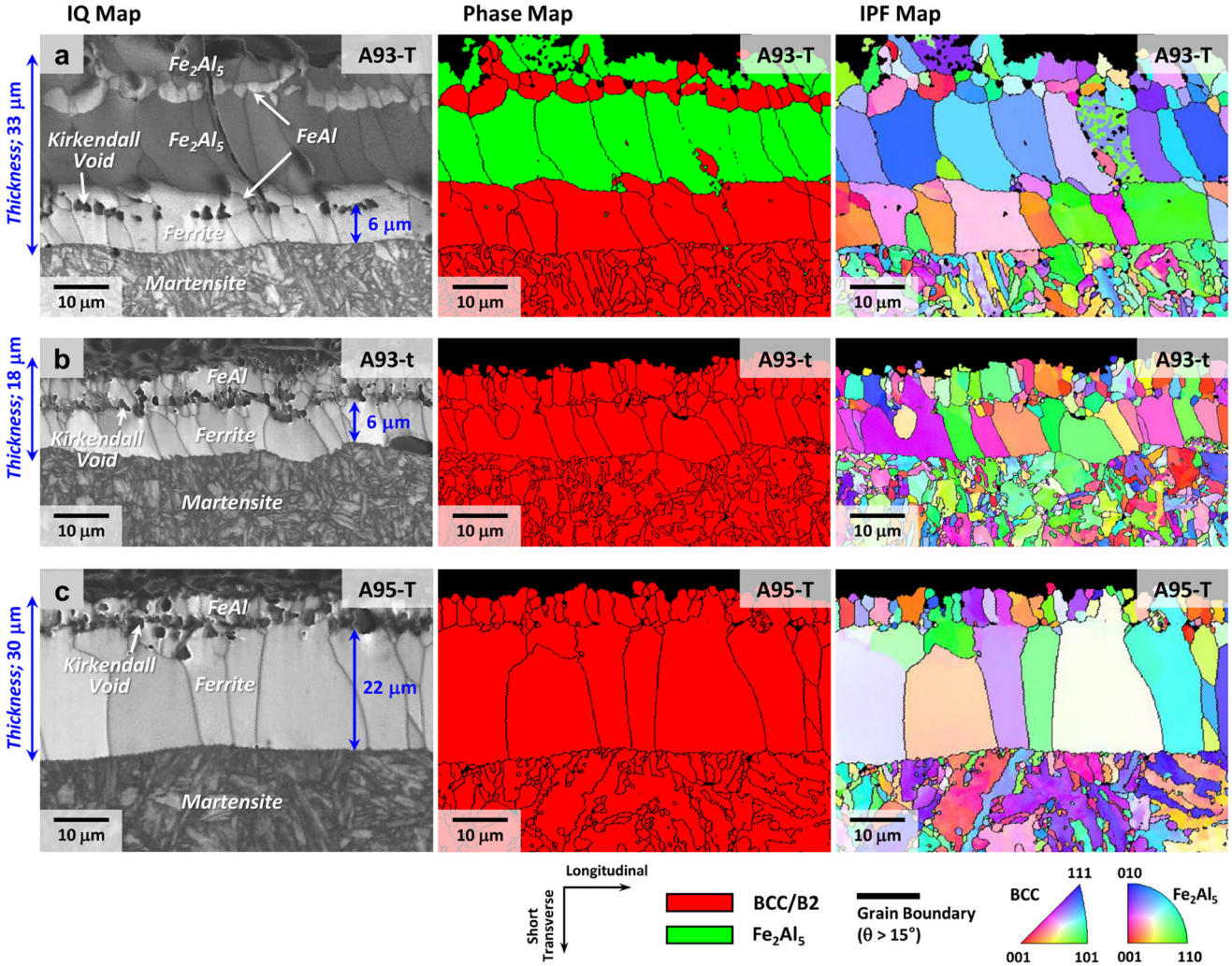

Fig. 7 Image quality maps, phase maps, and IPF for the three coating samples: A93-T, A93-t, and A95-T. (a) The A93-T consists of a surface Fe_2Al_5 layer, an intermediate FeAl phase, and a ferritic transition layer, with a total thickness of approximately 33 μm; (b) the A93-t contains only the FeAl phase and a ferritic transition layer, with a total thickness of roughly 18 μm; (c) the A95-T is composed of the FeAl phase and a significantly coarsened ferritic transition layer reaching a thickness of 22 μm. The IPF maps clearly illustrate the grain morphology and crystallographic orientation distribution of each phase. Reproduced with permission.[141] Copyright 2022, Elsevier.

connectivity without damaging the coating, thereby avoiding the local sampling errors inherent in two-dimensional measurement techniques.[144,145] Zhang *et al.*[146] quantified the pore space distribution in plasma electrolytic oxidation coatings using X-CT technology, but failed to detect the submicron pores observed by SEM. To more precisely analyze the dynamic evolution of pores, Zhu *et al.*[147] developed an image processing algorithm based on X-CT technology, combining Top-Hat segmentation with region growth. This algorithm significantly improved pore recognition rates and effectively separated pores from the coating background structure. Fig. 8 shows the three-dimensional pore cluster distribution with volume fraction statistics grouped by radius under this algorithm. Despite the advanced algorithm, the inherent spatial resolution limitations of current X-CT technology still make it difficult to clearly resolve the connectivity behavior of microcracks between pores, especially at the submicron scale. For this reason, X-CT technology must still be combined with high-resolution SEM, TEM, and other microscopic characterization techniques at this stage to compensate for its limitations in fine-structure characterization. Furthermore, the comprehensive utilization of various microscopy techniques to systematically characterize the microstructure of HBCs—particularly the evolution of pore size, distribution, morphology, and connectivity—is crucial for gaining a deeper understanding of the failure mechanisms of coatings under service conditions in hydrogen pipelines. This represents a key factor in evaluating the long-term durability and reliability of coatings, while also providing essential guidance for optimizing coating structures and enhancing hydrogen barrier performance.

5.1.2 Adhesion evaluation. The adhesion between a coating and its substrate is fundamental to maintaining the

© 2026 The Author(s). Co-published by the Institute of Process Engineering, Chinese Academy of Sciences and Royal Society of Chemistry

Open Access Article. Published on 14 May 2026. Downloaded on 6/5/2026 2:11:30 AM.
This article is licensed under a Creative Commons Attribution-NonCommercial 3.0 Unported Licence.

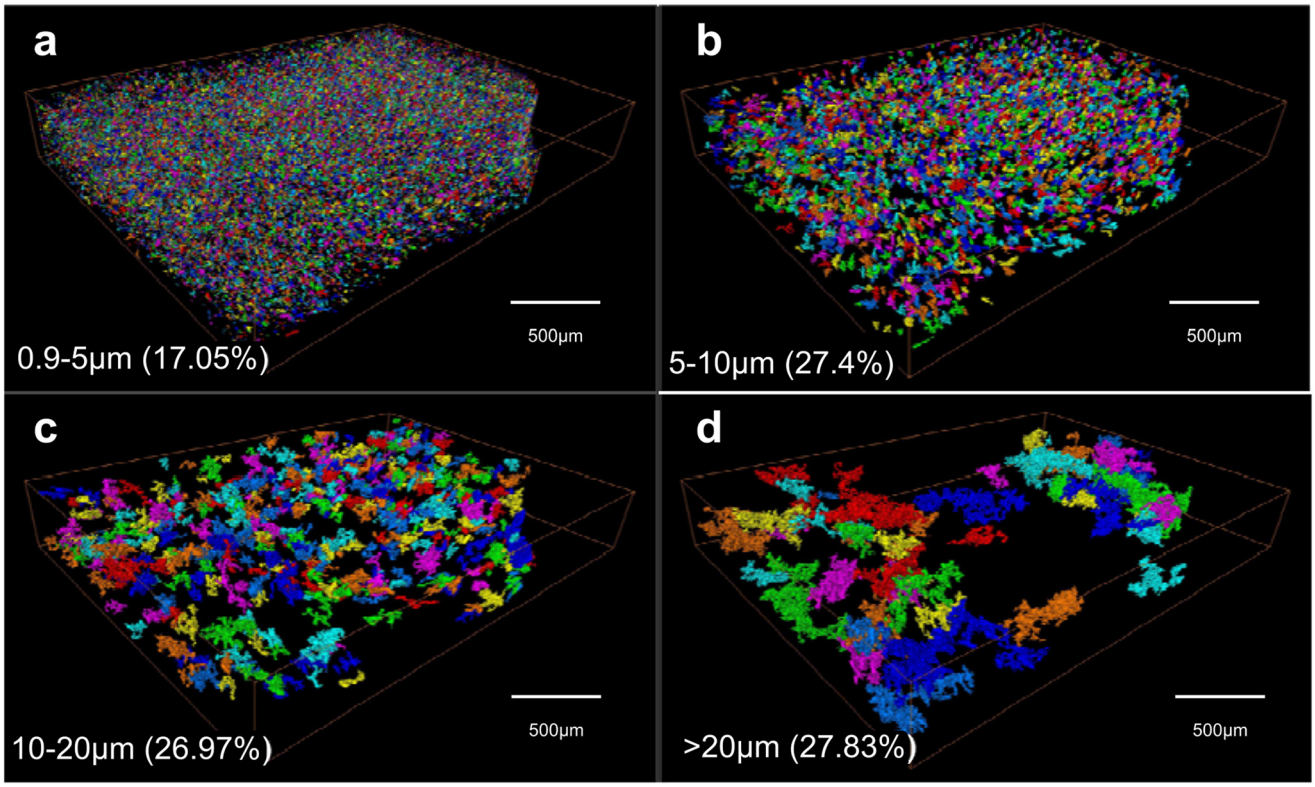

Fig. 8 Three-dimensional representation of pores with different pore radii extracted from ceramic coatings using top-hat segmentation combined with region growth. Pore size distribution and volume fractions: (a) 0.9–5 μm (17.05%), (b) 5–10 μm (27.4%), (c) 10–20 μm (26.97%), and (d) >20 μm (27.83%). Reproduced with permission.[147] Copyright 2019, Elsevier.

structural integrity of the coating and to providing long-term protection. It directly determines the durability of the coating under service conditions. Inadequate adhesion may lead to coating delamination during prolonged use, resulting in loss of intended functionality. Various methods are available for evaluating coating adhesion, including nano-indentation or nano-scratch testing, pulse laser induced shock spallation testing, blister, bulge and buckle testing, and acoustic emission testing.[148] Currently, the aforementioned evaluation methods are generally conducted in air environments, whereas hydrogen environments have been demonstrated to significantly impact coating adhesion.[149] To obtain adhesion data closer to actual coating operating conditions, testing under simulated service conditions in high-pressure hydrogen environments is crucial.

From another perspective, while high adhesion strength enhances the coating's resistance to spalling, excessively strong interfacial bonding can introduce new issues such as "film-induced brittle fracture". Traditional views held that only brittle substrates exhibited this phenomenon, but Guo[96] tested a brittle film/ductile substrate system (TiN/brass) and discovered that ductile substrates could also fracture due to cracks propagating from the coating. It was concluded that the film–substrate adhesion is a critical factor influencing substrate cracking. Under strong adhesion, cracks in the TiN coating directly penetrate the interface and propagate into the brass substrate, forming cleavage cracks approximately 1 μm deep. At this stage, no interfacial delamination occurs, and crack energy is directly transferred to the substrate. With weak bonding, crack propagation promotes delamination at the film–substrate interface, dissipating energy and preventing crack extension into the substrate, thereby avoiding substrate fracture. Therefore, in critical applications such as hydrogen transmission pipelines, the optimization of adhesion must be carefully balanced. Pursuing excessively high adhesion without considering the risk of film-induced substrate cracking may compromise the long-term safety of pipeline systems.

5.1.3 Thickness evaluation. Coating thickness significantly impacts hydrogen barrier performance. Current non-destructive testing methods for evaluating coating thickness include infrared thermal imaging thickness measurement, ultrasonic thickness measurement, and eddy current thickness measurement. Additionally, techniques based on terahertz time-of-flight and laser-induced plasma spectroscopy are also employed.[150] Two-dimensional microscopic analysis techniques are typical destructive testing methods. Coating thickness can be accurately determined through cross-sectional characterization. These techniques are widely applied owing to their high precision and reliable results. For instance, Chikada *et al.*[151] precisely measured the thickness of erbium oxide coatings using scanning transmission electron microscopy. The reported coating thicknesses ranged from 0.3 to 2.6 μm. Under the

© 2026 The Author(s). Co-published by the Institute of Process Engineering, Chinese Academy of Sciences and Royal Society of Chemistry

Open Access Article. Published on 14 May 2026. Downloaded on 6/5/2026 2:11:30 AM. This article is licensed under a Creative Commons Attribution-NonCommercial 3.0 Unported Licence.

ideal assumption of defect-free coatings, Chikada *et al.* inferred a positive correlation between hydrogen barrier performance and coating thickness, consistent with Kalin's observations. Using SEM analysis, Kalin *et al.*[20] examined aluminum oxide coatings of varying thicknesses prepared on $Cr_{18}Ni_{10}Ti$ surfaces *via* the molten hot-dip aluminum process, revealing enhanced hydrogen barrier effectiveness with increasing thickness. Constrained by current coating materials and preparation techniques, it is still a major challenge to achieve completely pore-free and crack-free coatings.

However, the relationship between coating thickness and hydrogen barrier efficiency is not a simple linear proportional relationship. Research by Li *et al.*[152] indicates that hydrogen permeability does not decrease significantly as the Al_2O_3 coating thickness increases within the range of 0.2–1.6 μm. This suggests that within this thickness range, the chemical barrier mechanism against hydrogen permeation at the aluminum oxide coating surface dominates, and the effect of thickness is not evident. Only when the thickness reaches a certain threshold do the physical barrier properties begin to manifest. At this point, hydrogen permeability decreases significantly with increasing thickness.[153] In addition, increasing coating thickness often carries the risk of performance degradation. Zhang Hua *et al.*[154] demonstrated that both surface quality and hydrogen barrier properties of aluminum oxide coatings prepared on SS316L surfaces exhibited a trend of initial improvement followed by decline as coating thickness increased. At a coating thickness of 0.11 μm, the coating displayed excellent hydrogen barrier performance, achieving a PRF of 315. As the thickness increased to 0.255 μm, cracks began to appear on the coating surface, leading to a decline in hydrogen barrier performance. Qamar *et al.*[45] also found that excessively thick SiC coatings are prone to cracking under high-temperature conditions. Therefore, for specific coating systems and service environments in hydrogen transport pipelines, it is necessary to determine the optimal thickness range that balances high hydrogen barrier performance with good surface integrity.

5.2 Efficiency evaluation

Numerous testing methods exist for evaluating hydrogen dissolution and permeation into metallic materials. Since each method employs distinct evaluation criteria, the appropriate technique is typically selected by considering the specific application and environmental conditions.

5.2.1 Vacuum gaseous hydrogen permeation tests. Vacuum gaseous hydrogen permeation testing is dependent on high-vacuum and high-temperature technologies, comprising three main units: the sample mounting and heating unit, the high-vacuum hydrogen charging chamber, and the high-vacuum hydrogen measurement chamber.[7] As shown in Fig. 9a, the high-vacuum hydrogen charging chamber and high-vacuum hydrogen measurement chamber maintain distinct vacuum levels to provide hydrogen diffusion driving force. The high-vacuum hydrogen charging chamber is connected to a hydrogen cylinder and utilizes a mass flow controller to supply constant-pressure hydrogen (a palladium hydrogen permeation membrane at the hydrogen nozzle enhances hydrogen purity). A heating system provides high-temperature conditions by heating the specimen, enhancing hydrogen atom diffusion through the metallic substrate. When hydrogen diffuses from the hydrogen charging chamber to the right side of the sample, hydrogen atoms combine into hydrogen molecules. After desorption, the increase in pressure is detected and measured by a high-sensitivity vacuum gauge (or other instruments such as quadrupole mass spectrometers that directly measure hydrogen concentration[33,35,40]). Since the pressure increase is proportional to the permeated hydrogen concentration, a dynamic curve of the hydrogen permeation process can be obtained, enabling quantitative monitoring of hydrogen permeation within the material. This method can be applied to evaluate the hydrogen barrier performance of hydrogen-resistant coatings under varying hydrogen pressures and temperatures. The hydrogen permeability can be calculated using the following equation:[155]

$$P = \frac{J \times L}{p^n} \tag{4}$$

where J is the hydrogen permeation flux in mol m^{-2} s^{-1}; L is the sample thickness in m; p is the hydrogen source supply pressure in Pa; n is the constant representing the form of hydrogen present in the material: n = 1/2 when present as atoms; n = 1 when present as molecules; P is the permeability in mol m^{-1} s^{-1} Pa^{-1}.

For metallic materials, vacuum gaseous hydrogen permeation testing is required to provide elevated temperatures for detecting hydrogen permeation. At temperatures approaching pipeline operating conditions, this test may fail to accurately detect permeated hydrogen atoms. For example, Okayasu and Sato[156] observed no hydrogen atoms detected in the vacuum hydrogen measurement chamber when heating low-carbon steel specimens after 48 hours of exposure to 0.7 MPa H_2 gas at 50 °C. Only when the sample was heated to 100 °C did hydrogen atom content reach 140 ppm (wt) after 24 hours of hydrogen charging. However, tests conducted at temperatures significantly higher than pipeline operating conditions cannot quantitatively analyze hydrogen permeation data of coatings under actual operating temperatures.

5.2.2 Electrochemical hydrogen permeation tests. The measurement of hydrogen permeation behavior in materials using the Devanathan–Stachurski (D–S) double-cell system is termed electrochemical hydrogen permeation testing. As shown in Fig. 9b, it consists of two independent electrolyte cells separated by a thin sheet specimen. The hydrogen-charged cell is positioned to the right of the specimen, enabling hydrogen injection into the specimen under

© 2026 The Author(s). Co-published by the Institute of Process Engineering, Chinese Academy of Sciences and Royal Society of Chemistry

Open Access Article. Published on 14 May 2026. Downloaded on 6/5/2026 2:11:30 AM.
This article is licensed under a Creative Commons Attribution-NonCommercial 3.0 Unported Licence.

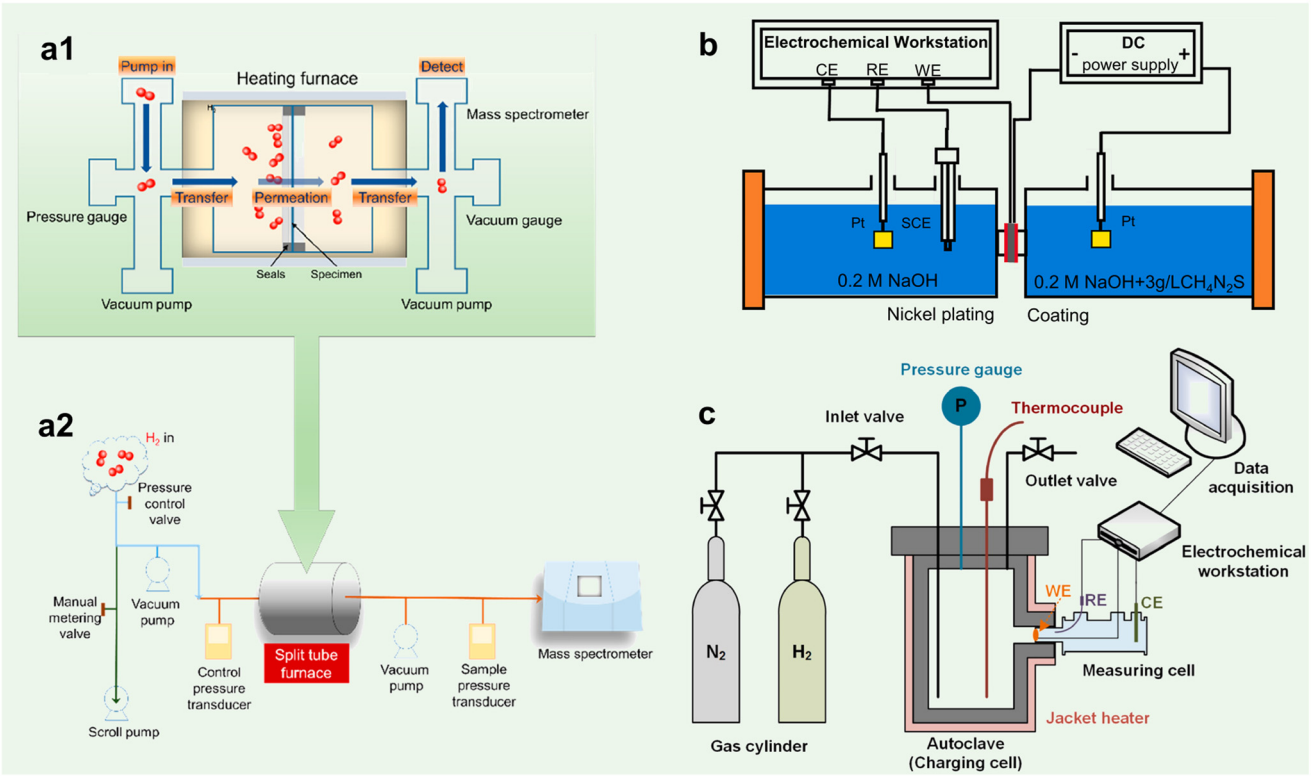

Fig. 9 (a1) Vacuum gaseous hydrogen permeation testing apparatus and (a2) process flow diagram. Reproduced with permission.[58] Copyright 2023, American Chemical Society; (b) schematic diagram of the electrochemical permeation measurement instrument. Reproduced with permission.[12] Copyright 2025, Elsevier; (c) schematic diagram of *in situ* gaseous hydrogen permeation test equipment. Reproduced with permission.[161] Copyright 2023, Elsevier.

constant current or constant potential conditions.[157] It acts as the cathode, where hydrogen ions migrate to the surface of the metal sheet sample, acquire electrons to form atomic hydrogen, and enter the specimen (some atomic hydrogen may combine into hydrogen molecules and desorb from the specimen surface; this can be mitigated by adding a poison to the electrolyte[155]). On the left side is a hydrogen measurement cell. The electrochemical workstation applies a constant potential to the left side of the sample, oxidizing all hydrogen atoms permeating from the hydrogen-infusion side into hydrogen ions. This records the hydrogen permeation current, yielding a current-*versus*-time hydrogen permeation curve. Analysis of this curve provides hydrogen permeation-related parameters.[12]

The steady-state hydrogen permeation current density i_∞ can be calculated by substituting into the steady-state hydrogen permeation diffusion flux equation:

$$J_\infty = \frac{i_\infty}{nF} \tag{5}$$

where F is the Faraday constant of 96 500 C mol^{-1}; n is the number of electrons transferred in the reaction; J_∞ is the steady-state hydrogen permeation diffusion flux, measured in mol m^{-2} s^{-1}.

The hydrogen diffusion coefficient can be calculated using the penetration time method or the time delay equation:

$$D_{app} = \frac{L^2}{15.3t_b} \tag{6}$$

$$D_{app} = \frac{L^2}{6t_{0.63}} \tag{7}$$

where D_{app} is the hydrogen diffusion coefficient in m^2 s^{-1}; L is the sample thickness in m; t_b is the transfer time (the time at which the tangent line at the inflection point of the permeation curve intersects the horizontal axis) in s; $t_{0.63}$ is the delay time (the time required for the permeation current to reach 0.63 times the steady-state permeation current value) in s.

Electrochemical hydrogen permeation testing is widely used for evaluating hydrogen barrier properties in non-high temperature service coatings due to its simple experimental setup, ease of operation, relatively low cost, and high accuracy of test results.[158–160] The primary limitation of this method is that the electrolytic hydrogen production process struggles to realistically simulate the permeation mechanism of high-pressure gaseous hydrogen in practical applications such as hydrogen storage and transportation. Additionally, prolonged immersion in electrolyte during testing may affect the surface condition of the specimens.[110]

5.2.3 *In situ* gaseous hydrogen permeation tests. To meet the laboratory simulation requirements for the actual operating temperatures and gaseous conditions of hydrogen

© 2026 The Author(s). Co-published by the Institute of Process Engineering, Chinese Academy of Sciences and Royal Society of Chemistry

Open Access Article. Published on 14 May 2026. Downloaded on 6/5/2026 2:11:30 AM. This article is licensed under a Creative Commons Attribution-NonCommercial 3.0 Unported Licence.

pipelines, an *in situ* gaseous hydrogen permeation test has been developed. It is based on the Devanathan–Stachurski double electrolytic cell, innovatively replacing the hydrogen charged side of the electrolyte cell with a high-pressure gas autoclave to achieve *in situ* hydrogen permeation measurement under high-pressure gaseous hydrogen environments.[161] As shown in Fig. 9c, the apparatus consists of a high-pressure gas vessel on the hydrogen-charged side, a hydrogen measurement cell, and the sample. Its hydrogen measurement principle is identical to that of the electrochemical hydrogen permeation test described in section 5.2.2. Hydrogen atoms diffusing from the gas vessel to the hydrogen measurement cell are oxidized by the applied anodic potential, yielding a hydrogen permeation current curve.

The *in situ* gaseous hydrogen permeation test more closely aligns with the actual service environment of pipelines, making this method widely adopted in hydrogen permeation research on pipeline steels. However, its application in evaluating the performance of HBCs for hydrogen transport pipelines remains relatively limited, primarily due to signal detection sensitivity. For bare steel specimens, detectable hydrogen permeation current signals are already extremely weak, typically in the microampere or even nanoampere range.[88] For coating specimens with superior hydrogen barrier properties, the permeation flux will further significantly decay, making it uncertain whether a stable detectable current signal can be generated. Therefore, overcoming the signal detection bottleneck and achieving high-pressure *in situ* gaseous permeation measurement of HBCs is crucial for evaluating coating performance under real-world service conditions. This, in turn, is decisive for guiding the design and application of highly reliable HBCs.

5.2.4 Thermal desorption spectrometry tests. The above tests all involve monitoring hydrogen permeation during hydrogen charging, whereas the thermal desorption spectrometry (TDS) test obtains the hydrogen diffusion coefficient based on the hydrogen release characteristics of pre-charged samples.[162] In TDS tests, pre-hydrogenation refers to the process of introducing hydrogen into the specimen beforehand *via* high-pressure hydrogen environments, aqueous solution electrolysis, or molten salt methods. For hydrogen-containing or pure hydrogen pipeline steel specimens, high-pressure hydrogen environments are typically used for pre-hydrogenation, and specimens are usually stored in liquid nitrogen to prevent hydrogen escape prior to measurement. During formal testing, the pre-hydrogenated specimen is continuously heated to a constant temperature in a vacuum furnace to induce desorption of internal hydrogen. A mass spectrometer monitors the instantaneous hydrogen release rate, yielding a hydrogen concentration *versus* time curve. Analysis of this curve, combined with the following equation,[163] enables determination of the material's hydrogen diffusion coefficient.

$$D_{\mathrm{app}} = \frac{2.3m}{\left(\frac{\pi}{l}\right)^2 + \left(\frac{2\beta_1}{d}\right)^2} \tag{8}$$

where D_{app} is the hydrogen diffusion coefficient in $m^2\ s^{-1}$; m is the slope of the linear decay segment in dimensionless; l is the sample length in m; β_1 is the root of the Bessel function; d is the sample diameter in m.

Depending on the heating method employed, TDS tests can also yield the function of hydrogen atom desorption rate (ppm s^{-1}) as a function of temperature (°C), thereby enabling analysis of the hydrogen trap type and its binding energy with hydrogen.[7,88] Yoo *et al.*[141] analyzed hot-pressed steel specimens with different coatings using TDS analysis. The results indicated that the A93-T coating (Fe_2Al_5 + FeAl + ferrite) exhibited the best hydrogen barrier properties, significantly outperforming the A93-t coating (FeAl + ferrite) and the A95-T coating (FeAl + coarsened ferrite). This conclusion is based on analysis of hydrogen atom desorption rate curves, where the peak area directly correlates to the total hydrogen content in the coating/substrate after pre-charging hydrogen, as shown in Fig. 10. The low-temperature peak area (approximately 50–100 °C) in Fig. 10a1 indicates hydrogen escaping from traps within the A93-T coating, which possess low hydrogen binding energy. The high-temperature peak area (approximately 100–200 °C) represents hydrogen escaping from traps within the substrate, which possess high hydrogen binding energy. Combining Fig. 10a2–a4, the hydrogen desorption peak area for the A93-T substrate is the smallest, indicating that the A93-T coating effectively blocked hydrogen atom permeation during the pre-hydrogenation process. From the perspective of complete desorption time, the A93-T substrate exhibited the longest hydrogen complete desorption time (7 weeks), indicating that the A93-T coating effectively restricted hydrogen atom escape during desorption. In summary, the A93-T coating demonstrates the optimal hydrogen barrier capability.

5.2.5 Inverse gas chromatography. Inverse gas chromatography (IGC) analysis is a well-established surface thermodynamic method. Different from hydrogen permeation tests, which detect hydrogen content, it indirectly reflects a coating material's hydrogen barrier capability by examining its interaction with hydrogen molecules. Generally, the stronger the interaction force between hydrogen molecules and the metal material surface, the easier it is for hydrogen molecules to adsorb and dissociate into hydrogen atoms on the surface. This ultimately increases the likelihood of hydrogen dissolving into the material interior, leading to reduced mechanical properties. IGC analysis operates on this principle: the test material is placed in a chromatographic column, while a carrier gas (*e.g.*, argon) carries the target gas molecules (such as hydrogen) as a "probe" into the column. The interaction strength between the material and the probe molecules is quantified by measuring the time taken for the probes to traverse the column and reach the detector.[164]

However, the key quantitative metric in IGC analysis—the residence time of hydrogen within the coating material—is susceptible to variations in the material's microstructure, leading to inconsistent test results.

© 2026 The Author(s). Co-published by the Institute of Process Engineering, Chinese Academy of Sciences and Royal Society of Chemistry

Open Access Article. Published on 14 May 2026. Downloaded on 6/5/2026 2:11:30 AM.
This article is licensed under a Creative Commons Attribution-NonCommercial 3.0 Unported Licence.

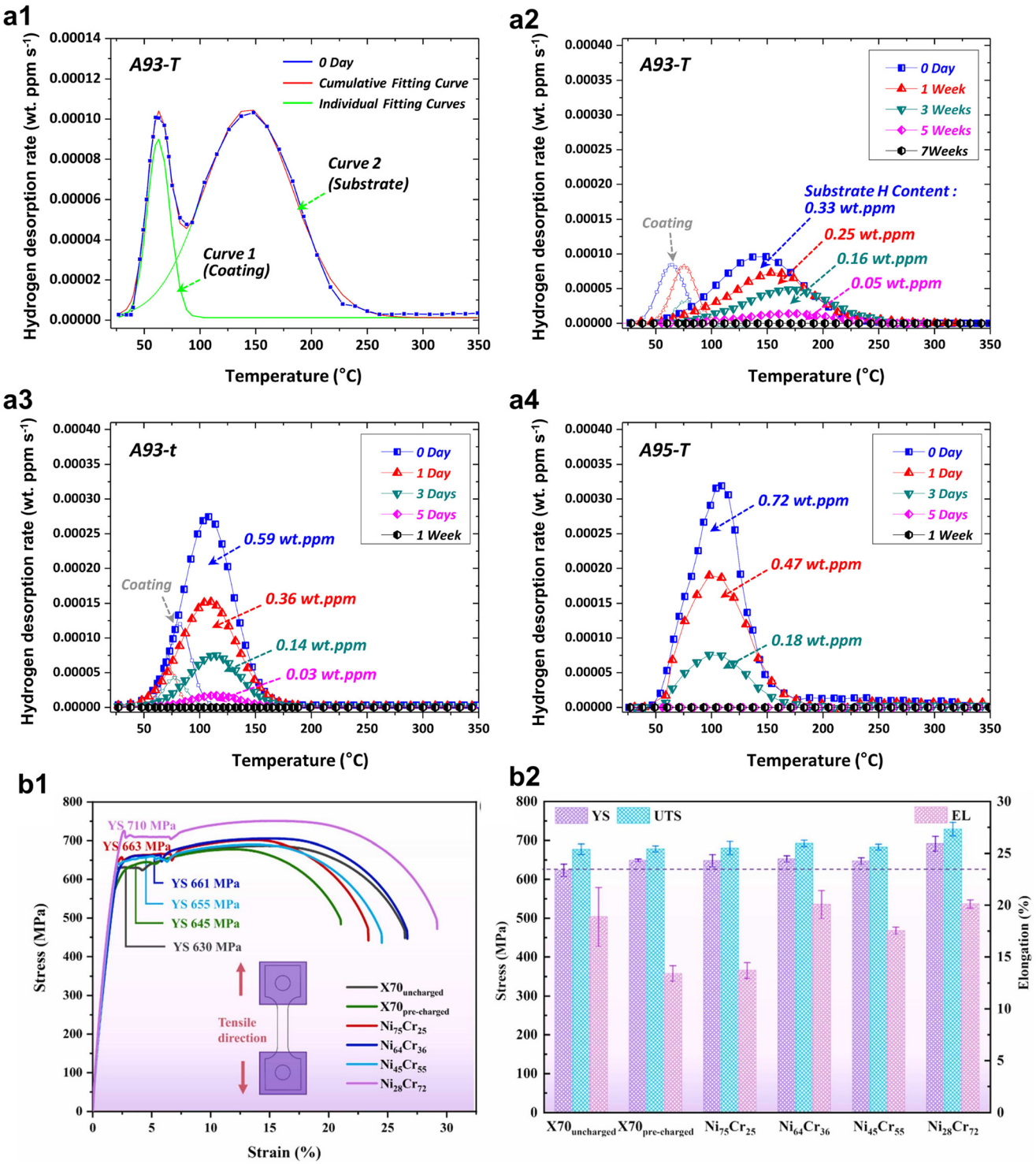

Fig. 10 Hydrogen desorption rate curves of (a1 and a2) A93-T, (a3) A93-t, and (a4) A95-T coatings/substrates obtained by TDS after pre-charging hydrogen. Reproduced with permission.[141] Copyright 2022, Elsevier; (b1) stress–strain curve, (b2) yield strength (YS), ultimate tensile strength (UTS), and elongation at fracture (EL) derived from (b1). Reproduced with permission.[19] Copyright 2024, Elsevier.

Consequently, IGC analysis provides only a rapid, quantitative method for evaluating hydrogen barrier performance in coatings and cannot be used for long-term hydrogen barrier testing under real high-pressure hydrogen environments.

5.3 Evaluation for the protective effect on mechanical properties

HBCs applied to pipeline steel in hydrogen environments prevent hydrogen permeation, thereby avoiding degradation

© 2026 The Author(s). Co-published by the Institute of Process Engineering, Chinese Academy of Sciences and Royal Society of Chemistry

Open Access Article. Published on 14 May 2026. Downloaded on 6/5/2026 2:11:30 AM.
This article is licensed under a Creative Commons Attribution-NonCommercial 3.0 Unported Licence.

of the steel's mechanical properties due to hydrogen-induced microstructural changes. This prevents hazards such as HE that threaten hydrogen energy transportation safety. Therefore, it is essential to conduct systematic evaluations of the protective efficacy of HBCs on pipeline steel's mechanical properties. The fundamental mechanical properties of pipeline steel, such as ductility and fatigue characteristics, are susceptible to hydrogen effects. Mainstream evaluation methods for these properties include slow strain rate tensile testing and fatigue crack propagation testing. Comparing the mechanical property changes of coated *versus* uncoated metallic materials under hydrogen exposure through these tests is a critical component of the hydrogen barrier coating evaluation system for hydrogen pipelines.

5.3.1 Slow strain rate tensile tests. Slow strain rate tensile tests (SSRT) are used to evaluate HE resistance by comparing results from slow strain tensile experiments conducted at constant elongation rates under hydrogen-filled conditions *versus* control media. Commonly compared data include elongation, reduction of area, fracture time, and maximum fracture stress. Existing research indicates that hydrogen primarily affects the tensile properties of pipeline steels by reducing ductility, specifically diminishing fracture elongation and reduction of area.[8] The HE index F_H (eqn (9)) can be calculated based on reduction of area to quantify a material's HE sensitivity and evaluate the extent of its mechanical property degradation.

$$\begin{cases} \mathrm{AR} = (S_0 - S_A)/S_0 \times 100\% \\ F_H = (\mathrm{AR}_0 - \mathrm{AR}_H)/\mathrm{AR}_0 \times 100\% \end{cases} \quad (9)$$

where S_0 and S_A are the cross-sectional areas of the specimens before and after stretching, respectively; and AR_0 and AR_H are the area reduction values in the inert and experimental gas (pure or hydrogen-doped) environments, respectively.

Numerous SSRT tests have shown that the application of HBCs is an effective strategy to significantly improve the HE resistance of pipeline steels in hydrogen environments. Samanta *et al.*[18] found that after cathodic hydrogen charging, the elongation at break of X70 steel specimens was reduced from 20.1% to 17.6%. When the specimens were coated with Ni–P coating with amorphous structure, the elongation at break exceeded 20% with or without a hydrogen environment, indicating that the coated specimens had lower HE susceptibility. Zhu *et al.*[165] compared two kinds of coated X80 steels in a hydrogen compressed natural gas environment, proving that epoxy resin coatings could significantly reduce the HE susceptibility of X80 steel. The protective effect of the ionic liquid-modified epoxy resin composite coating on X80 steel was even better, reducing the HE index of X80 steel from 34.44% to 16.17% under a 5 MPa hydrogen partial pressure environment. Liu *et al.*[47] investigated the effect of CrN coating density on protective performance. It was shown that a dense CrN coating formed by 2 min per cycle ion bombardment could maintain the fracture elongation and yield strength of X70 steel in a hydrogen environment at levels comparable to those in a non-hydrogen environment. This prevented degradation of the X70 steel's mechanical properties. Meng *et al.*[19] investigated the influence of microstructure in Ni/Cr composite coatings on protective performance. As shown in Fig. 10b, the coated specimens were observed to exhibit higher yield strength, tensile strength, and elongation at break compared to the uncoated substrate. Furthermore, the protective effect of coatings on steel mechanical properties improved with increasing Cr content. Among them, the $Ni_{28}Cr_{72}$-coated steel specimen with the highest Cr content exhibited the highest yield strength and tensile strength, reaching 691 ± 19 MPa and 728 ± 17 MPa respectively, with an elongation at fracture of 20.1 ± 0.4%. Therefore, existing research fully confirms that both inorganic and organic coatings can effectively block hydrogen permeation, thereby improving the mechanical properties of the substrate in hydrogen environments and reducing HE sensitivity.

5.3.2 Fatigue tests. Fatigue is a critical failure mechanism for metallic materials subjected to cyclic stress, encompassing properties such as fatigue crack growth rate, fatigue life, and fatigue limit. In-service natural gas pipeline steels face significant fatigue failure risks due to frequent pressure fluctuations and temperature variations.[7] This risk is exacerbated when pipeline steel carries hydrogen-containing fluids or pure hydrogen, primarily manifested through a reduction in the threshold stress intensity factor ΔK_0 and an increase in the fatigue crack growth rate da/dN. Currently, fatigue performance is typically evaluated according to ASTM E647 (standard test method for measurement of fatigue crack growth rates), established by the American Society for Testing and Materials.

However, research on the fatigue characteristics of coated specimens remains at a preliminary stage. For instance, although hydrogen pressure cycling tests were conducted by Junichiro Yamabe *et al.*[166] on notched coated tubular specimens in hydrogen at 85 °C and 95 MPa, demonstrating that the coating effectively improved the fatigue life of the stainless steel substrate in a hydrogen environment, the fatigue crack growth behavior of the coated specimens has not yet been analyzed. Therefore, to comprehensively evaluate and develop hydrogen-resistant coatings that provide comprehensive mechanical protection for pipeline steel in high-pressure hydrogen environments, fatigue testing of coated specimens under hydrogen conditions needs to be performed. Such studies are essential to address the current gaps in the fatigue performance evaluation system.

5.4 Applicability evaluation in pipeline transportation environments

In pipeline transportation environments, the durability of HBCs is influenced by the inherent properties of both the coating and substrate materials. Moreover, their delamination failure represents a typical thermo-mechano-chemical

© 2026 The Author(s). Co-published by the Institute of Process Engineering, Chinese Academy of Sciences and Royal Society of Chemistry

Open Access Article. Published on 14 May 2026. Downloaded on 6/5/2026 2:11:30 AM.
This article is licensed under a Creative Commons Attribution-NonCommercial 3.0 Unported Licence.

coupled process, as illustrated in Fig. 11. Therefore, to evaluate the compatibility of HBCs with pipelines, it is necessary to consider the effects of environmental coupling factors and coating/substrate performance.

5.4.1 The influence of temperature. Long-distance hydrogen transmission pipeline systems experience significant temperature fluctuations due to variations in transported media and diurnal/seasonal ambient changes. Under these conditions, the difference in the coefficient of thermal expansion (CTE) between the coating and the substrate induces interfacial thermal stress. This thermal stress reduces both the cohesion[167] and adhesion of the coating, representing a primary cause of coating failure. To mitigate temperature effects on coatings, the CTE of materials must be considered. The CTE is determined by atomic radius, bond strength, and crystal packing density.[124] It can be regulated through elemental composition design. Hayashi[168] combined experimental and molecular dynamics simulation methods to study yttria-stabilized zirconia (YSZ) coatings. It was found that as the Y_2O_3 content increased, the decreased Zr–O and Y–O distances led to an increase in binding energy of the crystal and bulk modulus, resulting in a reduced CTE. Optimization of the fabrication process can partially mitigate CTE mismatch. For example, ceramic layers deposited by magnetron sputtering often exhibit a columnar crystal structure. The gaps between columns provide buffer space for thermal expansion. Another feasible approach is the structural design of an interlayer. Materials with a CTE similar to that of the substrate are commonly used as an intermediate layer to enhance adhesion between the substrate and coating. However, although interlayers can partially alleviate CTE mismatch, inherent differences between layers remain unavoidable. These differences become more pronounced with increasing temperature, leading to the accumulation of thermal stress. This may result in crack propagation and eventual interfacial delamination. Therefore, temperature adaptability testing is essential to validate the structural stability of coating materials under thermal cycling conditions.

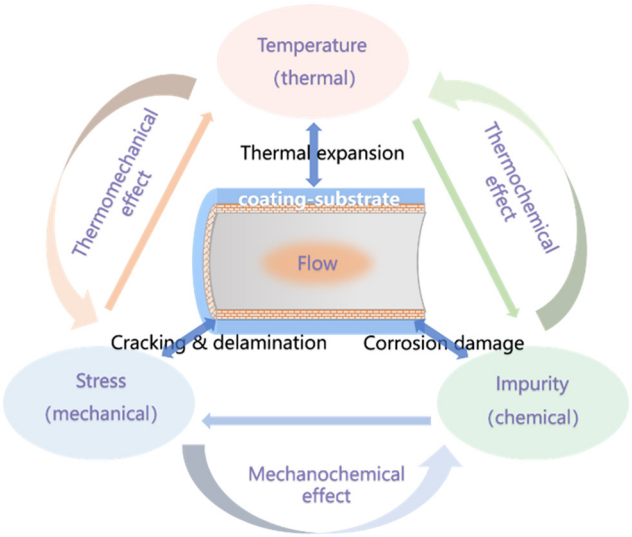

Fig. 11 Environmental coupling factors affecting the adaptability of hydrogen pipeline coatings.

5.4.2 The influence of stress. Interfacial stresses, including both thermal and mechanical stresses, are considered key factors leading to the failure of coatings during service. In addition to the thermal stresses induced by temperature fluctuations in the service environment, coatings prepared at elevated temperatures often contain residual thermal stress. Hydrogen transmission pipeline systems are also subjected to various mechanical stresses, such as bending stress and stresses generated by the transported media.[88,141] Among these, stresses induced by the transported media can fluctuate due to changes in downstream supply and demand. Under multi-source stresses, stress concentrations are formed at geometric discontinuities or interfacial defects within the coating. Once the critical stress is exceeded, microcracks initiate. Subsequent crack propagation leads to coating cracking or even delamination failure. Currently, the state of residual thermal stress can be evaluated using the Stoney equation:[124]

$$\sigma = \frac{1}{6}\frac{E_s T_s}{(1-\nu_s)t}\left(\frac{1}{R_n} - \frac{1}{R_0}\right) \quad (10)$$

where E_s, ν_s, t, T_s, R_0, and R_n represent the Young's modulus, Poisson's ratio, substrate thickness, coating thickness, and the radius of curvature of the substrate and coating, respectively. By controlling these parameters, the residual stress in the coating can be optimized to reduce the risk of failure. Furthermore, analyzing the stress state of the coating under environmental loading conditions and understanding its failure mechanisms under complex stress scenarios are essential for evaluating the suitability of HBCs for pipeline applications.

5.4.3 The influence of impurities. Hydrogen-blended natural gas pipelines typically contain impurities such as H_2S, CO_2, and Cl^-, presenting challenges of multi-component acidic corrosion. Existing internal coatings are usually made of inert materials with excellent chemical stability, which are difficult to react directly with corrosive media in the environment. However, surface defects in the coating—such as pores, cracks, or scratches—can provide pathways for the permeation of corrosive media. The permeation of these media disrupts the coating's microstructure and reduces its overall mechanical properties. Over time, corrosive media reach the coating/substrate interface, inducing localized corrosion of the metal. The accumulation of loose corrosion products at the interface further weakens coating adhesion. Eventually, under continuous exposure to corrosive conditions, macroscopic coating delamination occurs, resulting in a complete loss of protective functionality. Currently, electrochemical impedance spectrometry (EIS) is widely used to investigate the corrosion behavior of coating materials, evaluating their corrosion resistance through analysis of Nyquist and Bode plots.[83,86,169] It is generally

© 2026 The Author(s). Co-published by the Institute of Process Engineering, Chinese Academy of Sciences and Royal Society of Chemistry

Open Access Article. Published on 14 May 2026. Downloaded on 6/5/2026 2:11:30 AM. This article is licensed under a Creative Commons Attribution-NonCommercial 3.0 Unported Licence.

accepted that in Bode plots, the low-frequency impedance modulus is generally regarded as an indicator of corrosion resistance, with higher values corresponding to better performance.[86]

However, in actual corrosion processes, the synergistic effect of temperature and stress is considered a key accelerating factor. Meanwhile, corrosion itself also amplifies the influences of temperature and stress on the coating. Predicting the service life of coatings by accounting for thermo–mechano-chemical coupling factors—such as temperature, stress, and corrosive media—will be essential for the application of HBCs.

5.4.4 The influence of gas flow. The high-flow state of transported media is a distinctive feature of hydrogen transport in pipelines compared to other hydrogen application scenarios. Under flowing conditions, the actual hydrogen permeation behavior of barrier coatings is likely to be more complex. However, this factor has been largely overlooked in existing evaluations of the hydrogen resistance of coatings. Such a discrepancy fails to reflect the actual application effectiveness of HBCs. Existing studies have preliminarily indicated that flowing conditions can enhance hydrogen permeation within materials. Compared to static environments, hydrogen exhibits higher activation energy and mobility under flow, making it more likely to bind to specific sites on material surfaces and significantly increasing the probability of dissociative adsorption.[88] Nevertheless, there is still a lack of in-depth research on the hydrogen permeation behavior of barrier coatings under flowing conditions. This issue involves numerous complex factors, including fluid boundary layer effects, surface density and roughness, and gas components. To better evaluate the suitability of HBCs for pipeline transport conditions, it is essential to account for these complexities when analyzing the influence of flow on coating performance.

5.4.5 The influence of coating–substrate interactions. Strong adhesion to the substrate is a prerequisite for coatings with excellent pipeline adaptability. In this context, the coating, the coating/substrate interface, and the substrate should be considered as an integrated system. The deformation compatibility of this system is influenced by both hardness and toughness, which collectively determine its overall performance[124] and long-term service stability. Therefore, balancing the trade-off between hardness and toughness to develop hard yet tough coatings is crucial for further enhancing the pipeline adaptability of coatings.

Hardness is defined as the ability of a material to resist permanent plastic deformation under localized loading, which is specifically reflected in high wear resistance. This property enhances the coating's ability to resist erosion from flowing media. The toughness of hard coatings can be effectively improved through nanocrystalline or amorphous structural designs. Such microstructural modifications enhance deformation compatibility while maintaining wear resistance.[18] Ou *et al.*[170] produced a toughened CrN/Si_3N_4 multilayer coating through the addition of silicon. With increasing silicon content, the coating's microstructure transitioned from flaky columnar crystals to dense nanofibrous grains, achieving an elastic recovery rate of 58.5%. In a separate study, Samanta *et al.*[18] regulated phosphorus content to obtain amorphous NiP coatings in three alloy forms—near-eutectic, hypereutectic, and hypoeutectic—demonstrating superior toughness. As shown in Fig. 12a, wear tests indicated that the nanocrystalline structure of CrN/Si_3N_4 exhibits excellent deformation compatibility. Even under severe plastic deformation, excellent surface integrity was maintained. The amorphous structure of NiP not only provides toughness but also further enhances wear resistance in Fig. 12b. Under all applied loads, the three types of amorphous NiP coatings demonstrated lower wear depths. Furthermore, improving the deformation compatibility of the coating–substrate system can enhance resistance to crack propagation under coupled thermo-mechano-chemical conditions, thereby avoiding coating-induced brittle fracture.

Toughness refers to the ability of a material to absorb energy during plastic deformation until failure, which can be characterized by bending performance. In bend tests, the bend angle at peak load is used to evaluate the bendability of materials.[141] This parameter effectively reflects the deformation compatibility of the coating/substrate system. As shown in Fig. 13a–e, the failure process of the hard coating–substrate system (A93-T) can be divided into four main stages: (1) formation of micro V-cracks; (2) increase in the number and size of V-cracks; (3) initiation and propagation of shear cracks at the tips of V-cracks; (4) stable propagation of shear cracks leading to final failure. In comparison, the toughened coating/substrate system (A95-T) can absorb most of the energy from bending deformation. No cracks or defects were observed in the coating–substrate system before a bending load angle of 65°. As the bending load angle increased from 68° to 71°, wide groove-like defects developed into V-cracks on the coating surface. While the substrate remained unaffected, with no grooves or cracks observed. Eventually, when the bending load angle reached 74°, shear cracks initiated and propagated at the coating–substrate interface due to the inherent hardness mismatch, resulting in failure. Throughout this process, no significant V-cracks formed in the substrate during the entire process, which reveals that the toughened coating–substrate system possesses superior deformation compatibility, allowing it to absorb energy and mitigate crack propagation. In addition, hydrogen was observed to promote the aforementioned bending failure process. As shown in Fig. 13j–l, the fully hydrogen-desorbed specimen (7 weeks) exhibited the highest peak bending load angle, consistent with the uncharged specimen. As the hydrogen desorption time decreased (*i.e.*, hydrogen content increased), the bending load angles of the coating–substrate specimens decreased, indicating a reduction in deformation compatibility. To achieve a coating–substrate system that combines both hardness and toughness, the role of hydrogen must be considered. This is

© 2026 The Author(s). Co-published by the Institute of Process Engineering, Chinese Academy of Sciences and Royal Society of Chemistry

Open Access Article. Published on 14 May 2026. Downloaded on 6/5/2026 2:11:30 AM.
This article is licensed under a Creative Commons Attribution-NonCommercial 3.0 Unported Licence.

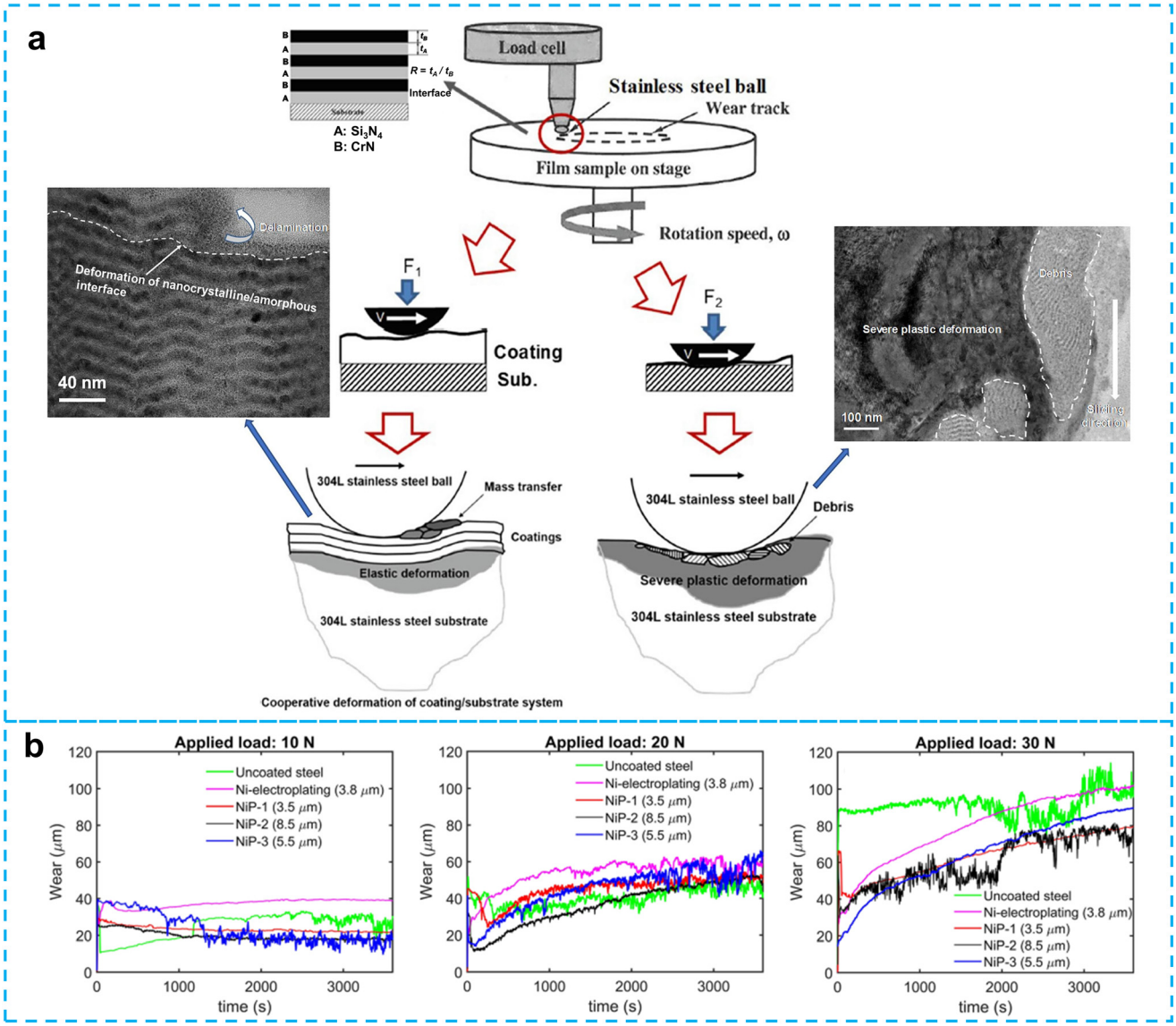

Fig. 12 (a) Deformation of the nanocrystalline structure in the CrN/Si_3N_4 multilayer coatings under different normal loads during dry sliding wear tests, with two HRTEM images showing details of coordinated deformation at the normal load of 1 N and 4 N. Reproduced with permission.[170] Copyright 2020, Elsevier; (b) Wear penetration depth *versus* test time for substrate and NiP-coated specimens under applied loads of 10 N, 20 N, and 30 N. Reproduced with permission.[18] Copyright 2022, Springer Nature.

essential for further improving the pipeline adaptability of HBCs.

5.5 Industrial performance indexes

To effectively bridge the gap between fundamental laboratory research and practical pipeline engineering requirements, and to provide a standardized reference for the future industrial application of HBCs, the proposed "full-chain evaluation framework" was aligned with existing industry standards. The key performance indexes, test methods, and representative standards for each evaluative dimension are summarized in Table 4.

It should be noted that the diversified and fragmented nature of the test methods and standards listed in the table objectively reflects the current absence of prescriptive standards specifically tailored for HBCs in hydrogen pipelines. The intrinsic differences between various coating materials result in evaluation methods that are often constrained to independent or even cross-disciplinary localized standards. Presently, industry practice predominantly relies on conventional internal pipeline coating standards, supplemented by specialized tests in high-pressure hydrogen environments to verify product suitability. Such a decentralized approach is detrimental to the selection of coating materials, the adoption of fabrication methods, the definition of performance indexes, and the establishment of industrial acceptance criteria. Just as ASME B31.12 has established the industry code for hydrogen pipelines, this full-chain evaluation framework is intended to foster

© 2026 The Author(s). Co-published by the Institute of Process Engineering, Chinese Academy of Sciences and Royal Society of Chemistry

Open Access Article. Published on 14 May 2026. Downloaded on 6/5/2026 2:11:30 AM.
This article is licensed under a Creative Commons Attribution-NonCommercial 3.0 Unported Licence.

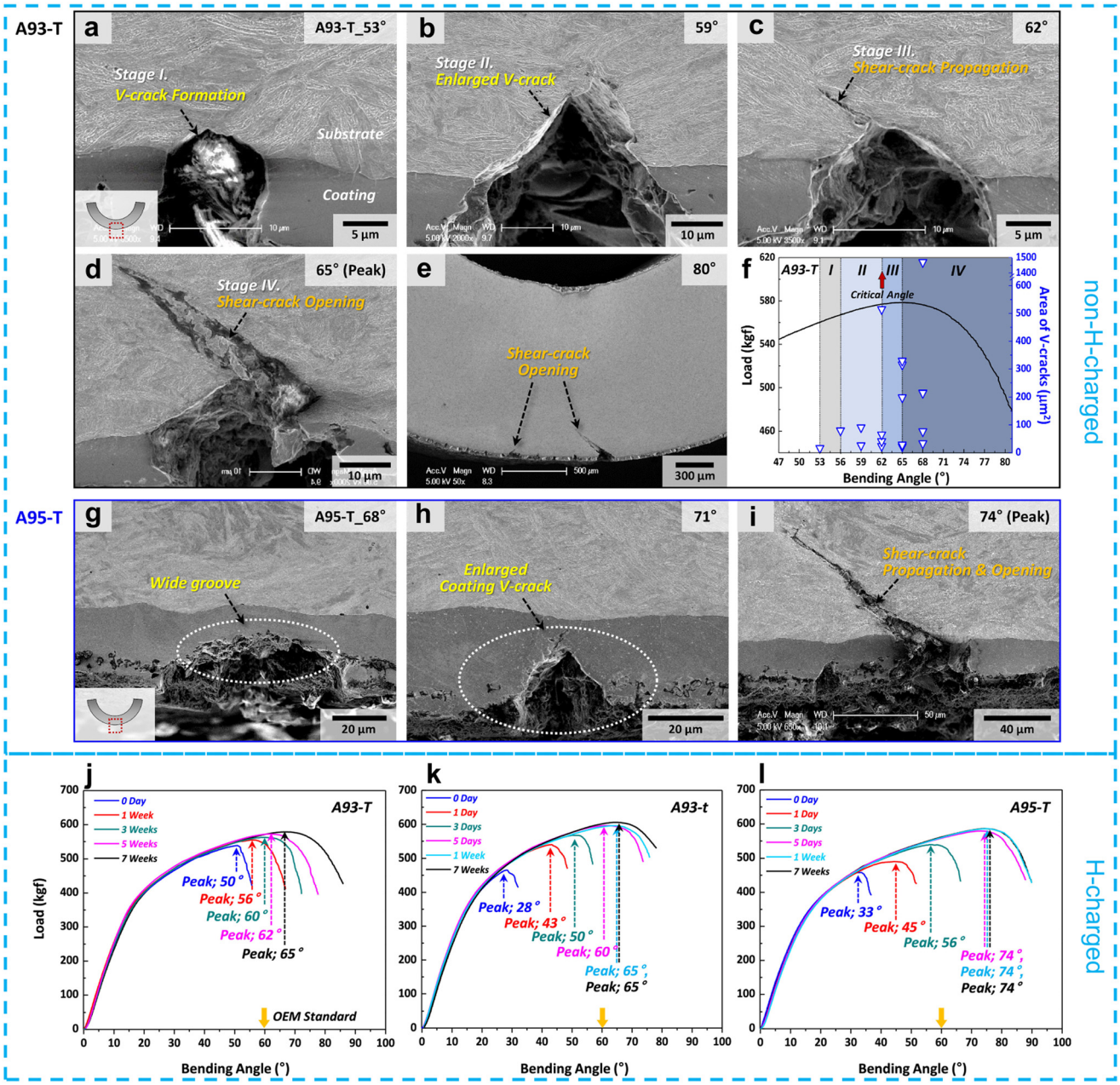

Fig. 13 (a–e) Continuous cracking process of the non-H charged A93-T and (g–i) A95-T coating–substrate systems during bending tests; (f) shows the variation of crack area with bending angle and the load-bending angle curve; (j–l) load-bending angle curves of the three H-charged coating–substrate systems. Reproduced with permission.[141] Copyright 2022, Elsevier.

consensus on the development of supporting standards for HBCs. The ultimate objective is to facilitate the transition of HBC applications from laboratory-scale research to industrial standardization.

6 Application of HBCs in industrial pipelines

To facilitate the transition of coating technologies from the laboratory to large-scale applications, a balance must be achieved among engineering feasibility, overall hydrogen barrier performance, and adaptability to complex service environments, while taking economic costs into account. Currently, polymer coatings applied by spraying are commonly used for corrosion protection in industrial pipelines, and surface pretreatment is employed to enhance the interfacial bond strength between the coating and the substrate.[171] In the field of hydrogen transport, the hydrogen blending ratio in high-pressure natural gas networks is generally 20% or lower. Under such conditions, hydrogen can be safely transported with virtually no modifications required for the existing pipeline infrastructure.[15] However, for

© 2026 The Author(s). Co-published by the Institute of Process Engineering, Chinese Academy of Sciences and Royal Society of Chemistry

Open Access Article. Published on 14 May 2026. Downloaded on 6/5/2026 2:11:30 AM. This article is licensed under a Creative Commons Attribution-NonCommercial 3.0 Unported Licence.

Table 4 Comparison of evaluation index for HBCs in pipeline applications

Evaluation dimensions	Performance indexes	Related test methods	Representative standard[15]	Recommended thresholds	Decision-making logic	Notes
Preparation quality	Density	Porosity measurement	ASTM B809	Depending on the type of coating and the test methods	Fundamental thresholds	At present, there is a distinct lack of unified, standardized methodologies for evaluating the comprehensive barrier performance of HBCs in pipeline applications. The majority of existing test techniques are implemented as adaptations of conventional standards
		microscopic characterization	ISO 21809-2			
	Adhesion	Scratch/indentation test	ASTM D6647			
		Blister/bulge/buckle test	ASTM D3359			
			ASTM D4541			
	Thickness/consistency	Non-destructive test	ASTM D7091			
		Microscopic characterization	ISO 2178			
Hydrogen barrier efficiency	Permeation rate	Hydrogen permeation test	ASTM D1434		Core indicators	
	PRF	TDS	ASTM G148			
		IGC	ISO 17081			
Mechanical protection performance	HE index	SSRT	ASTM G129		Service effectiveness	
			ASTM G142			
	Fatigue resistance	Fatigue test	ASTM E647			
		Pressure cycling test				
Applicability evaluation	Environmental tolerance	EIS	ISO 16773-2		Scenario adaptability	
			NACE TM0185			
	Coating–substrate performance	Wear test	ASTM			
		Bend test	D522/D522M			
		Peel test	ASTM G42			
		Scratch test				

application scenarios involving higher hydrogen blending ratios or even pure hydrogen, the extensive application of HBCs is deemed necessary as a critical mitigation measure against the risk of HE in pipelines. From the perspectives of cost and engineering feasibility, although extremely high hydrogen barrier efficiencies can be achieved *via* traditional techniques such as CVD and PVD, their large-scale application on pipelines spanning thousands of kilometers has not been reported.[14] It is primarily due to constraints imposed by vacuum chamber equipment and excessive energy consumption. Furthermore, the high heat input associated with such preparation methods often leads to microstructural coarsening of the substrate and residual stress accumulation, making it difficult to meet the quality requirements for high-standard engineering applications.[172] In contrast, combined with in-pipe robotic spraying technologies, polymer-based coatings can further facilitate the realization of low-cost *in situ* application.[173] Nevertheless, at critical locations within the pipeline network—particularly in regions exhibiting elevated fatigue risks or requiring an enhanced safety factor—the application of high-cost metallic or ceramic coatings is deemed engineeringly justifiable to secure absolute safety redundancy.

However, for long-distance pipelines with service lives spanning up to 30 years, the degradation and failure of coatings throughout their entire lifecycle cannot be overlooked. The failure mechanisms of these coatings evolve dynamically over the service period. In the short term, the quality of preparation is a key factor in coating failure. Geometric irregularities and residual stress concentrations at welds and heat-affected zones exacerbate localized hydrogen accumulation.[174,175] High hydrogen concentrations at the coating–substrate interface significantly accelerate coating damage or even delamination, leading to premature failure. Over the long term, coating degradation is largely determined by the service environment. Frequent cyclic loading within the pipeline is highly susceptible to inducing the initiation and propagation of fatigue microcracks in the coating. This process continuously impairs hydrogen barrier performance and accelerates hydrogen permeation, thereby amplifying the overall risk of coating failure. Furthermore, long-distance pipelines are typically equipped with cathodic protection systems. In the event of coating damage, hydrogen evolution reactions occur at the defects. The synergistic effect between evolved hydrogen and gaseous hydrogen can trigger catastrophic cathodic disbondment of the coating.[176] To address the challenges posed by these industrial applications, in-service pipeline coating robots offer an excellent comprehensive solution. By leveraging laser vision and 3D contour sensing, these robots can reconstruct weld seam topography in real time,[177] precisely plan spray gun orientation and movement trajectories, and ensure high-quality initial coating. More importantly, these robotic platforms enable the integration of surface pretreatment, *in situ* spraying, non-destructive testing, and localized coating repair. This multifunctional integration effectively addresses both short-term coating defects and long-term in-service degradation, making it crucial for ensuring the integrity of hydrogen pipeline networks throughout their entire lifecycle.

© 2026 The Author(s). Co-published by the Institute of Process Engineering, Chinese Academy of Sciences and Royal Society of Chemistry

Open Access Article. Published on 14 May 2026. Downloaded on 6/5/2026 2:11:30 AM.
This article is licensed under a Creative Commons Attribution-NonCommercial 3.0 Unported Licence.

Based on the five critical engineering dimensions identified above, a visual comparison of the large-scale application potential for four types of coating materials is presented in Fig. 14. The axes represent key comparative dimensions—namely economic feasibility, engineering feasibility, overall barrier performance, adaptability to complex environments, and long-term operational stability—ranging from "extremely low" to "extremely high". This relative distribution illustrates the trade-off relationships of the coating materials across various industrial standard dimensions. Notably, polymer-based composite coatings, which exhibit both superior economic and engineering feasibility, demonstrate significant potential for industrial-scale application.

The large-scale application of coatings further necessitates compliance with industrial acceptance standards. As previously discussed, the selection of industrial-grade coating materials should not be driven by the blind pursuit of extremely high PRF while disregarding practical engineering requirements. However, according to the analysis in section 5.5, specific evaluation standards currently do not exist for the use of HBCs as a mitigation measure for pipeline HE. In the existing ASME B31.12 standard, which is dedicated to hydrogen transport pipelines, the primary objective of coatings is the protection of the substrate against corrosion, erosion, and wear. This gap has resulted in a lack of industrial consensus regarding the application of HBCs in this context. Future research is required to further investigate the influences of coating materials, hydrogen barrier mechanisms, fabrication processes, and evaluation methodologies on the large-scale implementation of such coatings. Such efforts will facilitate the development of an application guideline for HBCs, ensuring compliance with pipeline design standards and maintaining long-term hydrogen barrier performance under diverse and complex service environments.

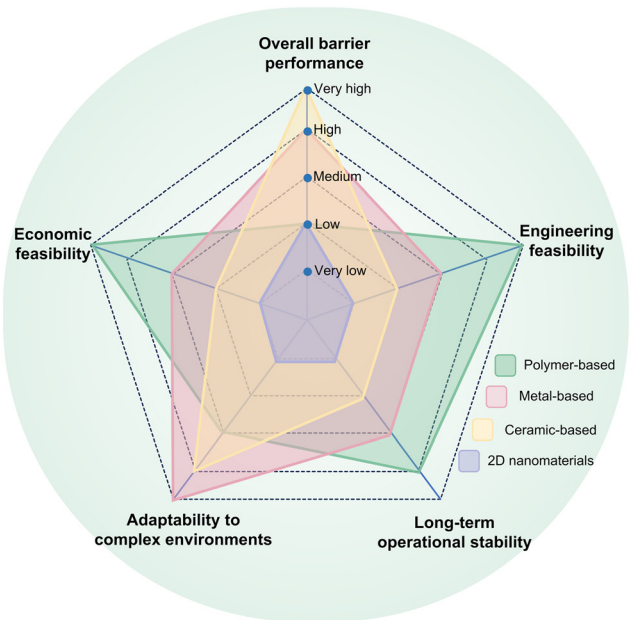

Fig. 14 A radar chart for the qualitative comparison of four mainstream HBCs in industrial applications.

7 Future development trend forecast analysis

High-performance, functionalized HBCs of excellent quality are considered essential for inhibiting hydrogen permeation, preventing hydrogen-induced failure, and ensuring the long-term safety of hydrogen pipelines. This review systematically summarizes four categories of HBCs and provides a comparative analysis of their hydrogen barrier properties. It also clarifies three hydrogen barrier mechanisms in inorganic materials: the physical barrier, the chemical barrier, and the trap capture mechanism, while the significant application potential of synergistic mechanisms in polymer composites incorporating functional fillers is emphasized. Furthermore, this review not only provides a comprehensive examination of preparation methods for HBCs but also synthesizes existing evaluation technologies. On this basis, it proposes a unified evaluation framework structured around four key criteria: preparation quality, hydrogen barrier efficiency, protective performance, and pipeline applicability. Finally, the requirements for HBCs in industrial applications are analyzed in detail.

However, the development of high-performance HBCs faces formidable challenges, primarily stemming from the specific technical requirements of hydrogen transport pipelines. These challenges are threefold: the high cost and technical difficulty of applying coatings over long distances, the complexity involved in predicting long-term service life, and the absence of a comprehensive performance test and evaluation system. To accelerate the development and enable the large-scale engineering application of these coatings for long-distance hydrogen pipelines, future research should focus on the following directions:

(1) Analysis of multi-scale hydrogen barrier mechanisms. The hydrogen barrier stability of coatings is governed by a combination of extrinsic service conditions and intrinsic material defects. Key pipeline operational factors (*e.g.*, thermal and pressure cycling, as well as corrosive medium) interact with inherent coating flaws (*e.g.*, micro-cracks and porosity introduced during fabrication), complicating hydrogen barrier mechanisms. A systematic investigation of hydrogen barrier performance is therefore required across nano-, micro-, and macro-scales under such multi-factor coupling. Future work should focus on establishing quantitative relationships between coating characteristic parameters (*e.g.*, porosity, micro-crack density) and key hydrogen barrier properties (*e.g.*, hydrogen diffusion coefficients, trap density). Clarifying the influence of these defect features on long-term barrier stability is essential to unravel the underlying inhibition mechanisms under realistic service environments.

(2) Material system design for functional coatings. The development of functional HBCs must be driven by the concurrent requirements of economic viability, superior

© 2026 The Author(s). Co-published by the Institute of Process Engineering, Chinese Academy of Sciences and Royal Society of Chemistry

Open Access Article. Published on 14 May 2026. Downloaded on 6/5/2026 2:11:30 AM. This article is licensed under a Creative Commons Attribution-NonCommercial 3.0 Unported Licence.

performance, and extended service life. Consequently, a thorough investigation is needed to elucidate the structure–property relationships between coating designs and their core properties (*e.g.*, hydrogen barrier efficiency, long-term stability, and substrate compatibility). Establishing a robust design framework founded on the "composition–structure–property" relationship is critical. This foundation will enable the creation of definitive guidelines for the design and optimization of coatings in engineering applications.

(3) Optimization of coating preparation processes and establishment of a comprehensive evaluation system. Two parallel initiatives are critical. First, the excellent engineering applicability of polymer-based composites necessitates the optimization of synthesis processes to develop coatings that combine exceptional hydrogen barrier performance, mechanical compatibility, and multifunctionality (*e.g.*, self-healing). Second, it is imperative to develop advanced testing and evaluation methods that faithfully replicate the thermo-mechano-chemical coupling encountered in real-world service, complemented by accurate life prediction models. This will enable the creation of a comprehensive, multi-metric performance evaluation system to rigorously validate coating reliability in complex, dynamic environments.

(4) Breakthroughs in application techniques for in-service pipeline coatings. To address the stringent cost and efficiency constraints, it is imperative to develop specialized application equipment and spraying techniques that enable high-quality, *in situ* coating on large-diameter pipelines under pressurized, in-service conditions. In parallel, standardized field-assessment methods for quantifying the interfacial overall performance of these coatings must be created. In the future, priority should be given to developing spraying robot technology that integrates surface pretreatment, *in situ* spraying, non-destructive testing, and localized repair in order to achieve a fully intelligent workflow. Together, success in these areas will pave the way for a comprehensive and practical engineering technology system for implementing HBCs on in-service pipelines.

Author contributions

Yuxi Chen: writing – original draft, validation, investigation. Cailin Wang: supervision, conceptualization, writing – review & editing, resourses. Cuiwei Liu: writing – review & editing. Xiusai Xu: writing – review & editing. Lianfeng Wu: writing – review & editing. Junjie Huang: writing – review & editing. Yuxing Li: conceptualization, writing-review & editing, funding acquisition.

Conflicts of interest

The authors declare no conflict of interest.

Data availability

No primary research results, software or code have been included and no new data were generated or analysed as part of this review.

Acknowledgements

This work is supported by the National Key Research and Development Program of China (2024YFE0211500), the Taishan Scholars Program for Young Experts of Shandong Province (tsqn202507114), and the Fundamental Research Funds for the Central Universities (25CX06004A).

References

1 G. Fan, H. Zhang, B. Sun and F. Pan, Economic and environmental competitiveness of multiple hydrogen production pathways in China, *Nat. Commun.*, 2025, **16**, 4284.
2 N. Johnson, M. Liebreich, D. M. Kammen, P. Ekins, R. McKenna and I. Staffell, Realistic roles for hydrogen in the future energy transition, *Nat. Rev. Clean Technol.*, 2025, **1**, 351–371.
3 S. Yuan, S. Zhang, J. Wei, Y. Gao, Y. Zhu and H. Wang, Materials selection, design, and regulation of polymer-based hydrogen barrier composite coatings, membranes and films for effective hydrogen storage and transportation: a comprehensive review, *Int. J. Hydrogen Energy*, 2024, **91**, 555–573.
4 F. Hofmann, C. Tries, F. Neumann, E. Zeyen and T. Brown, H_2 and CO_2 network strategies for the European energy system, *Nat. Energy*, 2025, **10**, 715–724.
5 Global hydrogen review, 2024, https://www.iea.org/reports/global-hydrogen-review-2024, (accessed 7 August 2025).
6 B. Sun, X. Zhang and S. Tu, Towards the intrinsic safety of hydrogen energy utilization: Progress and challenges in the study of hydrogen-induced damage, *Huagong Jinzhan*, 2025, **44**, 2898–2906.
7 X. Fan and Y. F. Cheng, Hydrogen pipelines and embrittlement in gaseous environments: An up-to-date review, *Appl. Energy*, 2025, **387**, 125636.
8 M. F. W. Chowdhury, C. V. Tapia-Bastidas, J. Hoschke, J. Venezuela and A. Atrens, A review of influence of hydrogen on fracture toughness and mechanical properties of gas transmission pipeline steels, *Int. J. Hydrogen Energy*, 2025, **102**, 181–221.
9 H. Yu, A. Díaz, X. Lu, B. Sun, Y. Ding, M. Koyama, J. He, X. Zhou, A. Oudriss, X. Feaugas and Z. Zhang, Hydrogen embrittlement as a conspicuous material challenge—Comprehensive review and future directions, *Chem. Rev.*, 2024, **124**, 6271–6392.
10 J. D. Fowler, D. Chandra, T. S. Elleman, A. W. Payne and K. Verghese, Tritium diffusion in Al_2O_3 and BeO, *J. Am. Ceram. Soc.*, 1977, **60**, 155–161.
11 E. C. E. Rönnebro, R. L. Oelrich and R. O. Gates, Recent advances and prospects in design of hydrogen permeation barrier materials for energy applications—A review, *Molecules*, 2022, **27**, 6528.
12 J. Liu, Y. Guo, X. Xing, X. Zhang, Y. Yang and G. Cui, A comprehensive review on hydrogen permeation barrier in the hydrogen transportation pipeline: Mechanism,

© 2026 The Author(s). Co-published by the Institute of Process Engineering, Chinese Academy of Sciences and Royal Society of Chemistry

Open Access Article. Published on 14 May 2026. Downloaded on 6/5/2026 2:11:30 AM. This article is licensed under a Creative Commons Attribution-NonCommercial 3.0 Unported Licence.

application, preparation, and recent advances, *Int. J. Hydrogen Energy*, 2025, **101**, 504–528.
13 E. Akbari-Kharaji, M. Shafaie, E. Sackett, J. Wood, M. B. Djukic and S. Alexander, Hydrogen barrier coatings: Application and assessment, *Int. J. Hydrogen Energy*, 2025, **180**, 151666.
14 Y. Li, M. Huard, K. Wong, X. Wang and K. F. Adane, Gap analysis of coating and liner for hydrogen pipeline, presented in part at International Pipeline Conference, Alberta, September, 2024.
15 Y. Li, M. Huard, K. Wong, X. Wang and K. F. Adane, Coatings and liners for hydrogen service pipelines, Canadian Standards Association, Toronto, 2024.
16 J. O. Noga, G. R. Piercy and J. T. Bowker, Uses and evaluation methods of potential hydrogen permeation barriers for nuclear reactor materials, Canadian Electrical Association, Montreal, 1985.
17 D. R. Chalfoun, T. M. Brizuela, C. Hurtado Noreña, F. Alvarez, A. Zavala and P. Bruzzoni, Evaluation of tungsten as a hydrogen permeation barrier in reduced activation steel F82H for nuclear fusion applications, *Int. J. Hydrogen Energy*, 2025, **136**, 833–842.
18 S. Samanta, K. Vishwanath, K. Mondal, M. Dutta and S. B. Singh, Electroless amorphous NiP coatings over API X70 steel: Resistance to wear and hydrogen embrittlement, *Met. Mater. Int.*, 2022, **28**, 397–411.
19 X. Meng, S. Xiao, C. Wu, W. Li, S. Fan, K. Shi and P. K. Chu, Enhanced hydrogen resistance of X70 pipeline steels by adaptive growth of NiCr composite coatings with cr/Fe_xNi_y inlaid structures, *J. Alloys Compd.*, 2024, **997**, 174932.
20 B. A. Kalin, V. L. Yakushin and E. P. Fomina, Tritium barrier development for austenitic stainless steel by its aluminizing in a lithium melt, *Fusion Eng. Des.*, 1998, **41**, 119–127.
21 G. W. Hollenberg, E. P. Simonen, G. Kalinin and A. Terlain, Tritium/hydrogen barrier development, *Fusion Eng. Des.*, 1995, **28**, 190–208.
22 D. K. Das, Microstructure and high temperature oxidation behavior of pt-modified aluminide bond coats on ni-base superalloys, *Prog. Mater. Sci.*, 2013, **58**, 151–182.
23 M. Goral, M. Pytel, K. Ochal, M. Drajewicz, T. Kubaszek, W. Simka and L. Nieuzyla, Microstructure of aluminide coatings modified by Pt, Pd, Zr and Hf formed in low-activity CVD process, *Coatings*, 2021, **11**, 421.
24 M. Shao, W. Mo, Y. Wu, Q. Sun, S. Xia, Y. Wang, H. Fang and K. Nishimura, Research on the microstructure and diffusion behavior of CVD aluminide coatings on inconel 718 superalloy, *Vacuum*, 2024, **228**, 113541.
25 L. Ye, H. Chen, G. Yang, B. Liu and Y. Gao, Oxidation behavior of Hf-modified platinum aluminide coatings during thermal cycling, *Prog. Nat. Sci.: Mater. Int.*, 2018, **28**, 34–39.
26 Z. Hong, L. Wang, W. Zhang, J. Yang, Y. Feng, J. Yang, H. Li, H. Yin, L. Zhang and X. Wang, Hydrogen isotope permeation behavior of AlCrFeTiNb, AlCrMoNbZr and AlCrFeMoTi high-entropy alloys coatings, *Coatings*, 2022, **12**, 171.
27 L. Hu, F. Zhong, J. Zhang, S. Zhao, Y. Wang, G. Cai, T. Cheng, G. Wei, S. Jia, D. Zhang, R. Yin, Z. Chen, C. Jiang and F. Ren, High hydrogen isotopes permeation resistance in (TiVAlCrZr)O multi-component metal oxide glass coating, *Acta Mater.*, 2022, **238**, 118204.
28 D.-G. Xie, Z.-J. Wang, J. Sun, J. Li, E. Ma and Z.-W. Shan, In situ study of the initiation of hydrogen bubbles at the aluminium metal/oxide interface, *Nat. Mater.*, 2015, **14**, 899–903.
29 D. Iadicicco, S. Bassini, M. Vanazzi, P. Muñoz, A. Moroño, T. Hernandez, I. García-Cortés, F. J. Sánchez, M. Utili and F. García Ferré, Efficient hydrogen and deuterium permeation reduction in Al_2O_3 coatings with enhanced radiation tolerance and corrosion resistance, *Nucl. Fusion*, 2018, **58**, 126007.
30 H. Wan, W. Min, D. Song and C. Chen, Research progress of hydrogen blocking coatings, *Mater. Chem. Phys.*, 2024, **328**, 130028.
31 E. Serra, H. Glasbrenner and A. Perujo, Hot-dip aluminium deposit as a permeation barrier for MANET steel, *Fusion Eng. Des.*, 1998, **41**, 149–155.
32 E. Serra, P. J. Kelly, D. K. Ross and R. D. Arnell, Alumina sputtered on MANET as an effective deuterium permeation barrier, *J. Nucl. Mater.*, 1998, **257**, 194–198.
33 J. Feng, M. Dan, F. Jin, M. Chen, L. Shen, H. Tong and G. Zhang, Preparation and properties of alumina coatings as tritium permeation barrier by plasma electrolytic oxidation, *Xiyou Jinshu Cailiao Yu Gongcheng*, 2016, **45**, 315–320.
34 J. Feng, M. Chen, H. Tong, F. Jin, M. Dan, Z. Xu, L. Shen and G. Zhang, Preparation of alumina coatings as tritium permeation barrier by a composite treatment of low temperature plasma, *Xiyou Jinshu Cailiao Yu Gongcheng*, 2017, **46**, 2837–2841.
35 S. Li, D. He, X. Liu, S. Wang and L. Jiang, Deuterium permeation of amorphous alumina coating on 316L prepared by MOCVD, *J. Nucl. Mater.*, 2012, **420**, 405–408.
36 T. Terai, T. Yoneoka, H. Tanaka, H. Kawamura, M. Nakamichi and K. Miyajima, Tritium permeation through austenitic stainless steel with chemically densified coating as a tritium permeation barrier, *J. Nucl. Mater.*, 1994, **212–215**, 976–980.
37 T. V. Kulsartov, K. Hayashi, M. Nakamichi, S. E. Afanasyev, V. P. Shestakov, Y. V. Chikhray, E. A. Kenzhin and A. N. Kolbaenkov, Investigation of hydrogen isotope permeation through F82H steel with and without a ceramic coating of Cr_2O_3–SiO_2 including $CrPO_4$ (out-of-pile tests), *Fusion Eng. Des.*, 2006, **81**, 701–705.
38 Q. Li, L.-B. Mo, J. Wang, K. Yan, T. Tang, Y.-C. Rao, W.-Q. Yao and J.-L. Cao, Performances of Cr_2O_3–hydrogen isotopes permeation barriers, *Int. J. Hydrogen Energy*, 2015, **40**, 6459–6464.
39 Z.-G. Wang, W.-D. Chen, S.-F. Yan, X.-K. Zhong, W. Ma, X.-W. Song, Y.-M. Wang and J.-H. Ouyang, Direct fabrication and characterization of zirconia thick coatings on zirconium hydride as a hydrogen permeation barrier, *Coatings*, 2023, **13**, 884.

© 2026 The Author(s). Co-published by the Institute of Process Engineering, Chinese Academy of Sciences and Royal Society of Chemistry

Open Access Article. Published on 14 May 2026. Downloaded on 6/5/2026 2:11:30 AM. This article is licensed under a Creative Commons Attribution-NonCommercial 3.0 Unported Licence.

40 V. Nemanič, P. J. McGuiness, N. Daneu, B. Zajec, Z. Siketić and W. Waldhauser, Hydrogen permeation through silicon nitride films, *J. Alloys Compd.*, 2012, **539**, 184–189.
41 Y. Wu, S. Zhu, Y. Zhang, T. Liu, Y. Rao, L. Luo and Q. Wang, The adhesion strength and deuterium permeation property of SiC films synthesized by magnetron sputtering, *Int. J. Hydrogen Energy*, 2016, **41**, 10827–10832.
42 P. Wang, J. Liu, Y. Wang and B. Shi, Investigation of SiC films deposited onto stainless steel and their retarding effects on tritium permeation, *Surf. Coat. Technol.*, 2000, **128–129**, 99–104.
43 K. Isobe, T. Yamanishi and S. Konishi, Tritium permeation behavior in SiC/SiC composites, *Fusion Eng. Des.*, 2010, **85**, 1012–1015.
44 T. Chikada, A. Suzuki and T. Terai, Deuterium permeation and thermal behaviors of amorphous silicon carbide coatings on steels, *Fusion Eng. Des.*, 2011, **86**, 2192–2195.
45 A. Qamar, A. Mahmood, T. Sarwar and N. Ahmed, Synthesis and characterization of porous crystalline SiC thin films prepared by radio frequency reactive magnetron sputtering technique, *Appl. Surf. Sci.*, 2011, **257**, 6923–6927.
46 T. Nishikiori, T. Nohira and Y. Ito, Electrochemical evaluation of high temperature hydrogen impermeability of TiN films and its dependence on film thickness, *Thin Solid Films*, 2002, **408**, 148–154.
47 L. Liu, Q. Ruan, S. Xiao, X. Meng, C. Huang, Y. Wu, R. K. Y. Fu and P. K. Chu, Fabrication and hydrogen permeation resistance of dense CrN coatings, *Surf. Coat. Technol.*, 2022, **437**, 128326.
48 J. Matějíček, J. Veverka, V. Nemanič, L. Cvrček, F. Lukáč, V. Havránek and K. Illková, Characterization of less common nitrides as potential permeation barriers, *Fusion Eng. Des.*, 2019, **139**, 74–80.
49 N. Ohtsu, T. Kozuka, Y. Shibata and M. Yamane, Effect of plasma nitriding on the structural stability and hydrogen absorption capability of Pd-coated Nb during thermal treatment, *Appl. Surf. Sci.*, 2017, **423**, 680–685.
50 R. Checchetto, M. Bonelli, L. M. Gratton, A. Miotello, A. Sabbioni, L. Guzman, Y. Horino and G. Benamati, Analysis of the hydrogen permeation properties of TiN-TiC bilayers deposited on martensitic stainless steel, *Surf. Coat. Technol.*, 1996, **83**, 40–44.
51 Z. Yao, J. Hao, C. Zhou, C. Shan and J. Yu, The permeation of tritium through 316L stainless steel with multiple coatings, *J. Nucl. Mater.*, 2000, **283–287**, 1287–1291.
52 J. Liu, H. Bi, Q. Zhang, S. Liu, H. Li and G. Cui, Design, fabrication, and hydrogen blocking performance of alumina/zirconia functional gradient coatings, *Ceram. Int.*, 2024, **50**, 45723–45738.
53 Y. He, E. Guo, F. Zhong, B. Fu, G. Cai, D. Zhang, C. Jiang and F. Ren, A novel method for preparing α-Al_2O_3 (Cr_2O_3)/Fe–Al composite coating with high hydrogen isotopes permeation resistance, *Ceram. Int.*, 2024, **50**, 20367–20375.
54 M. Zhang, R. Zhao, Y. Ling, R. Wang, Q. Zhou, J. Wang, Y. Li and Z. Zhang, Preparation of Cr_2O_3/Al_2O_3 bipolar oxides as hydrogen permeation barriers by selective oxide removal on SS and atomic layer deposition, *Int. J. Hydrogen Energy*, 2019, **44**, 12277–12287.
55 D. He, Y. Lei, C. Zhang, S. Li, X. Liu, H. Zhang, Q. Lv, Y. Wu and L. Jiang, Deuterium permeation of Al_2O_3/Cr_2O_3 composite film on 316L stainless steel, *Int. J. Hydrogen Energy*, 2015, **40**, 2899–2903.
56 Y. Wu, D. He, S. Li, X. Liu, S. Wang and L. Jiang, Deuterium permeation properties of Y_2O_3/Cr_2O_3 composite coating prepared by MOCVD on 316L stainless steel, *Int. J. Hydrogen Energy*, 2016, **41**, 7425–7430.
57 J. Chen, Y. Hou and G. Li, Synergistic regulation of hydrogen trapping-diffusion at grain boundaries and interfacial hydrogen resistance in La_2O_3/Y-doped Cr_2O_3-based coatings, *Surf. Coat. Technol.*, 2025, **513**, 132464.
58 Y. Li, F. Barzagli, P. Liu, X. Zhang, Z. Yang, M. Xiao, Y. Huang, X. Luo, C. Li, H. Luo and R. Zhang, Mechanism and evaluation of hydrogen permeation barriers: a critical review, *Ind. Eng. Chem. Res.*, 2023, **62**, 15752–15773.
59 Y. Kim, J. Baek, S. Kim, S. Kim, S. Ryu, S. Jeon and S. M. Han, Radiation resistant vanadium-graphene nanolayered composite, *Sci. Rep.*, 2016, **6**, 24785.
60 H. Yang, Z. Shao, W. Wang, X. Ji and C. Li, A composite coating of GO-Al_2O_3 for tritium permeation barrier, *Fusion Eng. Des.*, 2020, **156**, 111689.
61 H. Wan, X. Song, Z. L. Cheng, W. Min, D. Song and C. Chen, Construction and properties of graphene oxide hydrogen-blocking coatings, *Int. J. Hydrogen Energy*, 2024, **84**, 410–419.
62 M. Tamura and T. Kumagai, Hydrogen permeability of diamondlike amorphous carbons, *J. Vac. Sci. Technol., A*, 2017, **35**, 4D101.
63 M. Garitano, L. Mendizabal, O. Hernandez-Rodriguez, E. Tabares, F. J. López, P. L. Arias, M. Oregui and E. G. Berasategui, Development of barrier coatings based on diamond-like carbon for hydrogen storage and transportation, *Surf. Coat. Technol.*, 2025, **508**, 132122.
64 S. Saha, W. Son, N. H. Kim and J. H. Lee, Fabrication of impermeable dense architecture containing covalently stitched graphene oxide/boron nitride hybrid nanofiller reinforced semi-interpenetrating network for hydrogen gas barrier applications, *J. Mater. Chem. A*, 2022, **10**, 4376–4391.
65 M. Tamura, M. Noma and M. Yamashita, Characteristic change of hydrogen permeation in stainless steel plate by BN coating, *Surf. Coat. Technol.*, 2014, **260**, 148–154.
66 R. Checchetto, A. Chayahara, H. Horino, A. Miotello and K. Fujii, A study of deuterium permeation through thin BN films, *Thin Solid Films*, 1997, **299**, 5–9.
67 C. Tang, M. K. Grosse, P. Trtik, M. Steinbrück, M. Stüber and H. J. Seifert, H_2 Permeation behavior of Cr_2AlC and Ti_2AlC MAX phase coated Zircaloy-4 by neutron radiography, *Acta Polytech.*, 2018, **58**, 69.
68 W. Ling, K. Lai, J. Chen, F. Guo, D. Kang, Z. Zhao and J. Dai, Point defects and hydrogen-permeation behavior of MAX phase Cr_2AlC coating by first-principles studies, *Nucl. Mater. Energy*, 2023, **36**, 101486.

© 2026 The Author(s). Co-published by the Institute of Process Engineering, Chinese Academy of Sciences and Royal Society of Chemistry

Open Access Article. Published on 14 May 2026. Downloaded on 6/5/2026 2:11:30 AM. This article is licensed under a Creative Commons Attribution-NonCommercial 3.0 Unported Licence.

69 M. Tamura and H. Takizawa, TiAlN/TiMoN coatings as hydrogen barriers, *J. Mater. Sci. Eng. A*, 2019, **9**, 100–117.
70 T. Kim, J. Lee, S. Kim, E. Hong and H. Lee, Hydrogen permeation barrier of carbon-doped TiZrN coatings by laser carburization, *Corros. Sci.*, 2021, **190**, 109700.
71 J. Serafin, B. Dziejarski, G. Oindo Achieng, X. Vendrell, S. Chaitoglou and R. Amade-Rovira, Comprehensive analysis of MAX phase and MXene materials for advanced photocatalysis, electrocatalysis and adsorption in hydrogen evolution and storage, *J. Ind. Eng. Chem.*, 2025, **142**, 18–33.
72 K. Shi, X. Meng, S. Xiao, G. Chen, H. Wu, C. Zhou, S. Jiang and P. K. Chu, MXene coatings: Novel hydrogen permeation barriers for pipe steels, *Nanomaterials*, 2021, **11**, 2737.
73 Y. H. Auh, N. N. Neal, K. Arole, N. A. Regis, T. Nguyen, S. Ogawa, Y. Tsuda, A. Yoshigoe, M. Radovic, M. J. Green, H. Yamaguchi and J. L. Lutkenhaus, Nacre-like MXene/polyacrylic acid layer-by-layer multilayers as hydrogen gas barriers, *ACS Appl. Mater. Interfaces*, 2025, **17**, 31392–31402.
74 F. Sarrasin, P. Memari, M. H. Klopffer, V. Lachet, C. Taravel Condat, B. Rousseau and E. Espuche, Influence of high pressures on CH_4, CO_2 and H_2S solubility in polyethylene: Experimental and molecular simulation approaches for pure gas and gas mixtures. Modelling of the sorption isotherms, *J. Membr. Sci.*, 2015, **490**, 380–388.
75 S. Guan, P. Mayes, A. Andrenacci, D. Wong and B. Shaw, Advanced two layer polyethylene coating technology for pipeline protection, presented in part at International Corrosion Control Conference, Sydney, Australia, November, 2007.
76 T. P. McAndrew, M. Audenaert, J. Petersheim, D. Garcia and T. Richards, Polyamide-11 powder coatings: Exceptional resistance to cavitation erosion, in *New developments in coatings technology*, American Chemical Society, Washington, 2007, vol. 3, pp. 190–200.
77 S. Yuan, Y. Sun, C. Yang, Y. Zhang, C. Cong, Y. Yuan, D. Lin, L. Pei, Y. Zhu and H. Wang, A novel dual-functional epoxy-based composite coating with exceptional anti-corrosion and enhanced hydrogen gas barrier properties, *Chem. Eng. J.*, 2022, **449**, 137876.
78 L. Simon, R. MacDonald and K. Goerz, Corrosion failure in a lined sour gas pipeline—part 1: Case history of incident, NACE International, Alberta, 2010.
79 EUROPIPE pipes internally lined with epoxy flow coat ready for 100 percent hydrogen, https://hydrogen-central.com/europipe-pipes-lined-epoxy-flow-coat-100-percent-hydrogen/, (accessed 10 July 2025).
80 G. B. Janaki and J. R. Xavier, Evaluation of bi-functionalized alumina-epoxy nanocomposite coatings for improved barrier and mechanical properties, *Surf. Coat. Technol.*, 2021, **405**, 126549.
81 K. Cai and B. Jiang, Preparation and characterization of composite hydrogen barrier coatings with (graphene–epoxy resin)/(silicon carbide–epoxy resin)/(graphene–epoxy resin) sandwich structures, *Coatings*, 2025, **15**, 518.
82 L. Lei, J. Zhang, G. Li, Z. Ni and Y. Yan, Improve the gas-barrier and mechanical performance of epoxy resin by Co-modification from montmorillonite and polyethylene glycol, *Int. J. Hydrogen Energy*, 2024, **65**, 751–758.
83 S. Yuan, Y. Sun, C. Cong, Y. Liu, D. Lin, L. Pei, Y. Zhu and H. Wang, A bi-layer orientated and functionalized graphene-based composite coating with unique hydrogen gas barrier and long-term anti-corrosion performance, *Carbon*, 2023, **205**, 54–68.
84 A. Mathiazhagan and R. Joseph, Nanotechnology-a new prospective in organic coating -review, *Int. J. Chem. Eng. Appl.*, 2011, 225–237.
85 K. Huang, *Master's thesis*, General Research Institute for Nonferrous Metals, Beijing, 2024.
86 H.-X. Guo, Y.-L. Wei, J.-J. Liu, C.-Y. He and X.-H. Gao, Enhanced anti-corrosion and hydrogen resistance performance for epoxy resin composite coating with modified boron nitride, *Int. J. Hydrogen Energy*, 2025, **141**, 35–45.
87 L. Zhao, B. Yuan, Y. Geng, C. Yu, N. H. Kim, J. H. Lee and P. Li, Fabrication of ultrahigh hydrogen barrier polyethyleneimine/graphene oxide films by LBL assembly fine-tuned with electric field application, *Composites, Part A*, 2015, **78**, 60–69.
88 R. Zhang, C. Wang, C. Liu, H. Zhang, M. Zhu, Y. Song, T. Zhang and Y. Li, Gaseous hydrogen permeation of pipeline steels: A focused review, *Renewable Sustainable Energy Rev.*, 2025, **211**, 115304.
89 N.-E. Laadel, M. El Mansori, N. Kang, S. Marlin and Y. Boussant-Roux, Permeation barriers for hydrogen embrittlement prevention in metals – A review on mechanisms, materials suitability and efficiency, *Int. J. Hydrogen Energy*, 2022, **47**, 32707–32731.
90 X. Li, X. Ma, J. Zhang, E. Akiyama, Y. Wang and X. Song, Review of hydrogen embrittlement in metals: Hydrogen diffusion, hydrogen characterization, hydrogen embrittlement mechanism and prevention, *Acta Metall. Sin.*, 2020, **33**, 759–773.
91 S. Zheng, Y. Qin, W. Li, F. Huang, Y. Qiang, S. Yang, L. Wen and Y. Jin, Effect of hydrogen traps on hydrogen permeation in X80 pipeline steel —— A joint experimental and modelling study, *Int. J. Hydrogen Energy*, 2023, **48**, 4773–4788.
92 M. L. Martin, M. J. Connolly, F. W. DelRio and A. J. Slifka, Hydrogen embrittlement in ferritic steels, *Appl. Phys. Rev.*, 2020, **7**, 41301.
93 Y.-S. Chen, C. Huang, P.-Y. Liu, H.-W. Yen, R. Niu, P. Burr, K. L. Moore, E. Martínez-Pañeda, A. Atrens and J. M. Cairney, Hydrogen trapping and embrittlement in metals – A review, *Int. J. Hydrogen Energy*, 2025, **136**, 789–821.
94 H. K. Birnbaum and P. Sofronis, Hydrogen-enhanced localized plasticity—A mechanism for hydrogen-related fracture, *Mater. Sci. Eng., A*, 1994, **176**, 191–202.
95 B. Sun, H. Zhao, X. Dong, C. Teng, A. Zhang, S. Kong, J. Zhou, X.-C. Zhang and S.-T. Tu, Current challenges in the utilization of hydrogen energy-A focused review on the issue of hydrogen-induced damage and embrittlement, *Adv. Appl. Energy*, 2024, **14**, 100168.

© 2026 The Author(s). Co-published by the Institute of Process Engineering, Chinese Academy of Sciences and Royal Society of Chemistry

Open Access Article. Published on 14 May 2026. Downloaded on 6/5/2026 2:11:30 AM. This article is licensed under a Creative Commons Attribution-NonCommercial 3.0 Unported Licence.

96 T. Guo, L. Qiao, X. Pang and A. A. Volinsky, Brittle film-induced cracking of ductile substrates, *Acta Mater.*, 2015, **99**, 273–280.
97 Y. Bai, T. Guo, J. Wang, J. Gao, K. Gao and X. Pang, Stress-sensitive fatigue crack initiation mechanisms of coated titanium alloy, *Acta Mater.*, 2021, **217**, 117179.
98 A. Al-Borno, H. Pedraza, J. Rogozinski and J. K. Mistry, Coating the way to a hydrogen economy: Challenges ahead, presented in part at MECC 2023, Kingdom of Bahrain, November, 2023.
99 E. R. Gilbert, R. P. Allen, D. L. Baldwin, R. D. Bell, J. L. Brimhall, R. G. Clemmer, S. C. Marschman, M. A. McKinnon, R. E. Page, H. G. Powers and S. G. Chalk, Tritium permeation and related studies on barrier treated 316 stainless steel, *Fusion Technol.*, 1992, **21**, 739–744.
100 D. Iadicicco, S. Bassini, M. Vanazzi, P. Muñoz, A. Moroño, T. Hernandez, I. García-Cortés, F. J. Sánchez, M. Utili, F. García Ferré and F. Di Fonzo, Efficient hydrogen and deuterium permeation reduction in Al_2O_3 coatings with enhanced radiation tolerance and corrosion resistance, *Nucl. Fusion*, 2018, **58**, 126007.
101 K. Shi, S. Xiao, Q. Ruan, H. Wu, G. Chen, C. Zhou, S. Jiang, K. Xi, M. He and P. K. Chu, Hydrogen permeation behavior and mechanism of multi-layered graphene coatings and mitigation of hydrogen embrittlement of pipe steel, *Appl. Surf. Sci.*, 2022, **573**, 151529.
102 Y.-S. Chen, H. Lu, J. Liang, A. Rosenthal, H. Liu, G. Sneddon, I. McCarroll, Z. Zhao, W. Li, A. Guo and J. M. Cairney, Observation of hydrogen trapping at dislocations, grain boundaries, and precipitates, *Science*, 2020, **367**, 171–175.
103 B. Meng, C. Gu, L. Zhang, C. Zhou, X. Li, Y. Zhao, J. Zheng, X. Chen and Y. Han, Hydrogen effects on X80 pipeline steel in high-pressure natural gas/hydrogen mixtures, *Int. J. Hydrogen Energy*, 2017, **42**, 7404–7412.
104 D. Zhou, T. Li, D. Huang, Y. Wu, Z. Huang, W. Xiao, Q. Wang and X. Wang, The experiment study to assess the impact of hydrogen blended natural gas on the tensile properties and damage mechanism of X80 pipeline steel, *Int. J. Hydrogen Energy*, 2021, **46**, 7402–7414.
105 Y. H. Fan, B. Zhang, H. L. Yi, G. S. Hao, Y. Y. Sun, J. Q. Wang, E.-H. Han and W. Ke, The role of reversed austenite in hydrogen embrittlement fracture of S41500 martensitic stainless steel, *Acta Mater.*, 2017, **139**, 188–195.
106 Z. W. Shan, R. K. Mishra, S. A. Syed Asif, O. L. Warren and A. M. Minor, Mechanical annealing and source-limited deformation in submicrometre-diameter Ni crystals, *Nat. Mater.*, 2008, **7**, 115–119.
107 M. Li, H. Zhang, Y. Zeng and J. Liu, Adsorption and dissociation of high-pressure hydrogen on Fe (100) and Fe_2O_3 (001) surfaces: Combining DFT calculation and statistical thermodynamics, *Acta Mater.*, 2022, **239**, 118267.
108 Y. Sun and Y. F. Cheng, Thermodynamics of spontaneous dissociation and dissociative adsorption of hydrogen molecules and hydrogen atom adsorption and absorption on steel under pipelining conditions, *Int. J. Hydrogen Energy*, 2021, **46**, 34469–34486.
109 Y. He, Y. Li, C. Chen and H. Yu, Diffusion coefficient of hydrogen interstitial atom in α-Fe, γ-Fe and ε-Fe crystals by first-principle calculations, *Int. J. Hydrogen Energy*, 2017, **42**, 27438–27445.
110 K. Zhang, C. Li, M. Fang, L. Fang, Q. Wang and Y. Chang, Research progress and prospect of hydrogen permeation-resistance coatings, *Surf. Technol.*, 2025, **54**, 1–16.
111 S. K. Bull, T. A. Champ, S. V. Raj, R. C. O'Brien, C. B. Musgrave and A. W. Weimer, Atomic layer deposited boron nitride nanoscale films act as high temperature hydrogen barriers, *Appl. Surf. Sci.*, 2021, **565**, 150428.
112 R. Wang, Y. Tang, S. Li, Y. Ai, Y. Li, B. Xiao, L. Zhu, X. Liu and S. Bai, Effect of lattice distortion on the diffusion behavior of high-entropy alloys, *J. Alloys Compd.*, 2020, **825**, 154099.
113 G. K. Nayak, A. Kretschmer, P. H. Mayrhofer and D. Holec, On correlations between local chemistry, distortions and kinetics in high entropy nitrides: An ab initio study, *Acta Mater.*, 2023, **255**, 118951.
114 J. Li, H. Xu, J. Li, X. Chen, Y. Zhang, W. Liu, W. Li, C. Han, S. An, X. Wang and X. Qiu, Construction of inorganic-rich cathode electrolyte interphase on Co-free cathodes, *ACS Appl. Mater. Interfaces*, 2023, **15**, 26627–26636.
115 Z. Huang, J.-C. Lai, S.-L. Liao, Z. Yu, Y. Chen, W. Yu, H. Gong, X. Gao, Y. Yang, J. Qin, Y. Cui and Z. Bao, A salt-philic, solvent-phobic interfacial coating design for lithium metal electrodes, *Nat. Energy*, 2023, **8**, 577–585.
116 T. Otsuka, K. Goto, A. Yamamoto and K. Hashizume, Effects of shot-peening on permeation and retention behaviors of hydrogen in alpha iron, *Fusion Eng. Des.*, 2018, **136**, 509–512.
117 P. Tremblay, M. Savard, J. Vermette and R. Paquin, Gas permeability, diffusivity and solubility of nitrogen, helium, methane, carbon dioxide and formaldehyde in dense polymeric membranes using a new on-line permeation apparatus, *J. Membr. Sci.*, 2006, **282**, 245–256.
118 D. Zheng, J. Li, B. Liu, B. Yu, Y. Yang, D. Han, J. Li and Z. Huang, Molecular dynamics investigations into the hydrogen permeation mechanism of polyethylene pipeline material, *J. Mol. Liq.*, 2022, **368**, 120773.
119 J. Zhao, X. Li, X. Wang, Q. Zhang, Q. Yang, H. Yin, S. Zhang and C. Wu, Insights into the solubility of H_2 in various polyethylene matrices at high pressure: A coarse-grained MC/MD study, *Int. J. Hydrogen Energy*, 2023, **48**, 19619–19632.
120 J. Zhao, X. Wang, Q. Yang, H. Yin, B. Zhao, S. Zhang and C. Wu, Molecular dynamics simulation of H_2 in amorphous polyethylene system: H_2 diffusion in various PE matrices and bubbling during rapid depressurization, *Int. J. Hydrogen Energy*, 2022, **47**, 39572–39585.
121 H. Kanesugi, K. Ohyama, H. Fujiwara and S. Nishimura, High-pressure hydrogen permeability model for crystalline polymers, *Int. J. Hydrogen Energy*, 2023, **48**, 723–739.
122 J. K. Jung, I. G. Kim, K. T. Kim, K. S. Ryu and K. S. Chung, Evaluation techniques of hydrogen permeation in sealing rubber materials, *Polym. Test.*, 2021, **93**, 107016.

© 2026 The Author(s). Co-published by the Institute of Process Engineering, Chinese Academy of Sciences and Royal Society of Chemistry

Open Access Article. Published on 14 May 2026. Downloaded on 6/5/2026 2:11:30 AM.
This article is licensed under a Creative Commons Attribution-NonCommercial 3.0 Unported Licence.

123 J. K. Jung, I. G. Kim, K.-T. Kim, U. B. Baek and S. H. Nahm, Novel volumetric analysis technique for characterizing the solubility and diffusivity of hydrogen in rubbers, *Curr. Appl. Phys.*, 2021, **26**, 9–15.
124 Y. X. Ou, H. Q. Wang, X. Ouyang, Y. Y. Zhao, Q. Zhou, C. W. Luo, Q. S. Hua, X. P. Ouyang and S. Zhang, Recent advances and strategies for high-performance coatings, *Prog. Mater. Sci.*, 2023, **136**, 101125.
125 D. Levchuk, F. Koch, H. Maier and H. Bolt, Deuterium permeation through Eurofer and α-alumina coated Eurofer, *J. Nucl. Mater.*, 2004, **328**, 103–106.
126 D. Levchuk, H. Bolt, M. Döbeli, S. Eggenberger, B. Widrig and J. Ramm, Al–Cr–O thin films as an efficient hydrogen barrier, *Surf. Coat. Technol.*, 2008, **202**, 5043–5047.
127 K. T. Young, C. Smith, T. M. Krentz, D. A. Hitchcock and E. M. Vogel, Graphene synthesized by chemical vapor deposition as a hydrogen isotope permeation barrier, *Carbon*, 2021, **176**, 106–117.
128 Y. Fan, Y. Huang, B. Cui and Q. Zhou, Graphene coating on nickel as effective barriers against hydrogen embrittlement, *Surf. Coat. Technol.*, 2019, **374**, 610–616.
129 D. He, S. Li, X. Liu, C. Zhang, Q. Yu, Y. Lei, S. Wang and L. Jiang, Influence of microstructure on the hydrogen permeation of alumina coatings, *Int. J. Hydrogen Energy*, 2013, **38**, 9343–9348.
130 Y. Wu, D. He, H. Zhang, S. Li, X. Liu, S. Wang and L. Jiang, Preparation of yttrium oxide coating by MOCVD as tritium permeation barrier, *Fusion Eng. Des.*, 2015, **90**, 105–109.
131 T. Wang, J. Pu, C. Bo and L. Jian, Sol–gel prepared Al_2O_3 coatings for the application as tritium permeation barrier, *Fusion Eng. Des.*, 2010, **85**, 1068–1072.
132 Z. Yao, A. Suzuki, D. Levchuk, T. Chikada, T. Tanaka, T. Muroga and T. Terai, Hydrogen permeation through steel coated with erbium oxide by sol–gel method, *J. Nucl. Mater.*, 2009, **386–388**, 700–702.
133 C. Fazio, K. Stein-Fechner, E. Serra, H. Glasbrenner and G. Benamati, Investigation on the suitability of plasma sprayed Fe–Cr–Al coatings as tritium permeation barrier, *J. Nucl. Mater.*, 1999, **273**, 233–238.
134 M. Hajjami, A. Oubelkacem, Y. Benhouria, M. Kibbou, I. Essaoudi and A. Ainane, The structural, electronic and magnetic properties of Fe_3ZnC anti-perovskite, *Chin. J. Phys.*, 2024, **91**, 575–582.
135 Tz. Boiadjieva, L. Mirkova, H. Kronberger, T. Steck and M. Monev, Hydrogen permeation through steel electroplated with Zn or Zn–Cr coatings, *Electrochim. Acta*, 2013, **114**, 790–798.
136 P. Zhou, W. Li, B. Liu and X. Jin, Communication—hydrogen permeation resistance of nickel coating enhanced by adding the rare earth element Ce, *J. Electrochem. Soc.*, 2017, **164**, D1042–D1044.
137 G. Decher, Fuzzy Nanoassemblies: Toward layered polymeric multicomposites, *Science*, 1997, **277**, 1232–1237.
138 R. Rajasekar, N. H. Kim, D. Jung, T. Kuila, J. K. Lim, M. J. Park and J. H. Lee, Electrostatically assembled layer-by-layer composites containing graphene oxide for enhanced hydrogen gas barrier application, *Compos. Sci. Technol.*, 2013, **89**, 167–174.
139 E. Kashkarov, A. Obrosov, A. Sutygina, E. Uludintceva, A. Mitrofanov and S. Weiß, Hydrogen permeation, and mechanical and tribological behavior, of CrN_x coatings deposited at various bias voltages on IN718 by direct current reactive sputtering, *Coatings*, 2018, **8**, 66.
140 K. Zhang and Y. Hatano, Sealing of pores in sol–gel-derived tritium permeation barrier coating by electrochemical technique, *J. Nucl. Mater.*, 2011, **417**, 1229–1232.
141 J. Yoo, S. Kim, M. C. Jo, S. Kim, J. Oh, S.-H. Kim, S. Lee and S. S. Sohn, Effects of Al-Si coating structures on bendability and resistance to hydrogen embrittlement in 1.5-GPa-grade hot-press-forming steel, *Acta Mater.*, 2022, **225**, 117561.
142 D. He, S. Li, X. Liu, C. Zhang, S. Wang and L. Jiang, Influence of thermal annealing on composition, morphology and crystalline phase of alumina film deposited by MOCVD, *Xiyou Jinshu*, 2012, **36**, 762–766.
143 M. C. Oliver, R. Zheng, L. Huang and M. Mehana, Molecular simulations of hydrogen diffusion in underground porous media: Implications for storage under varying pressure, confinement, and surface chemistry conditions, *Int. J. Hydrogen Energy*, 2024, **65**, 541–547.
144 C. Wang, Y. Hua, S. Nadimi, Q. Hu, W. Taleb, J. Zhang, X. Liu, R. Zhang, X. Chen, A. Neville and Y. Li, Anti-corrosion characteristics of $FeCO_3$ and $Fe_xCa_yMg_zCO_3$ scales on carbon steel in high-PT CO_2 environments, *Chem. Eng. J.*, 2022, **431**, 133484.
145 C. Wang, Y. Hua, S. Nadimi, W. Taleb, R. Barker, Y. Li, X. Chen and A. Neville, Determination of thickness and air-void distribution within the iron carbonate layers using X-ray computed tomography, *Corros. Sci.*, 2021, **179**, 109153.
146 X. Zhang, S. Aliasghari, A. Němcová, T. L. Burnett, I. Kuběna, M. Šmíd, G. E. Thompson, P. Skeldon and P. J. Withers, X-ray computed tomographic investigation of the porosity and morphology of plasma electrolytic oxidation coatings, *ACS Appl. Mater. Interfaces*, 2016, **8**, 8801–8810.
147 W. Zhu, X. N. Cai, L. Yang, J. Xia, Y. C. Zhou and Z. P. Pi, The evolution of pores in thermal barrier coatings under volcanic ash corrosion using X-ray computed tomography, *Surf. Coat. Technol.*, 2019, **357**, 372–378.
148 X. Chen, C. Shaw, L. Gelman and K. T. V. Grattan, Advances in test and measurement of the interface adhesion and bond strengths in coating-substrate systems, emphasising blister and bulk techniques, *Measurement*, 2019, **139**, 387–402.
149 V. Nemanič, Hydrogen permeation barriers: Basic requirements, materials selection, deposition methods, and quality evaluation, *Nucl. Mater. Energy*, 2019, **19**, 451–457.
150 B. Cao, M. Wang, X. Li, M. Fan and G. Tian, Noncontact thickness measurement of multilayer coatings on metallic substrate using pulsed terahertz technology, *IEEE Sens. J.*, 2020, **20**, 3162–3171.
151 T. Chikada, A. Suzuki, T. Kobayashi, H. Maier, T. Terai and T. Muroga, Microstructure change and deuterium

© 2026 The Author(s). Co-published by the Institute of Process Engineering, Chinese Academy of Sciences and Royal Society of Chemistry

Open Access Article. Published on 14 May 2026. Downloaded on 6/5/2026 2:11:30 AM. This article is licensed under a Creative Commons Attribution-NonCommercial 3.0 Unported Licence.

permeation behavior of erbium oxide coating, *J. Nucl. Mater.*, 2011, **417**, 1241–1244.
152 Q. Li, J. Wang, Q.-Y. Xiang, K. Yan, W.-Q. Yao and J.-L. Cao, Study on influence factors of permeation reduction factor of Al_2O_3 -hydrogen isotopes permeation barriers, *Int. J. Hydrogen Energy*, 2016, **41**, 4326–4331.
153 A. Perujo and K. S. Forcey, Tritium permeation barriers for fusion technology, *Fusion Eng. Des.*, 1995, **28**, 252–257.
154 H. Zhang, S. Li, D. He, M. Du, Y. Wu, S. Wang, X. Liu and L. Jiang, Influence of thickness on hydrogen permeation properties of alumina coating, *Funct. Mater.*, 2016, **47**, 11141–11144.
155 C. Zhou, M. He, S. Xiao, K. Shi, H. Wu, S. Jiang, G. Chen and C. Wu, Review on hydrogen permeation barrier coatings on stainless steels, *Huagong Jinzhan*, 2020, **39**, 3458–3468.
156 M. Okayasu and M. Sato, Examination of hydrogen diffusivity in carbon steels using a newly developed hydrogen permeation system, *Exp. Mech.*, 2021, **61**, 1443–1453.
157 M. Kupka, K. Stępień and K. Nowak, Studies on hydrogen diffusivity in iron aluminides using the devanathan–stachurski method, *J. Phys. Chem. Solids*, 2014, **75**, 344–350.
158 X. Sun, J. Xu and Y. Li, Hydrogen permeation behavior in metastable austenitic stainless steels 321 and 304, *Acta Metall.*, 1989, **37**, 2171–2176.
159 M. Moshref-Javadi, H. Edris, A. Shafyei, H. Salimi-Jazi and E. Abdolvand, Evaluation of hydrogen permeation through standalone thermally sprayed coatings of AISI 316L stainless steel, *Int. J. Hydrogen Energy*, 2018, **43**, 4657–4670.
160 X.-Z. Wang, H. Luo and J.-L. Luo, Effects of hydrogen and stress on the electrochemical and passivation behaviour of 304 stainless steel in simulated PEMFC environment, *Electrochim. Acta*, 2019, **293**, 60–77.
161 C. Wang, J. Zhang, C. Liu, Q. Hu, R. Zhang, X. Xu, H. Yang, Y. Ning and Y. Li, Study on hydrogen embrittlement susceptibility of X80 steel through in-situ gaseous hydrogen permeation and slow strain rate tensile testsX80, *Int. J. Hydrogen Energy*, 2023, **48**, 243–256.
162 S. Frappart, A. Oudriss, X. Feaugas, J. Creus, J. Bouhattate, F. Thébault, L. Delattre and H. Marchebois, Hydrogen trapping in martensitic steel investigated using electrochemical permeation and thermal desorption spectroscopy, *Scr. Mater.*, 2011, **65**, 859–862.
163 G. A. Young and J. R. Scully, The diffusion and trapping of hydrogen in high purity aluminum, *Acta Mater.*, 1998, **46**, 6337–6349.
164 M. E. Hinman and I. Ulkem, Attempts for preventing hydrogen embrittlement and solving the infrastructure problems for hydrogen gas transmission lines – A practical IGC study based on surface thermodynamics, presented in part at AMPP Annual Conference + Expo, New Orleans, March, 2024.
165 Y. Zhu, G. Liu, Z. Cui, H. Yang, F. Liu, B. Jiang and L. Chen, Effect and mechanism of ionic liquid-polymer composite coating on enhancing hydrogen embrittlement resistance of X80 pipeline steel for hydrogen blended natural gas transportation, *Int. J. Hydrogen Energy*, 2024, **80**, 1305–1316.
166 J. Yamabe and S. Matsuoka, Hydrogen uptake, tensile, and fatigue properties of a barrier-coated, precipitation-hardened martensitic stainless steel with exposure to high-pressure hydrogen gas, *J. Pressure Vessel Technol.*, 2020, **142**, 41501.
167 H. Wei, J. Xia, W. Zhou, L. Zhou, G. Hussain, Q. Li and K. Ostrikov, Adhesion and cohesion of epoxy-based industrial composite coatings, *Composites, Part B*, 2020, **193**, 108035.
168 H. Hayashi, T. Saitou, N. Maruyama, H. Inaba, K. Kawamura and M. Mori, Thermal expansion coefficient of yttria stabilized zirconia for various yttria contents, *Solid State Ionics*, 2005, **176**, 613–619.
169 Z. Zhang, W. Zhang, D. Li, Y. Sun, Z. Wang, C. Hou, L. Chen, Y. Cao and Y. Liu, Mechanical and anticorrosive properties of graphene/epoxy resin composites coating prepared by in-situ method, *Int. J. Mol. Sci.*, 2015, **16**, 2239–2251.
170 Y. X. Ou, X. P. Ouyang, B. Liao, X. Zhang and S. Zhang, Hard yet tough CrN/Si_3N_4 multilayer coatings deposited by the combined deep oscillation magnetron sputtering and pulsed dc magnetron sputtering, *Appl. Surf. Sci.*, 2020, **502**, 144168.
171 Pipeline coating, https://fastercapital.com/content/Pipeline-coating–How-to-apply-and-maintain-the-pipeline-coating-using-coating-materials-and-equipment.html, (accessed 7 October 2025).
172 Z. Wang, C. Wang, L. Wu and G. Sun, Investigation on the microstructure and mechanical properties of X70 pipeline steel fabricated by laser-directed energy deposition, *Materials*, 2025, **18**, 4997.
173 C. P. Y. Chan, Z. Qu, K. H. Shiu, C. H. So, K. H. Koh, M. Farhan, C. Y. Ho, T. H. Wong and K. W. C. Lai, In-pipe maintenance robot using spray-in-place pipe technique for long-distance and complex pipe environment, *J. Field Robot.*, 2025, **42**, 1226–1243.
174 Y. Wang, X. Xu, Y. Ning, Y. Chen, C. Wang, C. Liu and Y. Li, Effect of non-metallic inclusions on hydrogen-induced cracking in pipeline steels: A focused review, *Eng. Fail. Anal.*, 2025, **180**, 109875.
175 Y. Sun and Y. F. Cheng, Hydrogen permeation and distribution at a high-strength X80 steel weld under stressing conditions and the implication on pipeline failure, *Int. J. Hydrogen Energy*, 2021, **46**, 23101–23112.
176 C. Gu, J. Hu and X. Zhong, The coating delamination mitigation of epoxy coatings by inhibiting the hydrogen evolution reaction, *Prog. Org. Coat.*, 2020, **147**, 105774.
177 A. Gunatilake, L. Piyathilaka, A. Tran, V. K. Vishwanathan, K. Thiyagarajan and S. Kodagoda, Stereo vision combined with laser profiling for mapping of pipeline internal defects, *IEEE Sens. J.*, 2021, **21**, 11926–11934.
178 D. Liu, Y. Wang, Y. Zhang, T. Ouyang, T. Zhou, X. Fang and J. Suo, Research on crack-filling heat treatment and hydrogen permeation test of self-healing tritium permeation barriers, *J. Therm. Spray Technol.*, 2018, **27**, 746–756.

© 2026 The Author(s). Co-published by the Institute of Process Engineering, Chinese Academy of Sciences and Royal Society of Chemistry